ISSN 2233-9485 (Print)
ISSN 2233-9574 (Online)

International Symposium on Magnetism and Magnetic Materials 2017

ABSTRACTS

Date November 29 - December 1 (Wed. - Fri.), 2017

Place Hwabaek International Convention Center (HICO), Gyeongju, Korea

Hosted by The Korean Magnetics Society

Sponsored by Hwabaek International Convention Center (HICO),
The Association of Korean Woman Scientists & Engineers (KWSE)

Digests of the International Symposium on Magnetism and Magnetic Materials 2017
The Korean Magnetics Society

International Symposium on Magnetism and Magnetic Materials 2017

ABSTRACTS

Date	November 29 - December 1 (Wed. - Fri.), 2017
Place	Hwabaek International Convention Center (HICO), Gyeongju, Korea
Hosted by	The Korean Magnetics Society
Sponsored by	Hwabaek International Convention Center (HICO), The Association of Korean Woman Scientists & Engineers (KWSE)

Notice

1. Presenters should follow the below guidelines.

1) The size of the board is 800 cm (width) by 1650 cm (height).
2) The scheduled posters should be displayed from 09:00 to 18:00 on the day of their session.
Poster Discussion will take place in the poster session room (205+206, 2nd Floor) from 09:00 to 09:50 and poster presenters must be present at their poster during this time.

2. Program at a Glance

Nov. 29 (Wed.)	14:00~	Registration		
	15:00~17:30	Blind Wine Tasting Challenge (105+106, 1st Floor)		
	17:30~19:00	Welcome Reception and Talk Concert (105+106, 1st Floor)		
Nov. 30 (Thu.)	08:30~	Registration		
	09:00~09:50	Poster Discussion (205+206, 2nd Floor)		Poster Session (205+206, 2nd Floor)
	09:50~10:00	Coffee Break		
	10:00~12:00	Ⓔ Special Session I (201+202, 2nd Floor)	Oral Session I (203, 2nd Floor)	
	12:00~13:30	Lunch		
	13:30~17:15	Special Session II (201+202, 2nd Floor)	Ⓔ Special Session III (203, 2nd Floor)	Oral Session II (204, 2nd Floor)
	17:15~17:30	Coffee Break		
	17:30~18:00	Plenary Session I (201+202, 2nd Floor)		
	18:00~18:30	KMS Regular General Meeting & KMS Awards (201+202, 2nd Floor)		
	18:30~20:00	Banquet (101+102+103+104, 1st Floor)		
Dec. 1 (Fri.)	08:00~	Registration		
	08:30~12:00	Ⓔ Special Session IV (201+202, 2nd Floor)	Special Session V (203, 2nd Floor)	
	12:00~12:10	Coffee Break		
	12:10~12:30	Poster Awards & Closing Ceremony (201+202, 2nd Floor)		

3. The Poster Awards Ceremony will take place in the main room (201+202, 2nd Floor) from 12:10 to 12:30 on December 1.
(If the winner (presenter) does not attend the ceremony, the awards will be cancelled.)

Nov. 29 (Wed.)

Time	PROGRAM
14:00 ~	**Registration**
15:00 ~ 17:30	**Blind Wine Tasting Challenge (105+106, 1st Floor)**
17:30 ~ 19:00	**Welcome Reception and Talk Concert (105+106, 1st Floor)** **'Magnetic sensor as the next generation core device'** Chair : Kwang Ho Shin (Kyungsung Univ.) Speakers : Kwang Ho Shin (Kyungsung Univ.), Geunbae Lim (POSTECH), Daesung Lee (KETI), Junseok Park (ETRI), Seok Bae (LG Innotek)

Nov. 30 (Thu.)

<table>
<tr><th>Time</th><th colspan="4">PROGRAM</th></tr>
<tr><td>08:30 ~</td><td colspan="4">Registration</td></tr>
<tr><td>09:00 ~ 09:50</td><td colspan="4">Poster Discussion (205+206, 2nd Floor)
Chairs : Cheol Soo Park (Hallym Polytechnic Univ.)/Ki-Suk Lee (UNIST)</td></tr>
<tr><td>09:50 ~ 10:00</td><td colspan="4">Coffee Break</td></tr>
<tr><td rowspan="5">10:00 ~ 12:00</td><td colspan="2">Ⓔ Special Session I
(201+202, 2nd Floor)
'Soft Magnetic Materials'
Chair : Sang-Im Yoo (Seoul Nat'l Univ.)</td><td colspan="2">Oral Session I
(203, 2nd Floor)
'Hard Magnetic Materials'
Chair : Dong Hwan Kim (Sunglim Group)</td></tr>
<tr><td rowspan="2">10:00 ~ 10:30</td><td rowspan="2">(Invited)S-I-1.
Amorphous and Nanocrystalline Materials for Soft Magnetic Applications
Giselher Herzer (Vacuumschmelze GmbH & Co.)</td><td>10:00 ~ 10:20</td><td>O-I-1.
Fabrication of Anisotropic Nd-Fe-B Magnet by Hot-deformation Process
Hee-Ryoung Cha (KIMS)</td></tr>
<tr><td>10:20 ~ 10:40</td><td>O-I-2.
Study on Microstructure and Coercivity of Thermally Processed Nd-Fe-B-type HDDR Material
Kyung Min Kim (Pukyong Nat'l Univ.)</td></tr>
<tr><td rowspan="2">10:30 ~ 11:00</td><td rowspan="2">(Invited)S-I-2.
Nanocrystalline-Based Magnetic Shielding Sheet for Wireless Power Transfer Applications
Dooho Park (Samsung Electro-Mechanics)</td><td>10:40 ~ 11:00</td><td>O-I-3.
High pressure synthesis, phase transformationand magnetic properties of nanocrystalline MnAl(C) magnets
Ping-Zhan Si (KIMS)</td></tr>
<tr><td>11:00 ~ 11:20</td><td>O-I-4.
Microscopic origin of the modification in the ferromagnetic properties of M type Sr hexaferrites by La and Co substitutions
Jae-Young Kim (IBS)</td></tr>
<tr><td colspan="4">Poster Session (205+206, 2nd Floor)
Session BM [Biomedical Magnetics]
Session HM [Hard-magnetic Materials]
Session MO [Magnetic Oxides and Multiferroics]
Session MT [Magnetic theory and calculations]
Session MD [Magnetization dynamics]
Session SA [Sensor and Applications]
Session SM [Soft-magnetic Materials]
Session SO [Spin orbit coupling and related phenomena]</td></tr>
</table>

Nov. 30 (Thu.)

<table>
<tr><th>Time</th><th colspan="6">PROGRAM</th></tr>
<tr><td rowspan="2"></td><td>11:00
~
11:30</td><td>(Invited)S-I-3.
FeCo-based Soft Magnetic Amorphous Alloys
Haein Yim (Sookmyung Women's Univ.)</td><td>11:20
~
11:40</td><td>O-I-5.
Thermomagnetic Stabilityof Exchange Coupled
Hard ($SrFe_{12}O_{19}$)/Soft(Fe-Co) Composites
Jihoon Park (KIMS)</td><td rowspan="2"></td></tr>
<tr><td>11:30
~
12:00</td><td>(Invited)S-I-4.
Spin dynamics of ferromagnetic Co/Pt multilayers over wide timescales
Dong-Hyun Kim (Chungbuk Nat'l Univ.)</td><td>11:40
~
12:00</td><td>O-I-6.
Magnetic properties of Y^{3+}-substituted SrM-type hexagonal ferrites prepared by solid state reaction
Kang-Hyuk Lee (Seoul Nat'l Univ.)</td></tr>
<tr><td>12:00
~
13:30</td><td colspan="6">Lunch</td></tr>
<tr><td rowspan="5">13:30
~
15:00</td><td colspan="2">Special Session II
(201+202, 2nd Floor)
'Magnetics for Defence'
Chairs : Derac Son (Hannam Univ.)/ Gwan Soo Park (Pusan Nat'l Univ.)</td><td colspan="2">Ⓔ Special Session III
(203, 2nd Floor)
'Women in radio-activation Analyses, and Magnetism'
Chairs : Haein Yim (Sookmyung Women's Univ.)/ Sam Jin Kim (Kookmin Univ.)</td><td colspan="2">Oral Session II
(204, 2nd Floor)
'Soft/Theory/Spin session'
Chair : Kwang Ho Shin (Kyungsung Univ.)</td><td rowspan="5">Poster Session
(205+206, 2nd Floor)
Session BM [Biomedical Magnetics]
Session HM [Hard-magnetic Materials]
Session MO [Magnetic Oxides and Multiferroics]
Session MT [Magnetic theory and calculations]
Session MD [Magnetization dynamics]
Session SA [Sensor and Applications]
Session SM [Soft-magnetic Materials]
Session SO [Spin orbit coupling and related phenomena]</td></tr>
<tr><td>13:30
~
14:00</td><td>(Invited)S-II-1.
Influence of Ship's Magnetic Field on Mine-War
Sungyong Lee (Navy Ordnance Ammunition Center)</td><td>13:30
~
14:00</td><td>(Invited)S-III-1.
Preparation of ^{57}Co sources for Mössbauer Spectroscopy
Malgorzatz Zoltowska (POLATOM)</td><td>13:30
~
14:00</td><td>(Invited)O-II-1.
Spin Circuit Model for Materials with Spin-Momentum Locking
Seokmin Hong (KIST)</td></tr>
<tr><td>14:00
~
14:30</td><td>(Invited)S-II-2.
Two-stage Flash-KD protocol for mock-up submarines without degaussing coils
Ki-Woong Bae (ADD)</td><td>14:00
~
14:30</td><td rowspan="2">(Invited)S-III-2.
Beta-voltaic battery and beta source using radioisotope Nickel
Young Rang Uhm (KAERI)</td><td>14:00
~
14:20</td><td>O-II-2.
Non-adiabatic spin-transfer torque for ferromagnetic domain wall
Hyeon-Jong Park (Korea Univ.)</td></tr>
<tr><td>14:30
~
15:00</td><td>(Invited)S-II-3.
Magnetic and Acoustic Virtual Target for OOO-class Submarine
Minho Kim (LIG Nex1)</td><td>14:30
~
15:00</td><td>(Invited)S-III-3.
Development of Turn-off Switching of NPT-IGBT under Fast Neutron Irradiation
Hani Baek (KAERI)</td><td>14:20
~
14:40</td><td>O-II-3.
Complementary spin transistors
using exchange-biased ferromagnetic electrodes
Youn Ho Park (KIST)</td></tr>
<tr><td>14:40
~
15:00</td><td>O-II-4.
Interfacial effect of Pt/$Ir_{20}Mn_{80}$ thin films
Thi Kim Hang Pham (Ewha Womans Univ.)</td></tr>
<tr><td>15:00
~
15:15</td><td colspan="6">Coffee Break</td></tr>
</table>

Nov. 30 (Thu.)

Time	PROGRAM						
15:15 ~ 17:15	15:15 ~ 15:45	(Invited)S-II-4. The Effect of Demagnetization depending on the thickness of the Vessel Sang Hyeon Im (Pusan Nat'l Univ.)	15:15 ~ 15:45	(Invited)S-III-4. Application of Activation Analysis to geological materials Mi-Eun Jin (KAERI)	15:15 ~ 15:35	O-II-5. Synthesis and Microwave Absorbing Property of Partially Zn-substituted Strontium Y-type hexaferrite Jae-Hyoung You (Seoul Nat'l Univ.)	**Poster Session (205+206, 2nd Floor)** Session BM [Biomedical Magnetics] Session HM [Hard-magnetic Materials] Session MO [Magnetic Oxides and Multiferroics] Session MT [Magnetic theory and calculations] Session MD [Magnetization dynamics] Session SA [Sensor and Applications] Session SM [Soft-magnetic Materials] Session SO [Spin orbit coupling and related phenomena]
	15:45 ~ 16:15	(Invited)S-II-5. A Study on the Signal Processing Techniques for Receiving Sensitivity Improvement of Active Proximity Magnetic Sensor Dae-Jung Kim (LIG Nex1)	15:45 ~ 16:15	(Invited)S-III-5. Co-electrodeposition of U-Mo in LiCl-KCl Melt Na-Ri Lee (KAERI)	15:35 ~ 15:55	O-II-6. Core loss improvement in the SMC composed of Fe-Al_2O_3 core-shell structure Sung Joon Choi (Seoul Nat'l Univ.)	
	16:15 ~ 16:45	(Invited)S-II-6. Orthogonal Fluxgate Sensor for Underwater Application Kwang Ho Shin (Kyungsung Univ.)					
	16:45 ~ 17:15	(Invited)S-II-7. A Study on 3-axis Flux-gate Magnetometer for Harbor Surveillance System Derac Son (Hannam Univ.)					
17:15 ~ 17:30	**Coffee Break**						
17:30 ~ 18:00	**Plenary Session I (201+202, 2nd Floor)** Chair : Pan Kyu Choi (MTI Co., Ltd.)						
	(Invited)P-I-1. The 4th Industrial Revolution and Creativity Hi-Jung Kim (KIST)						
18:00 ~ 18:30	**KMS Regular General Meeting & KMS Awards (201+202, 2nd Floor)**						
18:30 ~ 20:00	**Banquet (101+102+103+104, 1st Floor)**						

Dec. 1 (Fri.)

Time	PROGRAM			
08:00 ~	**Registration**			
08:30 ~ 12:00	**Ⓔ Special Session IV (201+202, 2nd Floor) 'Magnetic Materials for Electric Vehicles'** Chair : Wooyoung Lee (Yonsei Univ.)		**Special Session V (203, 2nd Floor) 'Medical Science Research'** Chair : Man-Seok Han (Kangwon Nat'l Univ.)	
	08:30 ~ 09:00	(Invited)S-IV-1. High Performance Nd-Fe-B-type Permanent Magnet with High Electrical Resistivity — H. W. Kwon (Pukyong Nat'l Univ.)	09:00 ~ 09:30	(Invited)S-V-1. Modified Oblique Sagittal MR imaging of rotator cuff tears: comparison with standard oblique sagittal images — Myung Sik Ju (Soonchunhyang Univ. Bucheon Hospital)
	09:00 ~ 09:30	(Invited)S-IV-2. High-Speed Electrical Machines - Applications, Key Issues and Challenges — Jian-Xin SHEN (Zhejiang Univ.)		
	09:30 ~ 10:00	(Invited)S-IV-3. On Electromagnetic Force Density Induced in Dipole Model of Materials — Hong Soon Choi (Kyungpook Nat'l Univ.)	09:30 ~ 10:00	(Invited)S-V-2. Development of Multi-purpose Quality Assurance Phantom for Verification of Treatment Plan of Volumetric Modulated Arc Therapy using Linear Accelerator — Hui-Su Won (Seoul Nat'l Univ. Bungdang Hospital)
	10:00 ~ 10:30	(Invited)S-IV-4. Fe-rich compounds with promising intrinsic magnetic properties as permanent magnetic materials — Y. Hirayama (National Institute of Advanced Industrial Science and Technology)	10:00 ~ 10:30	(Invited)S-V-3. Specific Absorption Rate Evaluation for Multi-Frequency Excitation — Yeunchul Ryu (Gachon Univ.)
	10:30 ~ 11:00	(Invited)S-IV-5. Design of Ferrite Magnet Flux Concentrated Permanent Magnet Synchronous motor with Cross-Laminated Rotor Core — Jaewoo Jung (Hyundai Mobis)	10:30 ~ 11:00	(Invited)S-V-4. Separation of photoneutron and photoproton in 10MV and 15MV Medical LINAC — Jeong Ho Kim (Konyang Univ. Hospital)
	11:00 ~ 11:30	(Invited)S-IV-6. Analysis and reduction of electromagnetic vibration of PM brush DC motors — Shanming Wang (Tsinghua Univ.)	11:00 ~ 11:30	(Invited)S-V-5. fMRI Brain Network Analysis techniques — Young-Jin Jung (Dongseo Univ.)
	11:30 ~ 12:00	(Invited)S-IV-7. Development of Heavy-Rare-Earth-Free Hot-deformed Nd-Fe-B Magnets for Traction Motors — Atsushi Hattori (Daido Electronics Co., Ltd.)	11:30 ~ 12:00	(Invited)S-V-6. Proposing a low-field bio-imaging method — Sang-Koog Kim (Seoul Nat'l Univ.)
12:00 ~ 12:10	**Coffee Break**			
12:10 ~ 12:30	**Poster Awards & Closing Ceremony (201+202, 2nd Floor)**			

CONTENTS

Nov. 29 (Wed.), 17:30~19:00
Session : 'Magnetic sensor as the next generation core device'

105+106, 1st Floor

Chair : Kwang Ho Shin (Kyungsung Univ.)

Nov. 30 (Thu.), 10:00~12:00
Special Session I 'Soft Magnetic Materials'

201+202, 2nd Floor

Chair : Sang-Im Yoo (Seoul Nat'l Univ.)

Nov. 30 (Thu.), 10:00~12:00
Oral Session I 'Hard Magnetic Materials'

203, 2nd Floor

Chair : Dong Hwan Kim (Sunglim Group)

Nov. 30 (Thu.), 13:30~17:15
Special Session II 'Magnetics for Defence'

201+202, 2nd Floor

Chairs : Derac Son (Hannam Univ.) / Gwan Soo Park (Pusan Nat'l Univ.)

Nov. 30 (Thu.), 13:30~16:15
Special Session III 'Women in radio-activation analyses, and magnetism'

203, 2nd Floor

Chairs : Haein Yim (Sookmyung Women's Univ.) / Sam Jin Kim (Kookmin Univ.)

Nov. 30 (Thu.), 13:30~15:55
Oral Session II 'Soft/Theory/Spin session'

204, 2nd Floor

Chair : Kwang Ho Shin (Kyungsung Univ.)

Nov. 30 (Thu.), 17:30~18:00
Plenary Session I

201+202, 2nd Floor

❀ Chair : Pan Kyu Choi (MTI Co., Ltd.)

Nov. 30 (Thu.), 09:00~18:00
Poster Session

205+206, 2nd Floor

❀ Chairs : Cheol Soo Park (Hallym Polytechnic Univ.) / Ki-Suk Lee (UNIST)

○ Session BM[Biomedical Magnetics]

○ Session HM[Hard-magnetic Materials]

○ Session MO[Magnetic Oxides and Multiferroics]

○ Session MT[Magnetic theory and calculations]

○ Session MD[Magnetization dynamics]

○ Session SA[Sensor and Applications]

○ Session SM[Soft-magnetic Materials]

Dec. 1 (Fri.), 08:30~12:00
Special Session IV 'Magnetic Materials for Electric Vehicles'

201+202, 2nd Floor

Chair : Wooyoung Lee (Yonsei Univ.)

Dec. 1 (Fri.), 09:00~12:00

Special Session V 'Medical Science Research'

203, 2nd Floor

Chair : Man-Seok Han (Kangwon Nat'l Univ.)

International Symposium on Magnetism and
Magnetic Materials 2017

Talk Concert

'Magnetic sensor as the next generation core device'

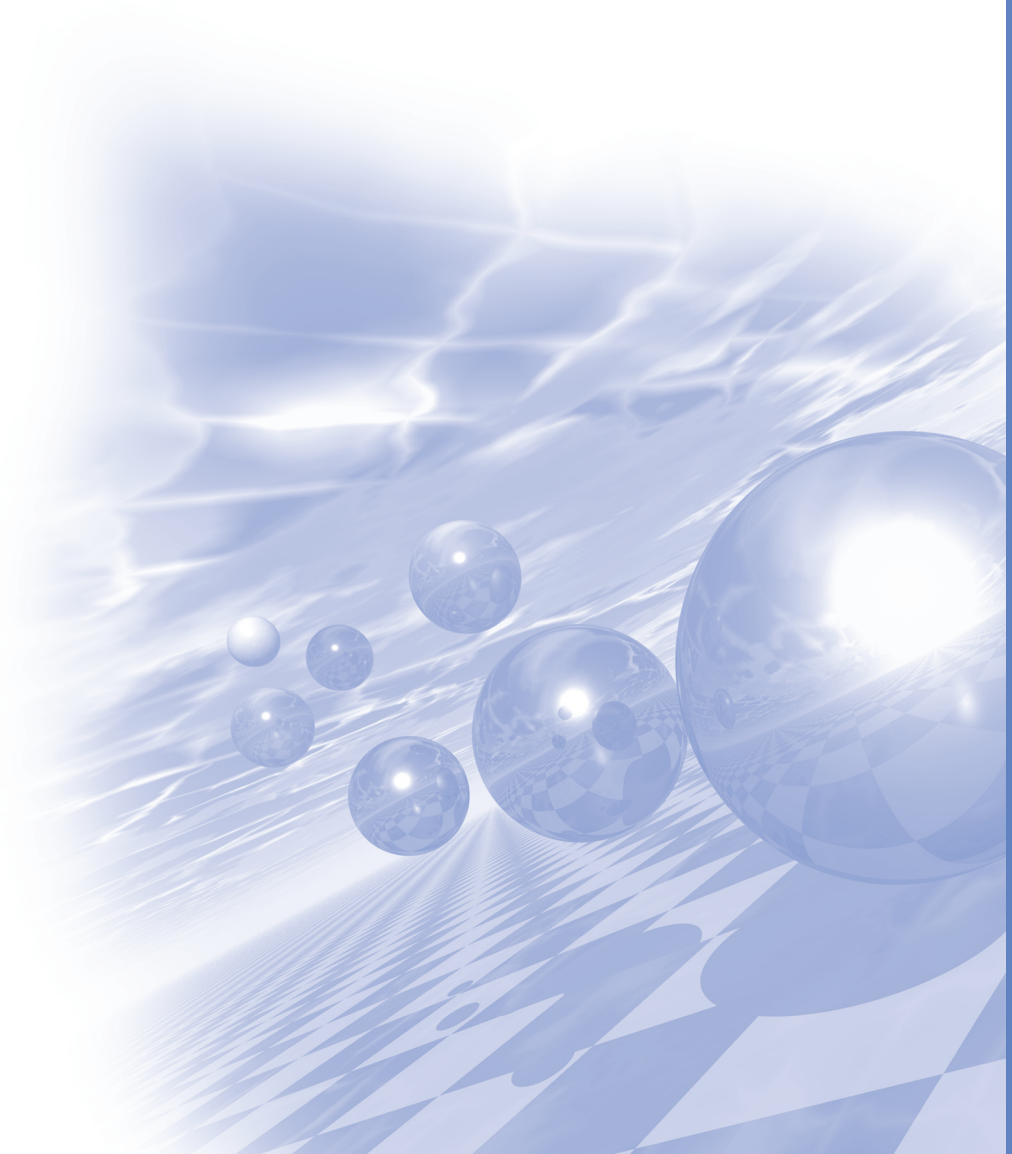

Present and Future of Magnetic sensors

Kwang-Ho Shin*
Kyungsung University, Korea

Nowadays, we can find magnetic sensors working in various applications; industrial, home electronics, military defense, bio/medical, IT, automobile, and etc. Non-specialists are not well aware of this status, but magnetic sensors are the most important of the various sensors. Recently, as the internet of things (IoT) became a hot topic of technical innovation, the importance of sensors is growing. Assuming the future of IoT technology development, the importance of magnetic sensors could be expected to increase sharply in near future. From the viewpoint of sensor technology, for the last 30 years, very rapid developments have been made in magnetic sensor area. However, it is hard to say that now technically saturated, because there is still room for much technical advancement. At this talk-concert, I would like to share some information related to magnetic sensors and discuss the future of the magnetic sensor with the audience.

Nano fabrication technology for new applications

Geunbae Lim*
Department of Mechanical Engineering, Pohang University of Science and Technology,
Chungam-ro 77, Pohang 37673, Korea

As semiconductor technology advances, Miceoelectromechanical System (MEMS) technology has drawn attention in the early 90s. Basically MEMS uses the scale effect that performance can be improved as device size become smaller, it has become new leading technology. However, hardware platform can hardly be commercialized and integrated into other technology because it varies according to its application. Only bio-application field using MEMS technology has been greatly expanded so far. Nanotechnology has gotten a spotlight in the early 2000s. It shows many unique characteristics/phenomena; it enables us to pursue new principle and to make new devices that were impossible in the macro world. In this presentation I will introduce new nano-fabrication technology for new applications

Suggestions for the development of the domestic sensor industry to prepare for the fourth industrial revolution

Daesung Lee*
Korea Electronic Technology Institute, Korea

Artificial intelligence (AI), Internet (IoT), drones, robots, autonomous vehicles, big data, and 3D printing are among the new industries that will lead the fourth industrial revolution. By the way it is the sensor that makes these industries possible and is the basis. For the control of robots, drones, and automobiles, information via sensors is essential for the new AI IoT service. Obtaining information through sensors is essential for robotics, drones, automobile control, and for new AI IoT services. BBC Research estimates that the global sensor market, which was $ 137.8 billion in 2017, will grow to $ 240.2 billion by 2022. In particular, the US Trillion Roadmap Summit expects sensor demand to grow at an annual average rate of more than 56%, taking into account the impact of the fourth industrial revolution. We will examine the sensor industry trend to prepare for this and look for ways to develop the domestic sensor industry which is relatively inferior.

IoT and Sensors

Junseok Park*
ETRI, Korea

Information technology systems of the future are increasingly focused on where data is generated and processed, how it's delivered and collected, and how quickly this data can move. Sensors and actuators are starting points of data generation from human and environments. Recently, a wide variety of potential application of IoT devices and sensors is emerging as an electronic consumer products in daily life use various sensors to provide new experience for its users. In this talk, I'd like to review the infrastructure of the Internet of Things(IoT), the role of sensors in the IoT, requirements of smart sensors, and it's potential applications.

Sensors for Internet of Things

Seok Bae*, Yuseon Kim
X-Task, CTO, LG Innotek

사물 인터넷은 사물들의 다수 센서로부터 수집된 정보가 인터넷 시스템과 연결되게 하는 기술로써 4차 산업 혁명의 가장 중요한 기술 분야중 하나이다. IoT 모듈은 전력부(배터리 혹은 에너지 하베스터), 모뎀, 제어부와 센서로 구성된다. IoT모듈의 성능 구현을 위하여 작고 효율적인 센서는 가장 중요한 부품이며 빛, 진동, 자기장 등의 다양한 특정 신호등을 센싱한다.

금번 논의에서는 상용화된 IoT 제품에 사용된 센서들의 요구 특성 등에 대해 논의하고자 한다.

The Internet of things (IoT) is the most important technical part of the 4th industrial revolution, which involves the internet system link to gathered data from sensors under the certain purpose and position. IoT module consists of power supply (include battery or energy harvesting device), wireless modem, control part and sensor. Small and efficient sensor is an essential component for the IoT module to detect the specific signal, such as light, vibration, and magnetic field.

In this talk, the required properties of sensors with the commercialized IoT products will be discussed

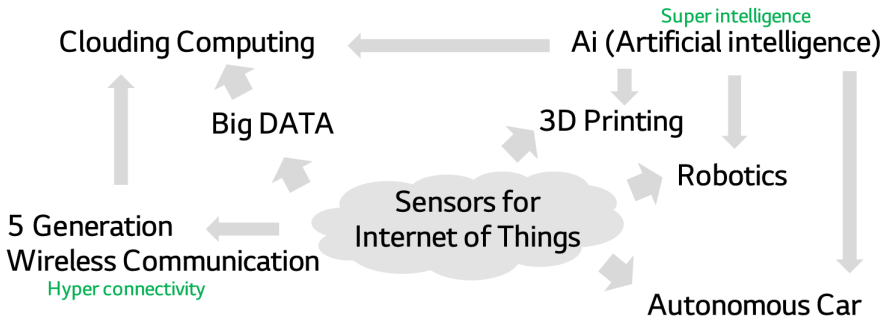

Fig. 1. Keywords in the 4th industrial revolution (1line spacing / image size: 300 dpi)

International Symposium on Magnetism and
Magnetic Materials 2017

Special Session I

'Soft Magnetic Materials'

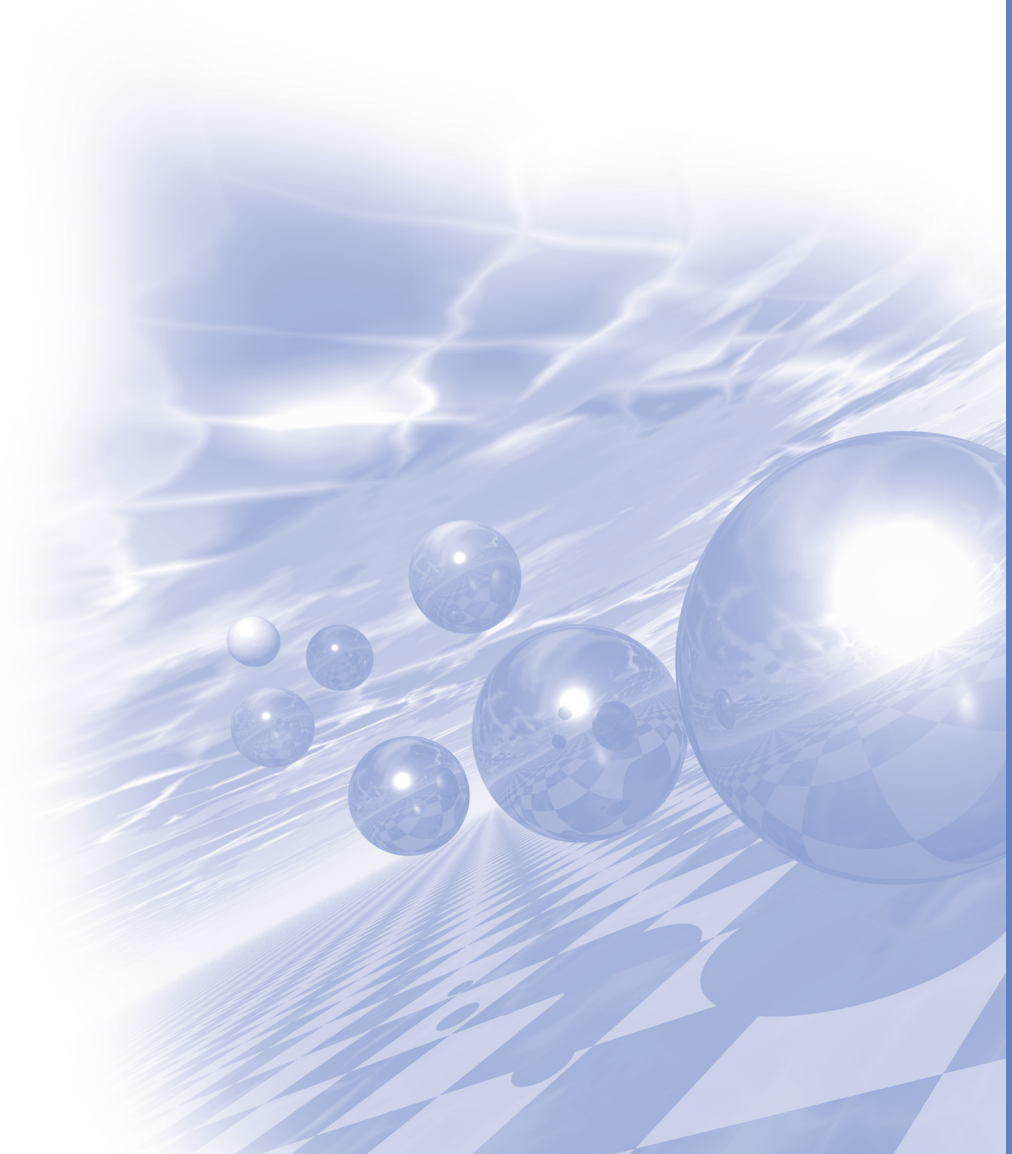

Amorphous and Nanocrystalline Materials for Soft Magnetic Applications

Giselher Herzer*
Vacuumschmelze GmbH & Co. KG, Grüner Weg 37, D-63450 Hanau, Germany
Email:gherzer@gmail.com

The talk surveys characteristic features of amorphous and nanocrystalline alloys for soft magnetic applications. Both materials have much in common starting from their way of production by rapid solidification as a thin ribbon and including the key factors which determine their magnetic properties. Thus, the magneto-crystalline anisotropy is randomly fluctuating on a scale much smaller than the domain wall width and, as a consequence, is averaged out by exchange interaction so that there is no anisotropy net effect on the magnetisation process, the prerequisite for good soft magnetic behaviour. Owing to their production inherent low thickness and relatively high electrical resistivity both materials additionally reveal favourably low losses up to several 100 kHz making them even competitive with MnZn ferrites.

Nanocrystalline alloys provide a particularly unique combination of high saturation induction, low magnetostriction, high permeability, low losses and good thermal stability. This allows to reduce the size and the weight of magnetic components. Apart from its technical performance, the material is also based on the inexpensive raw materials iron and silicon. Accordingly, nanocrystalline alloys are found in a steadily increasing number of applications previously served by amorphous Co-based alloys or MnZn ferrites.

Apart from low coercivity, soft magnetic applications also require a well-defined shape of the hysteresis loop with not necessarily the highest, but a specific level of permeability. This is accomplished by annealing induced magnetic anisotropies. Their orientation relative to the magnetic path controls the shape of the hysteresis loop and the magnitude, K_u, determines the permeability. In particular magnetic field annealing is a powerful tool in tailoring the hysteresis loop according to the demands of various applications. Still, tensile stress annealing provides a further opportunity to control the induced anisotropy. Appropriate choice of the alloy composition and the annealing conditions, thus, ultimately allows to vary K_u by about four orders of magnitude.

Nanocrystalline-Based Magnetic Shielding Sheet for Wireless Power Transfer Applications

Dooho Park*, Jung Young Cho, Sung-nam Cho, Tai-Yon Cho, Taejun Choi, Seungmin Lee, Seunghee Oh, San Kyeong, Chang Hak Choi, Jihyo Lee, Kangheon Hur
Corporate R&D Institute, Samsung Electro-Mechanics, Korea

The Wireless Power Transfer (WPT) technology has experienced a recent surge in interest with the rising popularity of mobile electronic devices. Common WPT scheme involves transmitter (Tx) and receiver (Rx) coils that are magneto-inductively coupled together. The specification of the system is indicated by the following three parameters: resonant frequency, self-inductance of the coils, and electromagnetic interference (EMI) characteristic. EMI characteristic is affected by attaching shielding materials such as ferrite and metal film that could change self- and mutual inductance. The requirements of shielding sheets for mobile devices are to be slim, controllable in magnetic properties and applicable for the WPT(100-300 kHz) / MST(2 kHz) / NFC(13.56 MHz)-integrated system which runs over wide frequency range. In this study, in order to provide the best solution for the requirements, nanocrystalline alloy has been employed for the new type of shielding sheet because of two advantages. One of advantages is that nanocrystalline Fe-Cu-Nb-Si-B alloys have higher permeability and lower core loss over wide frequency range than Mn-Zn ferrite and Fe-based amorphous alloy. The other advantage is that nanocrystalline ribbon has a benefit in thickness.

FeCo-based Soft Magnetic Amorphous Alloys

Haein Yim*
Department of Applied Physics, Sookmyung Women's University, Seoul 04310, Korea

Soft magnetic materials play important functional role in commercial products such as motors, sensors, and data storage devices which affect the human living ways. The FeCo-based amorphous alloys are among the best classes of soft magnetic materials due to their excellent magnetic performance including low coercivity (H_c), high saturation magnetization (M_s), and high permeability (μ). Therefore, the development of FeCo-based amorphous alloys with superior soft magnetic properties has been engaged interest in materials science and engineering research. Some have been widely used in application according to their unique characteristics. In this talk, we will overview our recent progresses toward the development of FeCo-based soft magnetic amorphous alloys. Rapidly solidified alloy ribbons were fabricated using a single copper roller vacuum melt spinning technique. We will focus on the newest of amorphous alloys and discuss on the details of their various characterization including structural, thermal, mechanical, and magnetic property.

Spin dynamics of ferromagnetic Co/Pt multilayers over wide timescales

Dong-Hyun Kim*
Department of Physics, Chungbuk National University, Cheongju 28644, Chungbuk, South Korea
Email : donghyun@cbnu.ac.kr

Magnetization dynamics on ultrafast time scales has recently attracted much attention due to possible application for fast-operating spintronic devices. The problem is basically linked with fundamental entities such as spin, electron, and lattice in the solid. Recently, huge interest has grown on the photo-induced demagnetization behavior of ferromagnetic system, where high energy photon pulse of femtoseconds pulse widths hit the sample with excitation of spin, electron, and lattice in the solid. On this non-equilibrium time scale, novel physical phenomena resulted from mutual intense interaction among spin, electron, and lattice are exhibited with a rich context, where we have successfully investigated phonon oscillation [1] and ultrafast magnetic cooling phenomenon [2]. Ultrafast spin-electron-lattice dynamics results explored by femtosecond pump-probe mageto-optical Kerr effect measurement will be reported with systematic analysis based on the 3-temperature model. On the other hand, magnetization reversal phenomenon mediated by magnetic domain wall evolution is a classical but a fundamental phenomenon, which should be clearly understood for further spintronic applications. We investigate magnetization dynamics over wide temporal scales ranging from femtosecond to kilosecond. Slow dynamics is directly observed by adopting a magneto-optical Kerr/Faraday microscopy [3]. Various details of magnetization dynamics over wide timescales will be briefly reviewed possibly with detailed microscopic features.

References

[1] C. H. Kim et al., Sci. Rep. **6**, 22054 (2016).
[2] J.-H. Shim et al., Nature Comm. **8**, 796 (2017).
[3] D.-T. Quachet al., IEEE T. Mag. **50**, 6500504 (2014).

Oral Session I

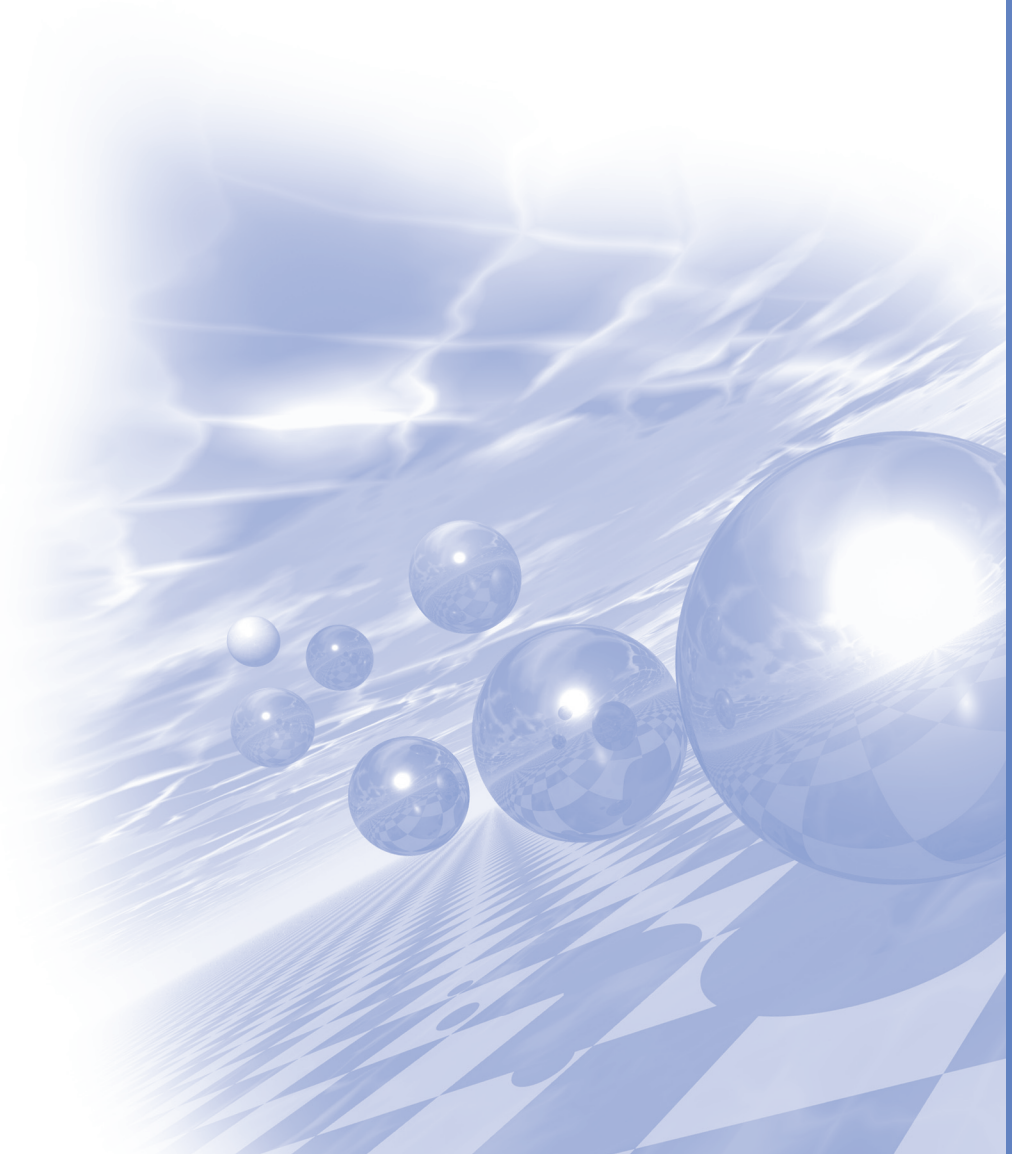

Fabrication of Anisotropic Nd-Fe-B Magnet by Hot-deformation Process

Hee-Ryoung Cha[1*], Jae-Gyeong Yoo[1], Youn-Kyoung Baek[1],
Hae-Woong Kwon[2], and Jung-Goo Lee[1]

[1]Powder&Ceramics Division, Korea Institute of Materials Science, Changwon, Korea
[2]Department of Materials Science and Engineering, Pukyong National University, Busan, Korea

The traction motors of hybrid and electric vehicles require permanent magnets with high coercivity and high maximum energy product. Currently, (Nd,Dy)-Fe-B sintered magnets has been used for traction motor due to the its outstanding magnetic properties. However, due to the resource problems of heavy rare earth (HRE) as Dy or Tb, HRE-lean or HRE-free high coercive Nd-Fe-B permanent magnets are demanded. Microstructure control such as grain size and grain boundary is necessary in order to increasing coercivity of magnets without HRE element. With regard to grain size, melt-spinning and hydrogenation–disproportionation–desorption–recombination (HDDR) are known as quite suitable method to decrease grain size down to the single domain size (~250 nm). The HDDR powder has coarser-grain compare to melt-spun powder though much smaller grain size than that of convention sintered magnet. Because of this relatively coarser-grain, the HDDR powder has an advantage during post-annealing as grain boundary diffusion process (GBDP), it can be treated at a relatively higher temperature compare to melt-spun powder. However, HDDR powder was used only for bonded magnet, though the fabricated bonded magnet has low maximum energy density. Thus, studies on sintering of HDDR powder are attracted attention for high performance HDDR magnet. Hot-deformation process has been used for the nano-crystalline powders in order to produce anisotropic bulk magnet. However, there were only a few studies examining the hot-deformation behavior of HDDR powders, whereas many studies have been done on that of melt spun powder.

In this study, hot-deformation process was employed to fabricate anisotropic bulk magnet. And the melt-spun powders and HDDR powders were used as initial powder in order to examine the effect of initial grain size on hot-deformation behavior. The deformation behavior of nano-grained magnetic powders was investigated systematically as a function of the strain, strain rate and temperature in order to optimize the deformation condition. After the hot-deformation, the grain morphology was changed from sphere to platelet. And the coercivity and remanence decreased and increased with increasing strain, respectively. The high deformation temperature and slow deformation rate reduce the coercivity further, inducing the grain growth and non-uniform Nd-rich grain boundary. With regard to the grain size, the large grain of HDDR powder was difficult for deformation and aspect ratio of grain produced with HDDR powders was lower than that of melt-spun powders after hot-deformation.

Study on Microstructure and Coercivity of Thermally Processed Nd-Fe-B-type HDDR Material

Kyung Min Kim[1*], Min Seok Kang[1], Hae-Woong Kwon[1], Tae Hoon Kim[2],
Cheol-Woong Yang[2], Jung Goo Lee[3], Ji Hoon Yu[3]

[1]Pukyong National University, Department of Materials Science and Engineering, Busan, Republic of Korea 48513
[2]Sungkyunkwan University, College of Materials Science and Engineering, Suwon, Republic of Korea 16419
[3]Korea Institute of Materials Science, Changwon, Republic of Korea 51508

1. Introduction

Share of an environment-friendly vehicle (HEV, EV) in a car market has drastically ballooned these days, and permanent magnet plays a vital role in traction motor of those vehicles. Magnet used in the traction motor of the vehicles is exclusively Nd-Fe-B-type by virtue of its superior magnetic performance. However, one of the downsides of Nd-Fe-B-type magnet is its rather low Curie temperature (~ 315 ^{o}C), and worse still, its operating temperature in the traction motor is unavoidably high (> 150 ^{o}C). The magnet, therefore, severely lacks thermal stability, in particular a poor thermal stability of coercivity is a major problem. As such, coercivity enhancement is a hot issue in the area of Nd-Fe-B-type magnet, and common approaches for enhancing coercivity in the magnet are; (1) substitution of some Nd atoms in the $Nd_2Fe_{14}B$ phase by heavy rare earth (HRE) atoms, such as Tb or Dy, (2) grain refinement. Enhancing coercivity by grain refinement is increasingly attracting great interest because it can avoid the use of expensive and scarce HRE. It would be desirable, therefore, to use a fine grain structured material like HDDR-treated Nd-Fe-B-type powder as starting material for fabrication of bulk magnet with high coercivity because the HDDR-treated Nd-Fe-B-type material inherently possesses fine $Nd_2Fe_{14}B$ grain structure. Several attempts have been made to exploit the HDDR powder as a starting material for consolidated bulk magnet with the intention of achieving high coercivity, but with little success. As consolidation of powder material commonly requires thermal processing, insight into the influence of thermal heating on the coercivity of the Nd-Fe-B-type HDDR material can hint at finding the best way for preparing high coercivity magnet. In the present study much emphasis was placed on the link between coercivity and grain boundary feature in the thermally processed Nd-Fe-B-type HDDR material.

2. Experimental

$Nd_{12.5}Fe_{80.8}B_{6.4}Ga_{0.3}$ alloy was HDDR-treated in a standard condition; hydrogenation at 350 °C for 60 min under 0.1 MPa hydrogen gas, disproportionation at 820 °C for 45 min under the 0.03 MPa hydrogen pressure, desorption and recombination at 820 °C for 30 min under a vacuum. The HDDR-treated powder with initial intrinsic coercivity of 14 kOe was swiftly heated up to desired temperature in controlled vacuum : high vacuum with around 5 x 10^{-6} mbar or lower vacuum with around 2 x 10^{-4} mbar. Cooling of the sample after heating was also performed in different mode quenching or slow-cooling (took approximately 30 min. from 900 ^{o}C to 500 ^{o}C). Magnetic characterization of the materials was performed by VSM after magnetizing with 5 T pulsing field. Microstructure of the material was examined using scanning electron microscopy (SEM), transmission electron microscopy (TEM) and chemical analysis was performed by using energy dispersive X-ray spectroscopy (EDS).

3. Results

Heat-treated $Nd_{12.5}Fe_{80.8}B_{6.4}Ga_{0.3}$ HDDR material exhibited consistently higher coercivity when it was quenched compared to when slow-cooled (Fig. 1). Higher coercivity in the quenched material was attributable to the grain boundary with lower Fe content. HDDR-treated material heated in high vacuum showed consistently higher coercivity than the material heated in lower vacuum, and this was attributed to less heavily oxidized surface. Reduced coercivity of the HDDR-treated material heated at moderate temperature was noticeably recovered at higher temperature, and this was attributed to lower Fe content in the grain boundary.

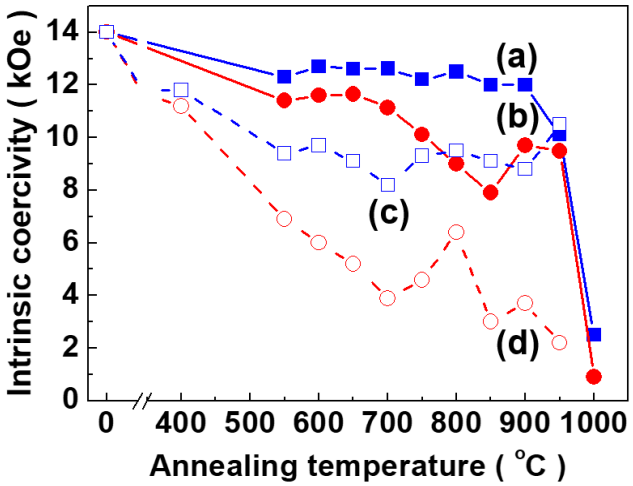

Fig. 1. Variations of intrinsic coercivity of the HDDR-treated $Nd_{12.5}Fe_{80.8}B_{6.4}Ga_{0.3}$ alloy after heating in different mode. (a) HVQ, (b) HVSC, (c) LVQ, and (d) LVSC.

High pressure synthesis, phase transformation and magnetic properties of nanocrystalline MnAl(C) magnets

Ping-Zhan Si[1,2*], Hui-Dong Qian[1], Jihoon Park[1], Chul-Jin Choi[1†]
[1]Powder & Ceramic Division, Korea Institute of Materials Science, Changwon, Gyeongnam, 51508, R. Korea
[2]College of Materials Science and Engineering, China Jiliang University, Hangzhou, 310018, China

Various techniques such as hot extrusion, backpressure equal channel angular extrusion, hot deformation, hot compaction, spark plasma sintering, and microwave sintering have been employed to make bulk MnAl magnets in the previous work. The precursors for hot extrusion and deformation are usually bulk materials while the precursors for the other methods are milled powders, which usually shows a higher coercivity and lower magnetization than that of the bulk. When the powders were consolidated in bulk magnets, both magnetization and coercivity would be decreased. The methods to make bulk samples usually involve high temperature processes that may result in a partial decomposition of the τ-phase, and thus a reduced magnetization. In this work, bulk MnAl and MnAl(C) magnets were prepared by pressing the as-prepared gas-atomized powders in pressures up to 4 GPa, which to some extent reduces the grain size into nanoscale and thus bulk nanocrystalline magnetic materials were obtained. The high-pressure process was conducted at room temperature or low temperatures and thus the magnetization of the powders was maintained while the coercivity was enhanced. The triggering temperatures of both displacive and massive phase transformation in the gas-atomized MnAl and MnAl(C) were determined by using magnetic measurements, based on which the annealing temperature to prepare the τ-phase of MnAl and MnAl(C) from ε-phase were optimized.

Acknowledgements

This work was supported by Creative Materials Discovery Program through the National Research Foundation of Korea (NRF) funded by the Ministry of Science, ICT and Future Planning under Grant Number 2016M3D1A1027800, and NSFC (Nos. 11074227, 51671177).

Microscopic origin of the modification in the ferromagnetic properties of M type Sr hexaferrites by La and Co substitutions

Yoon Young Koh[1], Jae-Young Kim[2*]
[1]Max Planck POSTECH center for Complex phase materials
[2]Center for Artificial Low Dimensional Electronic Systems, Institute for Basic Science (IBS)

M type hexaferrites are permanent magnets and they have been widely used in the applications such as motors and generators, microwave absorbing materials, and magnetic recording media. The high saturation magnetization and the large coercivity of them are originated basically from the uniaxial crystal structure of magnetoplumbite and the high frequency microwave response (>10 GHz) is associated with the unique ferrimagnetic spin arrangement of Fe ions in the five different local sites (2a, 2b, 4f1, 4f2, 12k). The ferromagnetic properties and the microwave response can also be modified by substituting La and Co for Sr or Ba and Fe ions. The smaller ionic size of La than those of Ba and Sr induces the structural transition at lower temperature and interestingly the excess charge supplied by the substituted La may induce local molecular magnetic anisotropy energy at Fe 2+ sites, which results in the higher coercivity and saturation magnetization. The substituted Co ions for Fe sites have smaller local magnetic moments then Fe ions and their preferable distribution is expected to change the magnetization too. In this work, we have measured X-ray Absorption Spectroscopy and X-ray Magnetic Circular Dichroism on a series of M type Sr hexaferrites which have different substitution ratios of La and Co. They directly show that the Fe 2+ are formed by the La substitution and they are localized at Oh sites. Also, the local symmetry distortion at Oh sites accompanied with Fe 2+ induces a large amount of orbital magnetic moment at the Fe 2+ sites.

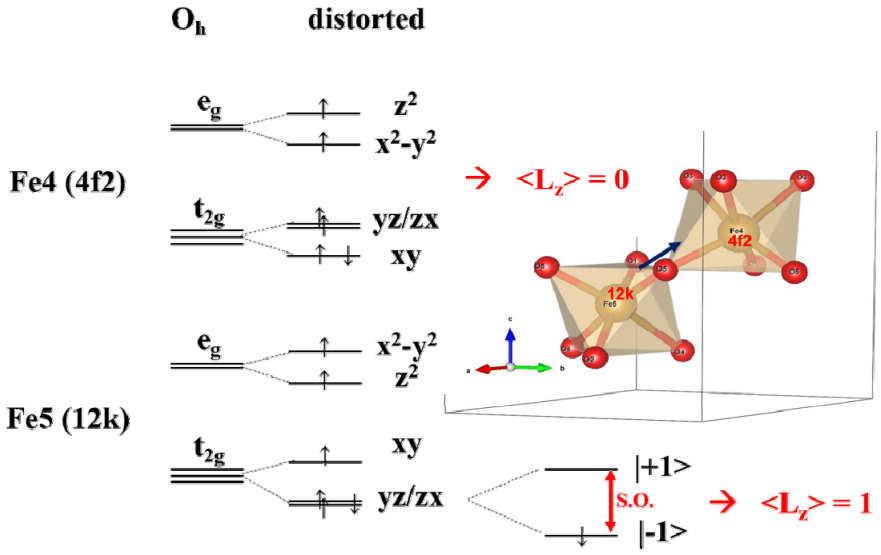

Fig. 1. How is the orbital moment unquenched by spin-orbit interaction under a particular lattice distortion in 12K site.

Thermomagnetic Stability of Exchange Coupled Hard ($SrFe_{12}O_{19}$)/Soft (Fe-Co) Composites

Jihoon Park*, Hui-Dong Qian, Ping-Zhan Si, Jong-Woo Kim, and Chul-Jin Choi†
Powder & Ceramic Division, Korea Institute of Materials Science, Changwon, Korea

Thermo-magnetic stability of magnetically exchange coupled hard/soft composite is not yet reported. Therefore, we have synthesized exchange coupled $SrFe_{12}O_{19}$(SrM)/Fe-Co spherical chain and SrM/Fe-Co nanoparticle composites to investigate thermo-magnetic stability, and measured saturation magnetization (σ_s), remanent magnetization (σ_r), and intrinsic coercivity (H_{ci}) of both single phase particles and SrM/Fe-Co composites over a temperature range of 23 to 300 °C.

Both composites reveal smooth and kink-free hysteresis loops with increased σ_r over most of temperature range, implying magnetic exchange coupling. Moreover, the temperature coefficients, i.e. $\alpha_s = \Delta\sigma_s/\sigma_s$, $\alpha_r = \Delta\sigma_r/\sigma_r$, and $\beta = \Delta H_{ci}/H_{ci}$, are enhanced to -0.162, -0.175, and -0.040 %/K for SrM/Fe-Co spherical chain and -0.170, -0.191, and -0.007 %/K for SrM/Fe-Co nanoparticle, respectively, from -0.183, -0.191, and +0.023 %/K for SrM. This suggests that exchange coupled SrM/Fe-Co composites are more thermo-magnetically stable than single phase SrM.

Acknowledgement

This work was supported by Creative Materials Discovery Program through the National Research Foundation of Korea (NRF) funded by the Ministry of Science, ICT and Future Planning under Grant Number 2016M3D1A1027800.

Magnetic properties of Y^{3+}-substituted SrM-type hexagonal ferrites prepared by solid state reaction

Kang-Hyuk Lee* and Sang-Im Yoo†
Department of Material Science and Engineering, Research Institute of Advanced Materials (RIAM),
Seoul National University, Seoul 151-744, Korea

Hexagonal ferrites have several advantages of excellent magnetic properties, chemical stability, and low cost compared with other magnetic materials. Among them, strontium ferrite ($SrFe_{12}O_{19}$) is one of M-type hexagonal ferrites and used as a permanent magnet in industrial applications since it possesses high Curie temperature, high coercivity, and high magnetic anisotropy. There have been various attempts to improve the magnetic properties of M-type hexaferrites. As such an effort, in this study, we tried to synthesize Y^{3+}-substituted Sr M-type hexagonal ferrites since the effect of the yttrium doping on the magnetic properties of Sr M-type hexagonal ferrites has never been reported yet. Hexaferrites with the nominal compositions of $Sr_{(1-x)}Y_xFe_yO_{19}$ (x = 0.0~0.5) (y = 10~12) were prepared by solid state reaction in air using strontium carbonate ($SrCO_3$), yttrium oxide (Y_2O_3) and iron oxide (Fe_2O_3) as raw materials. The raw materials were ball-milled for 24 h and calcined at 1100~1300 °C for 10 h in air. As-calcined powder were pressed into pellets and sintered at 1200~1300°C for 4 h in air. The samples were characterized by X-ray diffraction (XRD), vibrating sample magnetometer (VSM), and scanning electron microscope (SEM). The powder XRD patterns of $Sr_{0.5}Y_{0.5}Fe_{10}O_{19}$ calcined at 1200 for 10 h exhibited a single phase, and its maximum saturation magnetization (Ms) value of 66.872 emu/g was achieved from the sample sintered at 1300°C for 4 h in air. Details will be presented for a discussion.

Keywords: Hexaferrite, magnetic property, yttrium-substituted Sr M

International Symposium on Magnetism and Magnetic Materials 2017

Special Session II

'Magnetics for Defence'

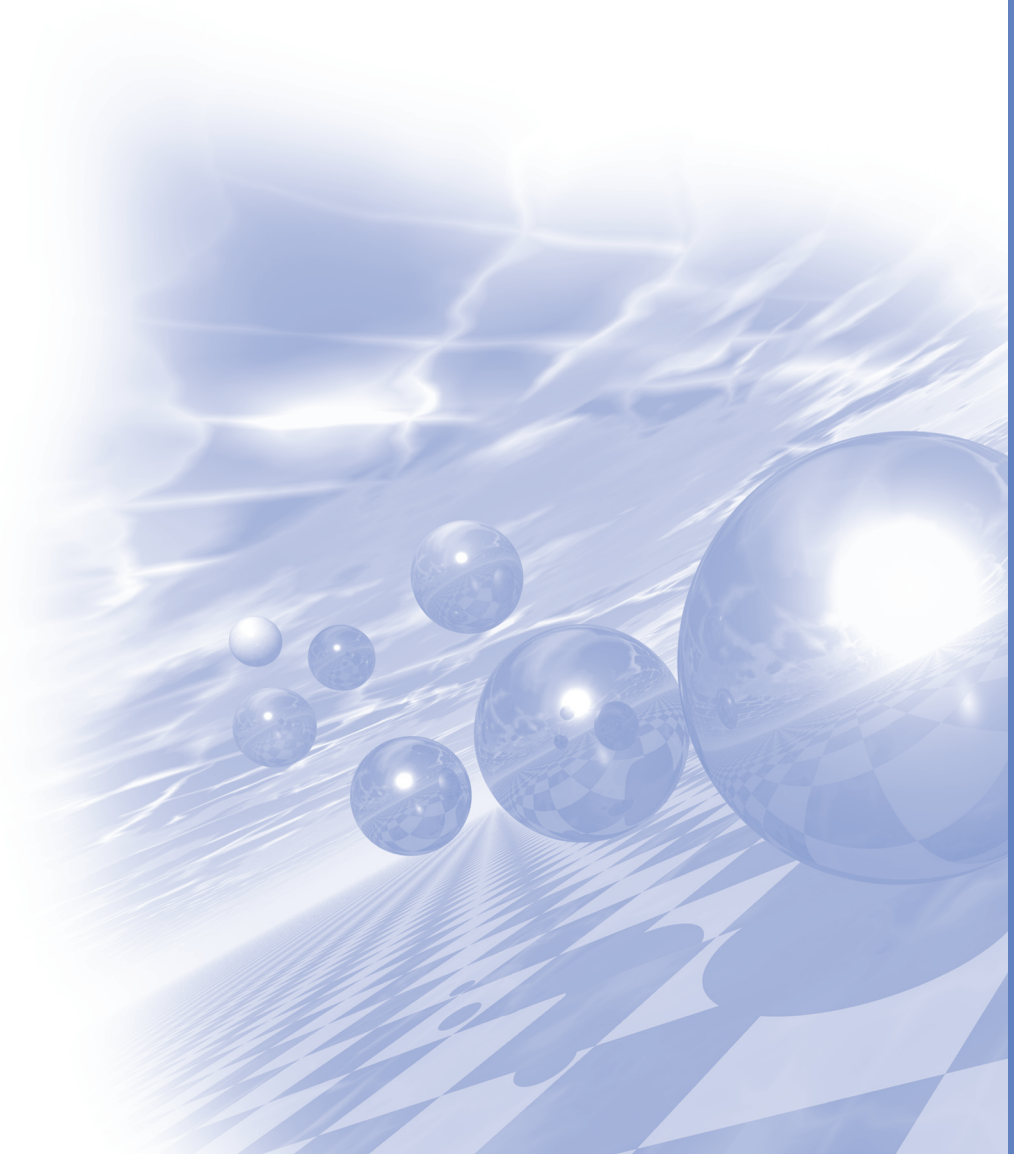

Influence of Ship's Magnetic Field on Mine-War

Sungyong Lee*
Navy Ordnance Ammunition Center, Korea

Two-stage Flash-KD protocol for mock-up submarines without degaussing coils

Ki-Woong Bae*, Hyun-Ju Chung, Chang-Seob Yang, Jun-Gi Hong, Woo-Jin Jeong
Sixth R&D institute, Agency for Defense Development

Conventional deperming protocols such as Biased Deperm-R suffer from poor magnetic stability. On the other hand, stable protocols such as Flash-D are rather complex and require long treatment time. In this proceeding, a modified Flash-D protocol was proposed. The proposed protocol omitted the second stage of Flash-D protocol, as a result, the treatment procedure was simplified in great deal while its magnetic stability was maintained.

1. Introduction

Ships need to be built with steel alloys to guarantee successful operation in harsh conditions. Steel alloys possess high permeability. Hence, ships built with steel alloys generate very strong magnetic fields, and can be easily detected by magnetic sensors. To protect ships from such threats and guarantee its operational robustness simultaneously, the importance of magnetic stealth technique cannot be underestimated. Among many magnetic stealth techniques, deperming protocols are crucial. [1]

A permanent vertical magnetization (PVM) is created in the Flash-D deperming protocol in order to cancel induced vertical magnetization (IVM). [2] The PVM is created by enforcing strong vertical magnetic field as bias. As a result, stable vertical magnetization can be created but the Flash-D protocol is rather complex and requires long time. In this paper, the Flash-D protocol was modified and a simpler, faster Flash-KD protocol was proposed.

2. Proposal of Flash-KD deperming protocol

In general terms, deperming protocols remove magnetization of ships by magnetically saturating ships with few strong horizontal current shots, then reducing the strength of consecutive shots, where each shot has opposing polarity. PVM can be generated by enforcing horizontal current shots in the presence of vertical magnetic bias. [3]

The Flash-D deperming protocol consists of 3 stages. In the first stage, decreasing horizontal current shots are enforced in the presence of strong vertical magnetic field as bias. Here, a strong bias is intentionally enforced to generate a strong PVM. In the second stage, the vertical bias is absent, and horizontal current shots are enforced with increasing strength. These increasing shots introduce magnetic shaking, which invokes creeping of weak vertical magnetization. In the third stage, current shots with decreasing strength are enforced in the absence of vertical bias, and this invokes the creeping of weak PVM again.

In the present work, the second stage of Flash-D was omitted to simplify the treatment procedure. This omission becomes possible based on the following assumptions:

1. The second and third stages of Flash-D protocol are intended to invoke creeping of PVM.

2. The second stage of Flash-D is required only for the strength of horizontal current shots can be decreased in the third stage.

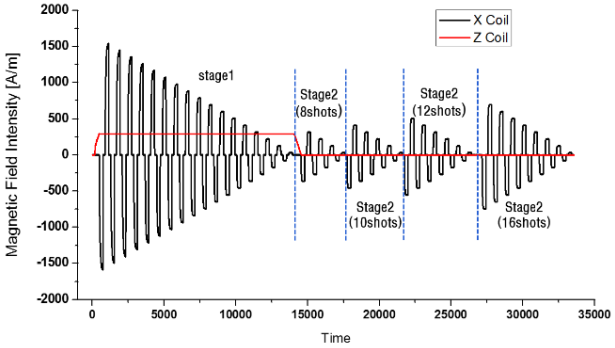

Fig. 1. Proposed 2-stage deperming protocol (Flash-KD)

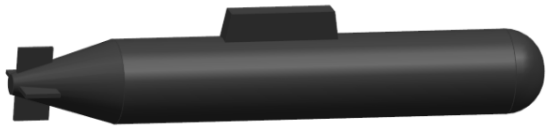

Fig. 2. Submarine model used in the experiment

With the omission, the magnetic treatment procedure can be simplified with minimal compromise in magnetic deperming performance. The proposed protocol is illustrated in Fig. 1. The number and strength of shots are increased (8 shots, 10 shots, etc.) in the second stage. This increases the amount of PVM creeping, and the optimal amount of PVM (=-IVM) can be found. Once the optimal PVM is found, the treatment time can be saved by applying the current shot that makes the optimal PVM.

3. Experiment results

The proposed Flash-KD protocol is simpler than the Flash-D protocol. The Flash-KD protocol is more stable and is capable of controlling PVM to be –IVM compared to Biased Deperm-R. In this paper, the proposed Flash-KD protocol was compared to the conventional Biased Deperm-R protocol to verify the validity of proposed Flash-KD protocol.

A miniature submarine was manufactured with SPCC material with the size of 1.75m in length and 0.265m in radius as shown in Fig. 2. A 3-axis magnetometer from Bartington inst. (Mag-03) whose resolution is less than 1 nT was used to compare the magnetic fields of two protocols. The sensor was located 0.27m above of the miniature submarine while the submarine was moved in south-north direction.

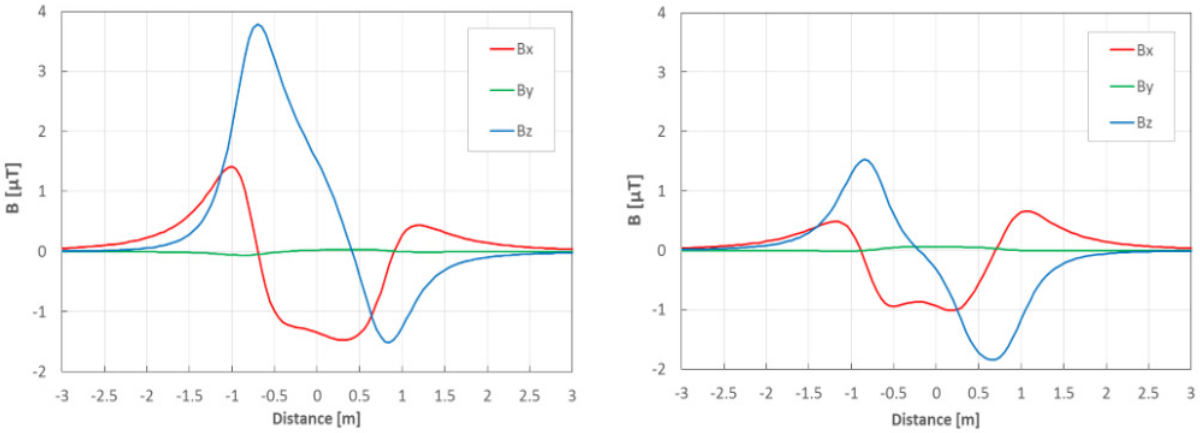

(a) (b)

Fig. 3. Induced magnetic fields of miniature submarine after applying (a) Biased Deperm-R protocol, (b) Flash-KD protocol.

The experiment was conducted at the non-magnetic laboratory in ADD. The non-magnetic lab is equipped with earth magnetic field compensation coils, deperming coils, and current amplifiers, so that it could facilitate subtle magnetic field measurement and deperming experiments. The lab was built with non-magnetic materials and the miniature was moved by a cart which was towed remotely in order to eliminate the effect of magnetic fields generating from driving motor.

Figs. 3(a) and (b) show the induced magnetic fields which were produced after applying Biased Deperm-R and Flash-KD protocols, respectively. With the Biased Deperm-R protocol, the PVM and IVM failed to cancel each other, therefore, the graph shows high peak value of 3.74μT as shown in Fig. 3(a). On the other hand, with the Flash-KD protocol, the PVM = -IVM, therefore, the peak value was reduced to 1.84μT and symmetric as shown Fig. 3(b). The peak value was reduced to about 49%.

The IVM was stronger than PVM after 8 or 10 current shots were enforced during the second stage of Flash-KD protocol. The PVM was stronger than IVM after 14 or more current shots were enforced. In above cases, PVM ≠ -IVM, however, when 12 current shots were enforced, PVM = -IVM as shown in Fig. 3(b).

4. Conclusion

In this paper, the second stage in Flash-D protocol was omitted, as a result, a simple and fast Flash-KD protocol was proposed. Experiments results demonstrated that the proposed Flash-KD method reduced peak magnetic field to half compared to conventional method. The proposed method is applicable to foster the treatment procedure of ROK Navy.

5. References

[1] J. Holmes, Reduction of a Ship's Magnetic Field Signatures, Morgan & Claypool, 2008.

[2] Official Website of the UNITED STATES NAVY <http://www.navy.mil>.

[3] J.-W. Kim, Deperming Method to Improve the Performance of Magnetic Stealth in Vessel, Ph. D. Soongsil Univ. Dec. 2016.

Magnetic and Acoustic Virtual Target for OOO-class Submarine

Minho Kim*, Sanggi Yoon, Sanghyuk Lee
LIG Nex1 Maritime R&D Lab, Korea

The OOO-class submarine was retired and it could not be used in the operation test and evaluation. The OOO-class submarine had been used as real-target for Harbor Underwater Surveillance System. The magnetic field of real-target is changed by demagnetization and it cannot be tested under the same conditions. The same target can also change the magnetic field according to time and earth coordinates. For these reasons, we became aware of the need for an underwater virtual target to simulate the magnetic/acoustic signal. The virtual target should be robust to changes in temperature, pressure and so on. And also the target must accurately generate the required values. The magnetic field generator consists of a magnetic core and a coil winding. A magnetic core is an oriented silicon steel strip. The acoustic transducers are placed in a towfish and generate the acoustic signal. The magnetic/acoustic generator is towed by a ship.

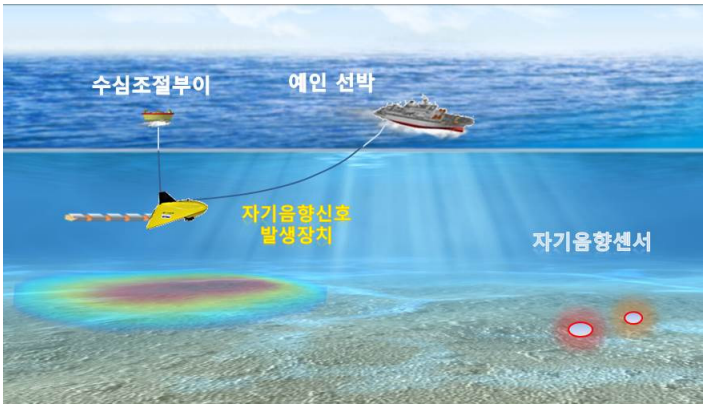

Fig. 1. Conceptual Diagram of Magnetic and Acoustic Virtual Target

The Effect of Demagnetization depending on the thickness of the Vessel

Sang Hyeon Im[1*], Hyun Ju Chung[2], Gwan Soo Park[1]
[1]School of Electrical and Computer Engineering, Pusan National University, Korea
[2]The 6th Research and Development Institute-3, Agency for Defense Development, Korea

The magnetic material has magnetic properties such as coercivity and permeability. A technique for removing the magnetic characteristics of a magnetic material is called a demagnetization. These demagnetizations are used in various fields, especially in the field of national defense research. Due to the development of technologies for detecting underwater magnetic fields generated in a ship, the importance of desorption studies to avoid them has been emphasized, and desorption studies have been carried out through various forms.

In order to carry out the demagnetization study, it is difficult to consider both the complex structure of the actual vessel and the various magnetic materials, so a simple model such as a hollo cylindrical specimen is used. A solenoid-type coil is created and a specimen is placed inside to apply an alternating and decreasing magnetic field from the outside. By reducing the residual magnetization in the specimen by the external magnetic field, the demagnetization is completed.

However, in the demagnetization study using the specimen, the magnitude of the magnetic field applied to the specimen becomes important because the size of the demagnetizing field varies depending on the length and thickness of the specimen. In the case of a real vessel, the demagnetizing field can be ignored because the thickness is very small compared to the length, but the specimen has a large ratio of length to thickness. Therefore, it is necessary to study the influence of the demagnetizing field depending on the thickness of the specimen.

In this study, by applying the same deperming protocol for all three types of specimens that have SS400 of magnetic materials and length of 300 mm but the thickness is 4.5 mm, 1.0 mm and 0.5mm, experiments were carried out and the results of demagnetization according to thickness were analyzed. As the experimental method, the specimen is placed inside the solenoid type coil and the same magnetic field was applied. After the deperming protocol was completed, the demagnetization results were compared by measuring the magnitude of magnetic flux density of the specimen through the sensor 18cm below the vertical direction.

According to the experiments performed, different experimental results were obtained even though the same deperming protocol were applied. This is because the demagnetizing field of each specimens are different. Since the magnetic material and length of the specimen are the same, but the thickness is different, each demagnetizing field is different. Depending on the thickness of the specimens, the demagnetizing factors are 0.0101, 0.0024 and 0.0012, respectively. That is, in order to actually apply a magnetic field of a desired magnitude of magnetic field, 11.1 times, 3.4 times and 2.2 times larger magnetic field is required to be applied to each of the specimens.

Therefore, a demagnetization study considering the demagnetizing field should be performed for the magnetic field actually applied inside the specimen.

Table 1. Demagnetizing Factor according to thickness of the specimens.

	4.5 mm	1.0 mm	0.5 mm
Demagnetizing factor	0.010087	0.002374	0.001155

A Study on the Signal Processing Techniques for Receiving Sensitivity Improvement of Active Proximity Magnetic Sensor

Dae-Jung Kim[1*], Chang-Seob Yang[2], Hyun-Ju Chung[2]
[1]LIGNex1, Korea
[2]Agency for Defense Development, Korea

In the underwater guided weapon field, which uses active magnetic sensor as proximity fuse, it is necessary to improve receive sensitivity to improve target detection performance. Also, the time delay for analyzing the received signal to identify the target must be minimized. Thus, in this paper, we apply the moving average technique to improve the receive sensitivity while minimizing the time delay in processing the received signal, demonstrate its effectiveness through simulation.

Orthogonal Fluxgate Sensor for Underwater Application

Kwang-Ho Shin[1*], Sang-Ho Lim[2], Chang-Seob Yang[1]
[1]Kyungsung University, Korea
[2]Korea University, Korea
[3]The 6th R&D Institute, Agency for Defense Development, Korea

Although the orthogonal fluxgate (OFG) mechanism was discovered long time ago, it is relatively recent that it has received great attention as a high-sensitivity magnetic sensor. The OFG sensor has big advantage in its simple structure as well as high sensitivity; its sensitivity is almost the same level with an ordinary fluxgate sensor (parallel type), and it has only one coil to pick-up output signal while the parallel type fluxgate must have two coils for excitation and signal pick-up. These aspects make the OFG very useful for underwater defense application. Fig. 1 shows the photograph and the measured noise figure (~ 12 Hz) of the fabricated OFG sensor. As shown in Fig. 1(b), the magnetic signal noise is below 5 pT in the frequency of 1 ~ 12 Hz, although the 3 dimensional sensor element has quite smaller (10◈10◈10 mm) than ordinary fluxgate sensor. It is well known that the output signal and/or sensitivity of fluxgate sensor are proportional to the magnetic core size and the number of winding coil for signal pick-up. However, the fabricated OFG sensor has very high sensitivity, even if it has small size and simple electronics. We have been successful to enhance the sensitivity with optimization of the operation frequency and the mechanism of that makes the magnetic domain wall disappear.

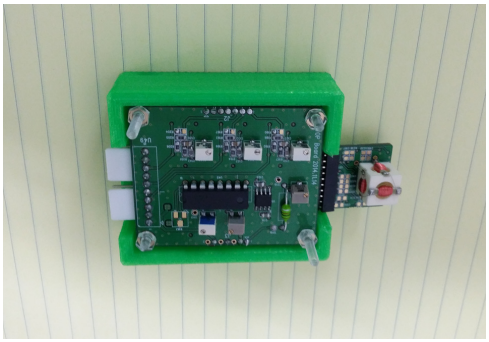

(a)

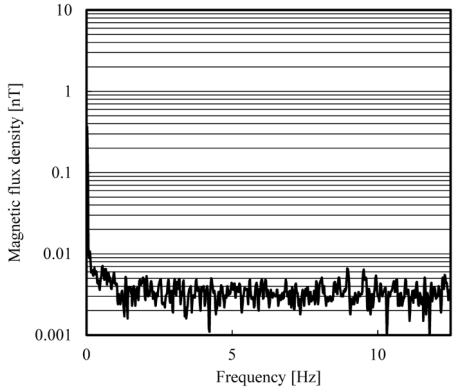

(b)

Fig. 1. Photograph of the fabricated orthogonal fluxgate sensor(a) and noise figure of the sensor ~ 12Hz.

A Study on 3-axis Flux-gate Magnetometer for Harbor Surveillance System

Eunhae Kim[1] and Derac Son[2*]
[1]Sensorpia Co., Korea
[2]Hannam university, Korea

To surveil unidentified objects which are moving in harbor, passive and active sonar, and magnetic field detection technologies have been used. Magnetic field detection technology becomes more important due to higher detection probability. Measurement of earth magnetic components i.e. south-north, east-went, and vertical and their change due to the object are ideal. But we cannot know attitude of the magnetometer which are laid under see. Due to this problems, total of magnetic field measurement have been used to observe magnetic objects. In this case orthogonal between 3-axis are very important.

In this work we developed 3-axis flux-gate magnetometer which has higher orthogonality using special algorithm.

To improve detection ability, elimination of earth magnetic field between magnetometers is important and we designed and constructed magnetometer have precise scale factor and very low output drift.

International Symposium on Magnetism and
Magnetic Materials 2017

Special Session III

'Women in radio-activation analyses, and magnetism'

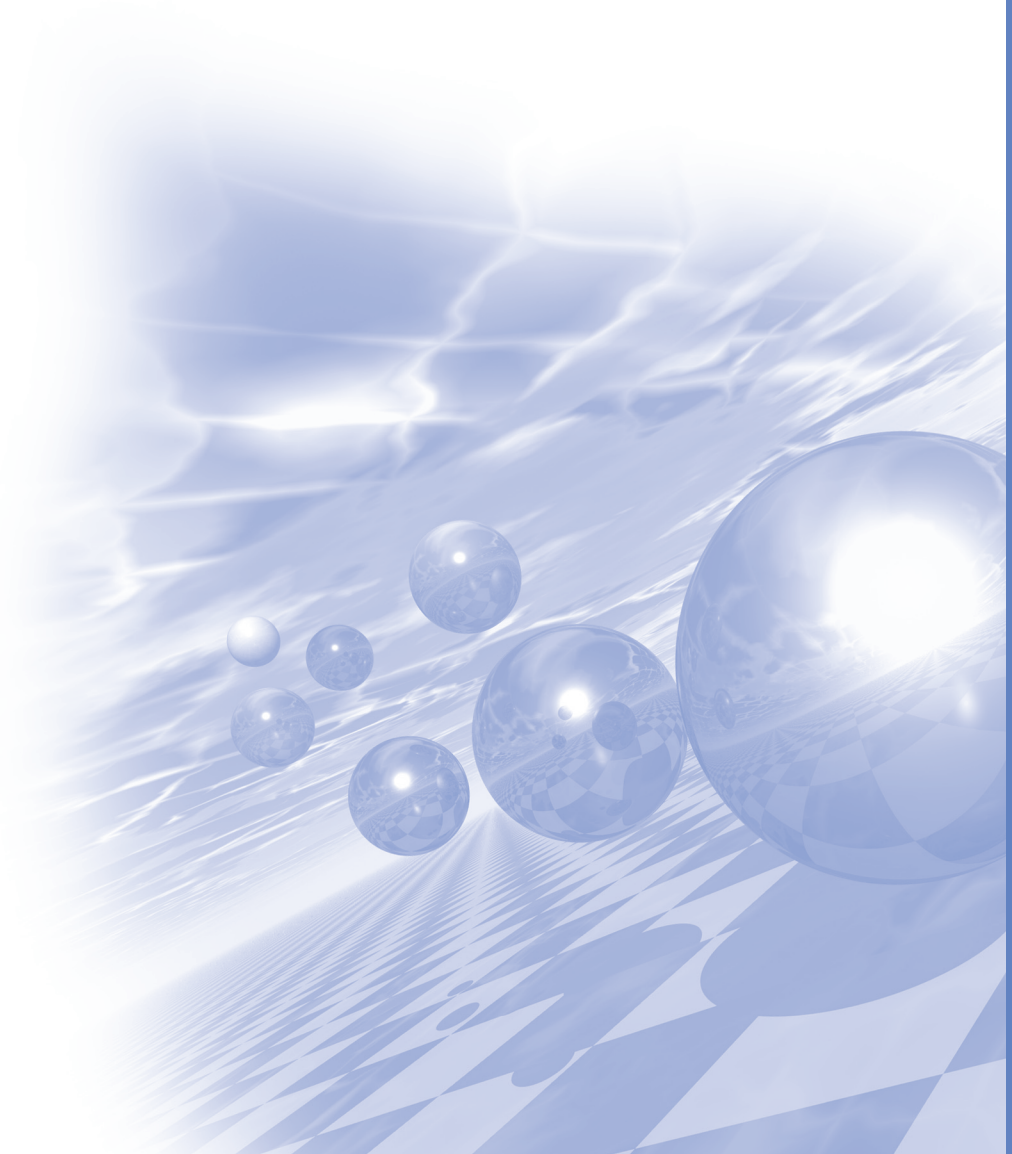

Preparation of ^{57}Co sources for Mössbauer Spectroscopy

Małgorzata Żółtowska*, Izabela Cieszykowska, Tomasz Janiak,
Tadeusz Barcikowski, Mieczysław Mielcarski
National Centre for Nuclear Research Radioisotope Center POLATOM, Poland

Cobalt-57 sources applied in Mössbauer Spectroscopy, utilizing the effect of recoilless gamma emission, are used in investigations of many processes proceeding in crystal lattice of solids. The method of preparation of ^{57}Co sources was developed in RC POLATOM.

The preparation of Mössbauer sources comprised electrodeposition of carrier-free ^{57}Co on rhodium foil [1] followed by thermal diffusion of ^{57}Co into rhodium matrix [2]. A series of experiments were performed in order to determine the optimal conditions for electrodeposition of cobalt on rhodium foils 6um thick.

Electrochemical cell consisting of platinum anode and rhodium disc as the cathode was chosen. The electrolyte was an aqueous solution of ammonia citrate 25g/l, hydrazine hydrate 25/l and carrier-free ^{57}Co in the form of ^{57}Co(II) in 0,1M HCl.

The diffusion of ^{57}Co into rhodium lattice was carried out by annealing the foil at temperature of 1100˚C at high vacuum, in quartz tube. The ^{57}Co active cores were encapsulated in cylindral Ti capsules with Be windows. The Mössbauer spectra were measured to verify the quality and efficiency of the testing sources.

The experiments performed allow making an optimum choice of the electrodeposition parameters of carrier-free ^{57}Co on rhodium foil. The highest efficiency approaching 100% and the best rate of deposition were obtained using current density 50mA/cm^2 and electrolyte volume – 5ml. The best results of diffusion of electrodeposition cobalt-57 onto rhodium matrix was obtained in an annealing process at 1100˚C in vacuum over 10^{-6} hPa.

The main spectra parameters of the prepared sources are fairly acceptable with respect to the typical obtainable values for α-Fe absorbers in Mössbauer spectroscopy. The results obtained confirm that the deposited layer diffused almost completely into rhodium matrix without substantial loss of the activity deposited.

References

[1] I.Cieszykowska, M.Żółtowska, M.Mielcarski (2011) Electrodeposition of carrier-free ^{57}Co on rhodium as an approach to the preparation of Mössbauer sources. Applied Radiation and Isotopes 69, 142-145

[2] I.Cieszykowska, M.Żółtowska, P.Zachariasz, A.Piasecki, T.Janiak, M.Mielcarski (2011) Thermal diffusion of ^{57}Co into rhodium matrix as a second step in preparing Mössbauer Sources. Applied Radiation and Isotopes 69, 1193-1197

Beta-voltaic battery and beta source using radioisotope Nickel

Young Rang Uhm[1*], Byung Gun Choi[2], Kwang Jae Son[1], Sang Mu Choi[1] and Jin Joo Kim[1]

[1]Affiliation A, Korea1Radioisotope Research Division, Korea Atomic Energy Research Institute (KAERI), Daejeon, 34057 Korea

[2]Human Interface SoC Research Section, Electronics and Telecommunications Research Institute (ETRI)

A betavoltaic battery that converts the decay beta energy of radioisotope into electricity offers advantages for application requiring a long lifetime without recharging and minimum maintenance. And, it is used in many low-power applications since it can operate effectively in extreme environmental condition such as space and deep sea. Ni-63, a pure beta-emitting source, is proper to the power source of a radioisotope battery because of its low energy spectrum (E_{evg}=17.4 KeV) and long half-life of 100.1 years. In this study, we fabricate a beta-voltaic micro battery and design radioisotope-based hybrid battery using Ni-63 as energy source. To establish preparation of betavoltaic source, natural Ni was electroplated on the Ni plate. The procedure of Ni deposited onto Ni foil was established using two different electroplating baths: the acid-based buffer (pH4) containing boric acid, sodium chloride, and saccharin, and the alkaline-based buffer (pH10) containing hydrazine hydrate and ammonium citrate. The deposition yield of the alkaline electrolyte is relatively higher than those of the acidic bath. Also, finer grain size was obtained at a citrate bath. A betavoltaic battery was prepared using a radioactive Ni-63 attached to a 3D single trenched P-N absorber. The optimum thickness of a Ni-63 layer was determined to be about 2 μm, when regarding the minimum self-shielding effect of beta (β) particles. In the case of combining secondary cells, the electricity generated from beta-voltaic battery is stored in secondary cell.

Development of Turn-off Switching of NPT-IGBT under Fast Neutron Irradiation

Hani Baek[1,2*], Gwang Min Sun[1], Chansun Shin[2], Gihyun Kwon[2]
[1]Neutron Utilization division, Korea Atomic Energy Research Institute, Korea
[2]Mataerials Science and Engineering Dept. Myongji University, Korea

The insulated-gate bipolar transistor (IGBT) is a unique device that combines the low forward voltage drop of a bipolar junction transistor (BJT) and the high input impedance and fast switching of a metal oxide semiconductor field effect transistor (MOSFET). But, turn-off delay time of the IGBT is increased by the tail-current due to stored minority carrier in n-drift region when the device is turned off. Also there is a disadvantage that the reverse current becomes large and power loss increased. These power losses which is the biggest factor that reduces the energy efficiency of the IGBT. To improve this, recently research has been conducted to improve the switching speed by controlling the lifetime of minority carriers of IGBT. A lattice defect is intentionally formed in n-drift region of the IGBT so as to act on a deep energy level in the energy band. These deep energy levels acts as minority carrier recombination centers and control the lifetime of the minority carrier in the IGBT to minimize the turn-off delay time.

In this study, the 600V NPT-IGBTs were irradiated by fast neutrons from the MC-50 cyclotron at the Korea Institute of Radiological & Medical Science. Fast neutron irradiation with various doses of energy have been carried out into IGBTs as a wafer state. The electrical properties, such as threshold voltage (V_{TH}), on-state forward voltage drop (V_{CE}), breakdown voltage (BV), leakage current (I_L) and turn-off delay time were analyzed and compared with non-irradiated.

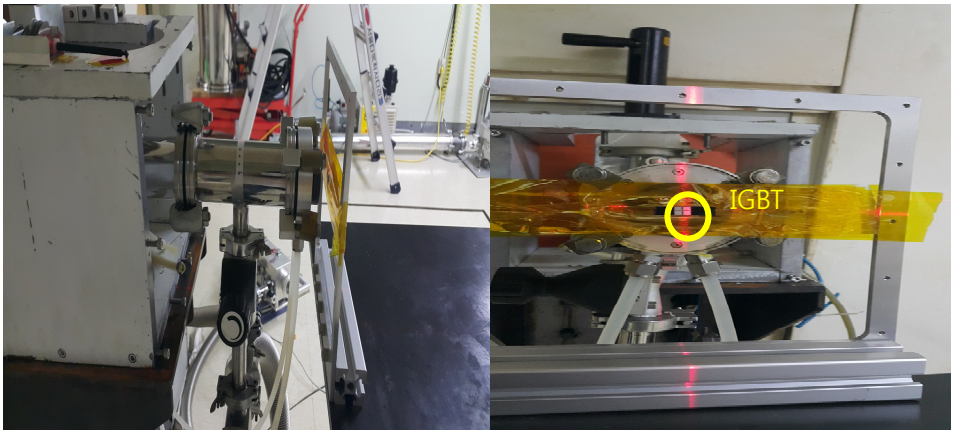

Fig. 1. 600V NPT-IGBT were irradiated by fast neutrons

Application of Activation Analysis to geological materials

Mi-Eun Jin[1,2*], Yong-Joo Jwa[1], Gwang Min Sun[2], Seonbok Yi[3],
Zsolt Kasztovszky[4] and Ildikó Harsányi[4]

[1]Department of Geological Sciences, Gyeongsang National University, Korea
[2]Neutron Utilization Research Division, Korea Atomic Energy Research Institute, Korea
[3]Department of Archaeology, Seoul National University, Korea
[4]Centre for Energy Research, Hungarian Academy of Sciences, Hungary

Recently, as the use of analytical instruments increases, reference materials play a very important role in obtaining more precise and accurate data. In particular, geostandards (Geological reference materials) are essential for analytical research and has been widely used for a chemical analysis to obtain accurate geochemical data. Besides, it is useful to evaluate the accuracy of the analysis and to develop and improve analytical techniques. There is a trend that demands for calibration increases as various analytical instruments and techniques are newly invented and applied. The geostandards which are the targets of a geological survey such as rocks, ore, minerals, soils, and sediments contain various elements in high concentration. Currently, there is no follow-up work about the study on Korean geostandards since 1990's. Also, it is difficult to obtain reference materials provided by foreign standard materials research institutes (e.g. NIST, USGS by Unite State and GSJ by Japan). Therefore, it is necessary to develop Korean geostandards that can represent Korean rocks.

We selected some representation granite samples and conducted petrological studies to produce Korean geostandards. Samples were taken from the Jurassic (KJG-2) granites. The samples were prepared by standard pulverization process and analyzed by XRF and PGAA. XRF is currently one of the most widely used analytical techniques in the determination of the major elements and REE in the rock samples. Large numbers of precise analyses can be made in a relatively short time. The PGAA(Prompt Gamma-ray Activation Analysis) method is one of the nuclear analysis techniques, which measures the immediate gamma ray emitted during the irradiation of the target nuclide with neutrons. We performed to determine the concentration of major and minor elements of the KJG-2. Moreover, we checked the homogeneity of the samples, which is defined by the concentration of elements of interest and their average values, absolute and relative standard deviations and so on. XRF was performed using an instrument (BRUKER S8 TIGER) at the Center for Research Facilities of Gyeongsang National University, and PGAA was carried out at Centre for Energy Research, Hungarian Academy of Sciences, Hungary.

Co-electrodeposition of U-Mo in LiCl-KCl Melt

Na-Ri Lee[1*], Gwang-Min Sun[1], Sang-Eun Bae[2], Tae-Hong Park[2]
[1]Neutron Utilization Research Division, Korea Atomic Energy Research Institute, Korea
[2]Nuclear Chemistry Research Division, Korea Atomic Energy Research Institute, Korea

U-Mo nuclear fuel that is possible a manufacture by the recycling of spent nuclear fuel and contains high uranium densities has received attention as a nuclear fuel for next generation research reactors. Since high temperature molten salt has wide electrochemical potential windows, it is able to reduce and deposit of all metals. U-Mo nuclear fuel can be manufactured more easily by using the characteristics of high temperature molten salt in the production of U-Mo nuclear fuel. In this work, U-Mo co-electrodeposition was investigated in a high temperature LiCl-KCl molten salt using transient electrochemical technique (CV, cyclic voltammetry), scanning electron microscopy (SEM), energy dispersive spectroscopy (EDS), and X-ray diffraction (XRD). Prior to performing U-Mo co-electrodeposition, the electrochemical behavior of Mo and U in LiCl-KCl molten salt was investigated. The electrodeposition of Mo occurred in LiCl-KCl melt at more negative potential than -0.3 V *vs.* $Ag|Ag^{+}$ and the amount of electrodeposited Mo was increase of the overpotential. Due to deposition potential of U more negative than Mo, co-electrodeposition of U-Mo was appeared 3-D dendritic structure. However, a flat U-Mo thin film was deposited using a diffusion-controlled electrodeposition.

Oral Session II

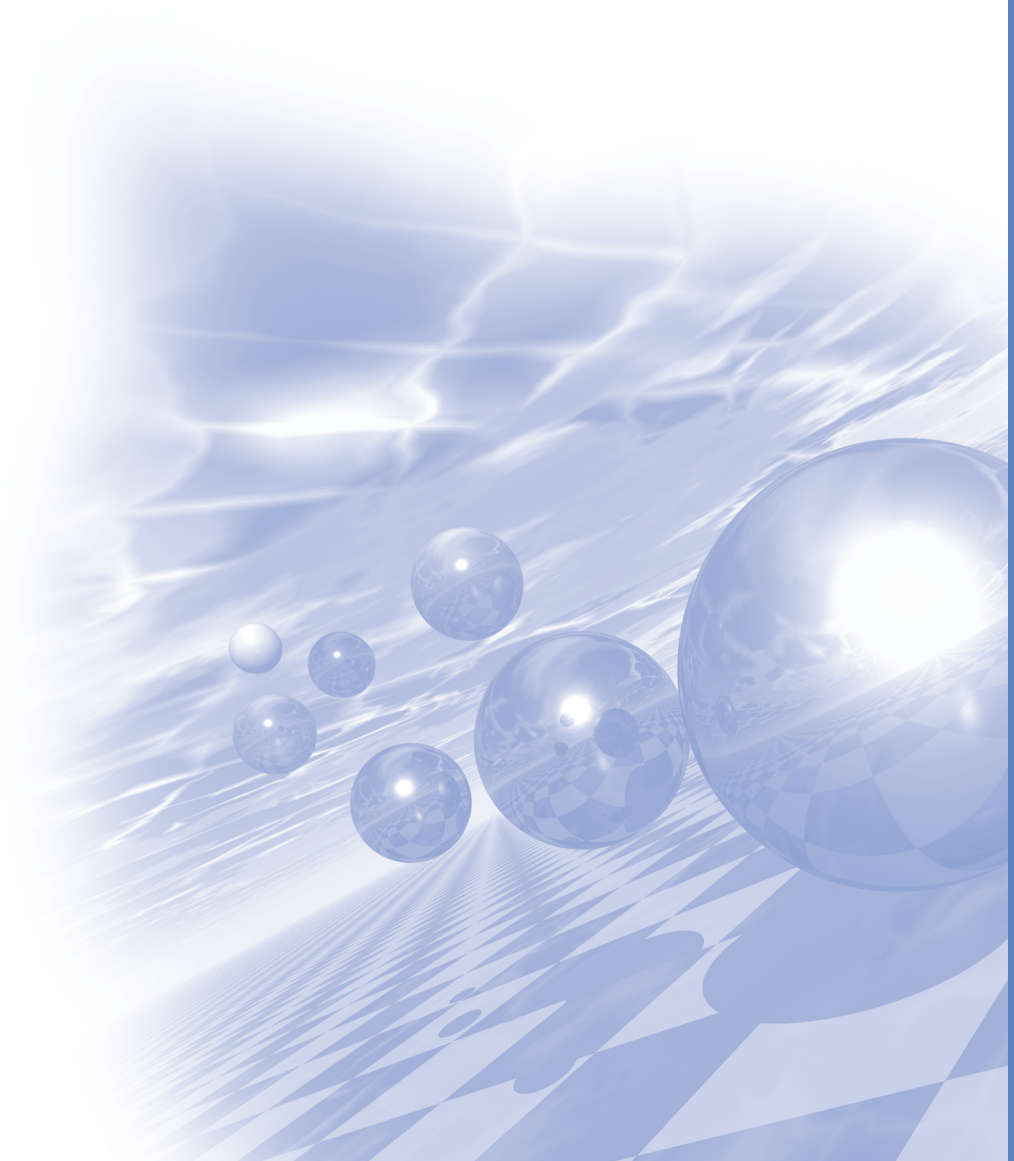

Spin Circuit Model for Materials with Spin-Momentum Locking

Seokmin Hong*
Center for Spintronics, Korea Institute of Science and Technology (KIST), Korea

The spin circuit model in spintronics has provided compact and modular approach in understanding and analyzing various phenomena in materials including normal metals, ferromagnets ant their interfaces. Recently materials with high spin orbit coupling are shown to provide an alternative way to create spin current that is often large enough to switch magnets with interesting applications.

In this talk, I review recent progress of spin circuit representation in materials with spin-momentum locking that is applicable to topological insulators, Rashba channels, and surface of heavy metals (Pt, Ta, and W), which is extending the previous spin circuit model with new predictions.

Non-adiabatic spin-transfer torque for ferromagnetic domain wall

Hyeon-Jong Park[1*], Jung Hyun Oh[2], Kyung-Jin Lee[1,2]
[1]KU-KIST Graduate School of Converging Science and Technology, Korea University, Seoul 02841, Korea
[2]Department of Materials Science and Engineering, Korea University, Seoul 02841, Korea

One of the most important issues for devices using domain wall motion is reducing threshold current density to move domain wall because of adiabatic spin-transfer torque. One of solutions is non-adiabatic spin-transfer torque. It acts like magnetic field to domain wall and ideally can move domain wall with no threshold. We analysis sources of non-adiabatic spin transfer torque which originate from spin relaxation [1], intrinsic spin-orbit coupling [2], spin mistracking [3]. Both spin relaxation and intrinsic spin-orbit coupling are independent of magnetization configurations, i.e., domain wall in this work, but spin mistracking is enhanced in rapid change in magnetization configurations. Moreover, intrinsic spin-orbit coupling is independent of spin-dependent scattering but spin relaxation is enhanced in large spin-dependent scattering. In these manners, we can separate magnitudes of each origin of non-adiabatic spin-transfer torque. We will numerically study these origins based on linear response theory code and evaluate an effective non-adiabaticity (, which represents a ratio between adiabatic and non-adiabatic spin-transfer torque, for quantitative analysis.

References

[1] S. Zhang et al., Phys. Rev. Lett. **93**, 127204 (2004).
[2] K.-W. Kim et al., Phys. Rev. B **92**, 224426 (2015).
[3] J. Xiao et al., Phys. Rev. B **73**, 054428 (2006).

Complementary spin transistors using exchange-biased ferromagnetic electrodes

Youn Ho Park[1*], Jun Woo Choi[1], Joonyeon Chang[1], and Hyun Cheol Koo[1,2†]

[1]Center for Spintronics, Korea Institute of Science and Technology (KIST), Seoul 02792, Republic of Korea
[2]KU-KIST Graduate School of Converging Science and Technology, Korea University,
Seoul 02481, Republic of Korea
[†]E-mail address: hckoo@kist.re.kr

The spin field effect transistor (spin-FET), proposed by Datta and Das, is one of the most popular concepts for next generation devices due to low power consumption, high speed, and nonvolatility. The main operation of spin-FET is that the control of spin-procession angle by a gate electrode in a semiconductor quantum well [1]. In this device, the spin-polarized current is injected from a ferromagnetic source and detected by the other ferromagnetic drain. While travelling spin polarized current from the injector to the detector in a semiconductor quantum well, the angle of spin-procession angle is decided by Rashba field which is controlled by a gate electrode. To be utilized for the logic gate, we should operate spin transistor without external magnetic field and parallel- and antiparallel types of spin-FET (P-ST and AP-ST) which can replaced conventional *n*- and *p*-MOS.

The Rashba field arises along the *y*-axis, so the magnetization direction of source and drain should be along the *x*- or *z*-axis, i.e. perpendicular to the Rashba field (B_{Ry}), to induce spin precession. In this experiment, we choose the ferromagnetic electrodes (FM) with magnetization along the *x*-axis. The lateral sizes of FMs are 0.5 μm × 15 μm and are 0.8 μm × 15 μm, respectively. Since the shape anisotropy would lead to a FM magnetization along the *y*-axis, we employ an exchange bias field along the *x*-axis using $Co_{84}Fe_{16}/Ir_{22}Mn_{78}$ bilayers. During the sputtering of $Co_{84}Fe_{16}$ and $Ir_{22}Mn_{78}$, we applied magnetic fields of +20 mT and −20 mT along the *x*-axis, respectively. Due to interfacial exchange interaction between the $Co_{84}Fe_{16}$ and $Ir_{22}Mn_{78}$, the first interfacial layer of $Ir_{22}Mn_{78}$ has the same magnetization direction as the $Co_{84}Fe_{16}$ layer. The antiferromagnetic order of $Ir_{22}Mn_{78}$ causes subsequent layers to have alternating magnetizations. The antiferromagnetic order is very stable, so that the ferromagnetic $Co_{84}Fe_{16}$ layer retains its magnetization direction even without a magnetic field. The ferromagnet/anti-ferromagnet bilayers have +35.5 mT and −36.3 mT of exchange bias. We also calculated the spin transistor operation using those parallel and antiparallel types spin-FET [2].

References

[1] H. C. Koo *et al.*, Science, 325, 1515 (2009).

[2] Y. H. Park *et al.*, Scientific Reports 7, 46671 (2017)

Interfacial effect of Pt/$Ir_{20}Mn_{80}$ thin films

Thi Kim Hang Pham*, Ja Ryun Lee, Tae Hee Kim†
Department of Physics, Ewha Womans University, Seoul 03760

$Ir_{20}Mn_{80}$ has attracted increasing interest as a promising candidate for spintronic applications since $Ir_{20}Mn_{80}$ owns their large spin-orbit coupling and the non-collinear spin textures [1]. However, how the interfacial effect Pt/$Ir_{20}Mn_{80}$ thin films controls its magnetoresistance (MR) and resistivity, has been far less explored. Hence, investigations of the $Ir_{20}Mn_{80}$ layer thickness dependence in the structure of Pt/$Ir_{20}Mn_{80}$ thin films are also demonstrated in this work.

Here, we report the interface microstructure of $Ir_{20}Mn_{80}$ thin films determined by Atomic Force Microscopy (AFM), and MR of 3 nm Pt/x nm $Ir_{20}Mn_{80}$ (x = 1.5, 3.0 and 5.0 nm) thin films. A Pt/$Ir_{20}Mn_{80}$ thin film was successively deposited at room temperature using Ultra High Vacuum-Molecular Beam Epitaxy (UHV-MBE). Our results show that $Ir_{20}Mn_{80}$ thin film with thickness of less than 3 nm formed with excellent layer structure toward Frank-van der Merwe growth, $Ir_{20}Mn_{80}$ thin film with 1.5 nm thickness formed with Volmer-Weber island growth due to remarkable surface roughness. Moreover, we obtain MRs and resistivities strongly depend on the interfacial properties of Pt/$Ir_{20}Mn_{80}$ thin films. Our results indicate that controlling the interface properties of Pt/$Ir_{20}Mn_{80}$ thin films has a promising prospect application in future spintronic devices.

Reference

[1] H. Chen, Q. Niu, and A. H. MacDonald, Phys. Rev. Lett. **112**, 017205 (2014).

Synthesis and Microwave Absorbing Property of Partially Zn-substituted Strontium Y-type hexaferrite

Jae-Hyoung You*, Sung Joon Choi, Sunwoo Lee, and Sang-Im Yoo†
Department of Materials Science and Engineering, Research Institute of Advanced Materials (RIAM),
Seoul National University, Seoul 151-744, Korea
†Sang-Im Yoo, e-mail: siyoo@snu.ac.kr

Strontium Y-type hexaferrite ($Sr_2Me_2Fe_{12}O_{22}$; Sr_2Me_2Y, where Me is a divalent transition metal ion), is a ferrimagnetic material possessing soft magnetic property with saturation magnetization (M_s) value around 30–40 emu/g. The Sr_2Me_2Y hexaferrites have been widely studied for microwave antenna application as they exhibit planar magneto-crystalline anisotropy in *c*-plane, and thus high permeability in the microwave range. Since Zn^{2+} is known to increase real and imaginary permittivity of Sr_2Me_2Y, we tried to synthesize and identify the magnetic property and microwave absorbing property of partially Zn^{2+}-substituted Sr_2Me_2Y hexaferrites ($Sr_2Zn_xFe_{2-x}Y$, where $0.0 \leq x \leq 2.0$)) which have not been reported yet. For this purpose, the samples with different x values were annealed at the temperature region of 1000–1350 ˚C for 2 h in the PO_2 of 10^{-3} atm. As a result, single-phase polycrystalline samples of $Sr_2Zn_xFe_{2-x}Y$ for x = 0.0–1.5 were obtained by annealing in the PO_2 of 10^{-3} atm, while Sr_2Zn_2Y was only obtainable by annealing in air. The magnetic hysteresis loop measurement revealed that M_s values of the samples increased with increasing x from 0.0 to 1.0 with maximum M_s value of 44.4 emu/g, and then decreased with further increased x value. The complex permittivity and permeability measurement results in the frequency range of 8–18 GHz and microwave absorbing property will be also presented for a discussion.

O-II-6

Core loss improvement in the SMC composed of Fe-Al_2O_3 core-shell structure

Sung Joon Choi*, Sunwoo Lee, Jae-Hyoung Yoo, and Sang-Im Yoo
Department of Materials Science and Engineering, and Research Institute of Advanced Materials,
Seoul National University, Seoul 151-744, Korea

The soft magnetic composites (SMC) have attracted great attention of many applications for electrical devices, transformers, and motors. It is quite well-known that considerably large high-frequency AC losses of magnetic metal powder can be effectively reduced by insulation coating due to a reduced macroscopic eddy current loss between metal particles. A thin coating of the insulator on the surface of magnetic metal particles is considered to be highly desirable for high performance SMC, but reports on this topic are very limited at the moment. In this study, we controlled the coating time to examine the magnetic properties and microstructures of soft magnetic composites (SMCs) with different coating thickness. To evaluate the core losses of samples, the toroidal cores were fabricated by mixing Al_2O_3-coated Fe powder with a resin. The microstructural analysis of Fe powder coated with Al_2O_3 was conducted using field emission-scanning electron microscope (FE-SEM) and transmission electron microscope (TEM). The magnetic properties were characterized by performing inductance analysis and B-H curve analyzer. In accordance with our expectation, reduction in core loss by insulation coating was larger in higher AC frequencies. Details will presented for a discussion.

This study was supported by a Grant from world class 300 (0417-20150129).

International Symposium on Magnetism and Magnetic Materials 2017

Plenary Session I

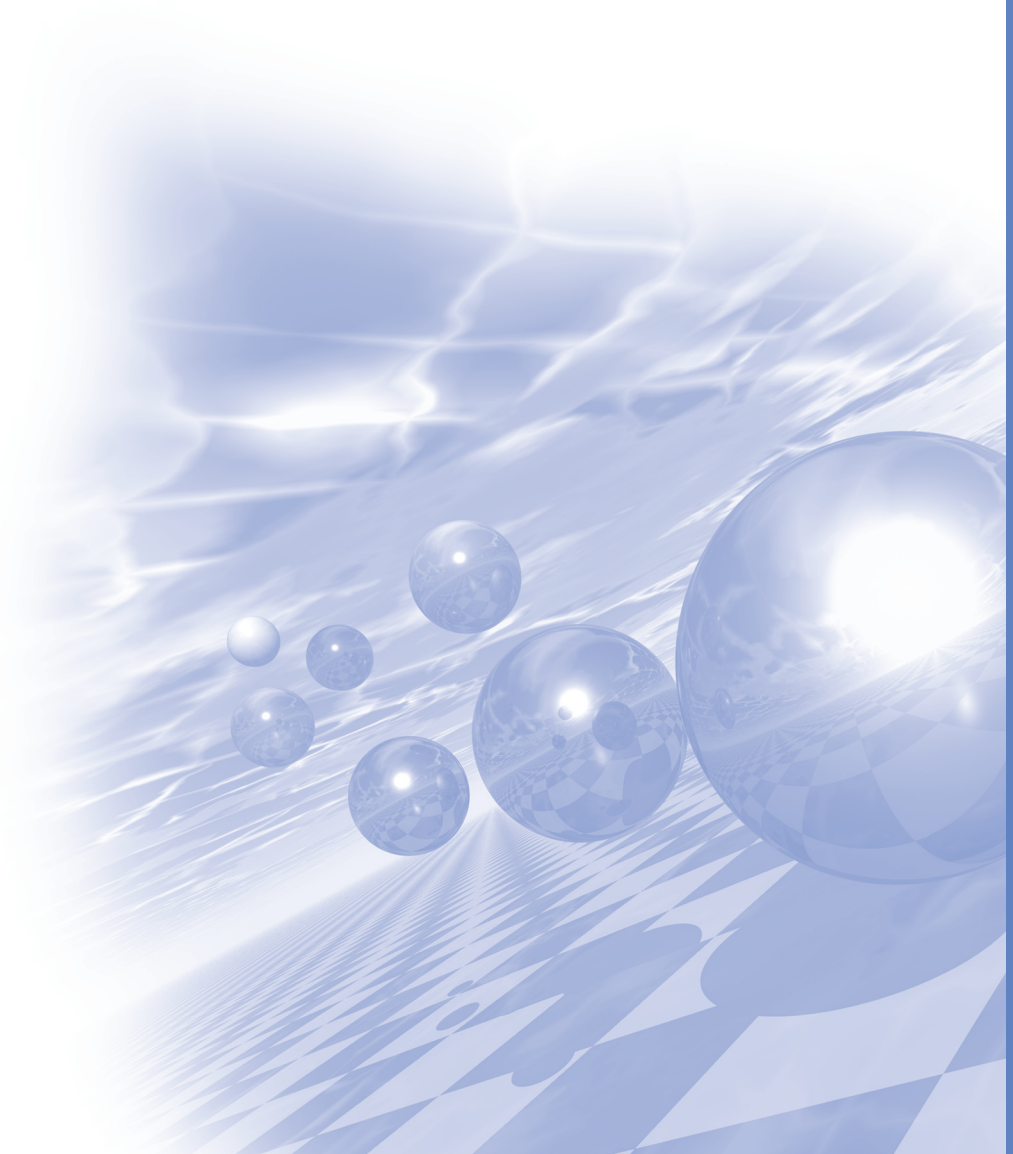

The 4th Industrial Revolution and Creativity

Hi-Jung Kim*
Korea Institute of Science and Technology

Many experts comment that creativity is the most important thing in the 4th industrial revolution era to apply and develop the fusion technologies integrating hardware-hardware as well as hardware-software technologies.

But it is very difficult to educate and improve creativity because it include many emotional or mental factors such as imagination and curiosity except physical one such as knowledge and infrastructure.

In this lecture I will introduce the past creative examples on some magnetics related inventions such as the telephone by A. Bell, the a.c. generator and motor by N. Tesla and the personal computer and iPod by S. Jobs. Finally I will discuss about five key factors on creativity such as expert knowledge, creative environment, boldness, internal motivation and imaginative power.

International Symposium on Magnetism and Magnetic Materials 2017

Poster Session

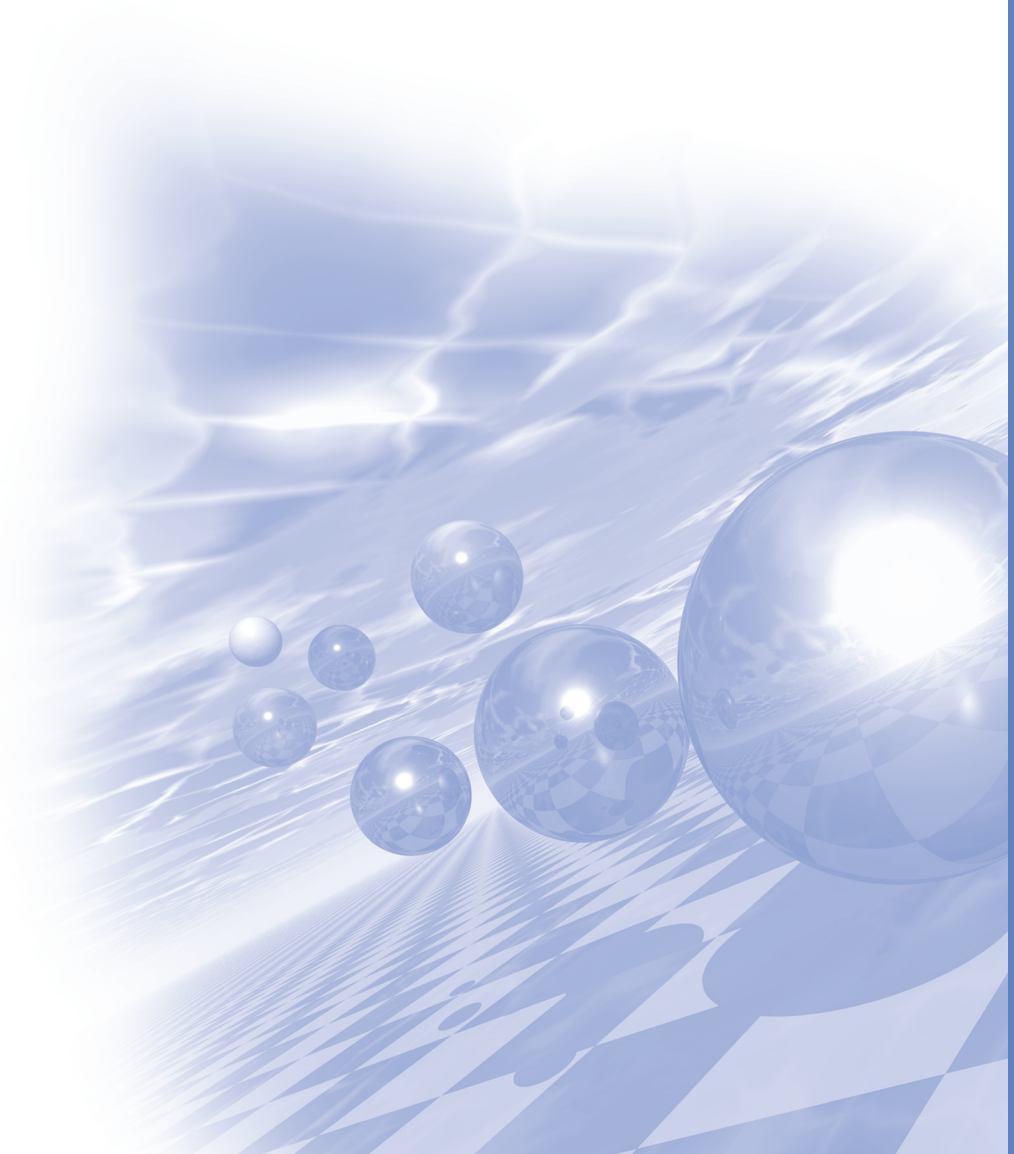

MR/CT Compatible Phantom for MR-only based Radiotherapy

Min-Joo Kim[1,2*], Sohyun Ahn[1], Seu-Ran Lee[2], Tae Suk Suh[2]
[1]Department of Radiation Oncology, Yonsei Cancer Center, Yonsei University College of Medicine, Yonsei University Health System
[2]Department of Biomedical Engineering, Research Institute of Biomedical Engineering, The Catholic University of Korea College of Medicine

1. Introduction

CT is conventionally used in radiation treatment planning since the high standard of geometrical accuracy offered by the images obtained with this technique. The ultimate goal of a CT image for radiation treatment is to establish a direct connection between Hounsfield units (HU) and information on the electron density of each tissue in order to enable the calculation of the dose. However, treatment planning using CT alone is incapable of delivering an accurate delineation of the target volume for some clinically relevant sites. Magnetic resonance (MR)-only based radiotherapy, where MR images are utilized for target delineation in radiation treatment, has been increasingly utilized because the images obtained with this technique offer superior contrast in comparison to CT images, when displaying soft tissues. However, multiple imaging modality is time consuming and involves extra costs. Image registration accuracy remains an issue to be solved to establish a fully MR-images based radiation treatment. We hypothesize that one single phantom, named hybrid MR/CT compatible phantom, used for acquisition of MR and conventional CT images could be applied for MR-only radiation treatment in terms of target delineation and radiation dose calculation. Since various tissue equivalent samples have been developed and inserted in the hybrid MR/CT compatible phantom, regions of interest from one single sample on a MR and CT image could represent tissue equivalent both for signal intensity (SI) on MR images and for HU on CT images. In addition, the relation between SI and HU from the same sample image section could be directly applied into the conversion process from HU to relative electron density in treatment planning system for dose calculation. Based on our strategy described above, the development process of a hybrid MR/CT compatible phantom was proposed and its characteristics were determined.

2. Materials and Methods

Several studies in MR related research have developed various kinds of production techniques for tissue equivalent materials for MR by utilizing various chemical components for their purpose, MR related research. One of the chemical components used in that reference research was carrageenan, which was blended from various kinds of seaweeds. The carrageenan was used as gelling agent to make rigid gel of sufficient strength to fabricate a torso with the added benefit of more elasticity. Moreover it is more resistant to cracking than agar gel, and it can be stored for an extended time. Agaros was used as T2 modifier. GdCl3 was used as T1 modifier. NaN3 was used as an antiseptic: it is highly soluble in water and very acutely toxic. The mixture of components used to mimic each organ has already been shown in previous studies of the reference group except for the amount of K2Co3 in each tissue equivalent material, since their previous study was focused on the development of tissue equivalent materials for MR imaging. To demonstrate the suitability of our mixing process, the uniformity of each

sample was calculated. For MR images, the percent image unit was calculated for all samples using the largest square-shaped region of interest on the sagittal plane. This value could be interpreted as the uniformity in the vertical direction for each sample. Furthermore, the average and standard deviation of a circular ROI for 7 slices of CT axial plane image was calculated for each sample as an evaluation of the uniformity of the horizontal direction of each sample. In our study, a sample with a standard deviation within 5% was classified as acceptable in terms of uniformity. The developed phantom was designed to equip 14 plugs (diameter: 37 mm; height: 66 mm for imaging section, airtight container) which contained various tissue equivalent materials for MR and CT imaging. Measurement, image acquisition using the developed phantom for MR imaging with 14 tissue equivalent samples, and all the tests on the samples mentioned above were done using 3.0 T scanner (Achieva Tx 3.0T, Philips Medical Systems, Netherlands) with 32 channel sensitivity encoding (SENSE) head coil and Somatom Sensation 64 (Siemens Medical Solutions, Forchheim, Germany).

3. Results and Discussion

We designed a hybrid MR/CT compatible phantom for radiation oncology and proposed it for MR-only based radiotherapy for the tasks of MR images generation, including image target delineation and radiation dose calculation without the need of any supplementary information from CT. To our knowledge, this study was firstly designed and proposed the concept of the development of the hybrid MR/CT compatible phantom.

Modulation of CT images by adding K2Co3 was successfully demonstrated in our study. The amount of K2Co3 to make tissue equivalent materials for CT image was determined as described. The development of tissue equivalent materials for MR images still requires further research as implied by the results of T1-T2 measurement, which failed to reach an agreement with the reference data. In these cases the SI from a MR image could not be compared to the HU value from the CT and a relationship in the same tissue equivalent material between the two values could not be successfully established.

4. Conclusion

This study highlights the importance of MR image phantoms in the field of radiation oncology. A hybrid MR/CT compatible phantom for MR and CT image acquisition was designed and the relation between MR and CT images for MR-only based radiotherapy, in terms of target delineation and radiation dose calculation, investigated. In addition, various tissue-equivalent materials for both MR and CT imaging, to be inserted into the developed phantom, were described.

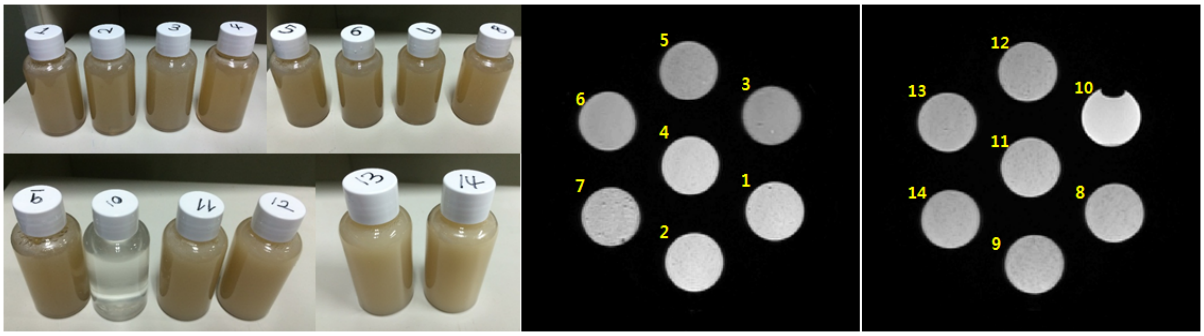

Fig. 1. 14 different developed tissue-equivalent materials (Left) and its MR image for each plug listed in Table 1 with TR 1500, TE 35. (Air plug listed in Table 1 was not shown in this figure. Number 14 plug was replaced with Air plug in final experiment.)

Study on the Mobility of Red Blood Cells by Pulsed Magnetic Field Stimulation

Jae Kwon Sim*, Hyun-Tak Shin, Do Gwun Hwang, Hyunsook Lee†
Department of Oriental Biomedical Engineering, Sangji University Wonju, South Korea
†Corresponding Author : Hyunsook Lee, hslee@sangji.ac.kr

Exposure to pulsed magnetic field (PMF) has been shown to have a therapeutic uses for a variety of medical conditions including angiosis, musculoskeletal disorders, soft-tissue regeneration, nerve, and neurological disorders. It is known that aggregation and displacement of stacked red blood cells (RBCs) have influence on the blood flow, and increase vascular resistance in the blood circulatory system. The present study has been investigated the dependence of the change in aggregation and mobility of RBCs on PMF stimulus duration. Our PMF stimulator system was designed to generate a PMF with a maximum intensity variation of 0.27 T at a transition time of 0.102 ms, with pulse intervals of 1 Hz. Live blood analysis was used in order to compare the rouleau formation of RBCs before and after PMF stimulus and the movement of RBCs was recorded using video camera attached to the microscope.

Figure 1(a) shows the mobilities of RBC after PMF stimulus of 5 to 20 min. The morphologies of RBCs observed after PMF stimulus of 10 min. showed almost separated RBCs each other and their mobilities are very fast up to 200% compared to before stimulus. However, as increasing stimulation duration to 15 and 20 minutes, the RBCs aggregated again and the number of stacked cells increased, and the mobilities after stimulus decreased, compared with before stimulus. For the longer or shorter stimulus than 10 min. the RBCs were stacked almost same as non-stimulation and their mobilities were slower than those of before stimulus, for male subject. The reason is considered as the longer exposure to PMF may give a bad influence on nerve system and ionic channel of cells. Figure 1(b) shows the activated time taken to stop the motion of RBCs on the slide glass, as function of PMF stimulus duration. The movement of RBCs last a long time up to 170 s and 128 s, respectively, for PMF stimulus of 10 min. for male and 5 min. for female. For longer exposure time of 15-20 min. and 5 min., the RBCs movement stop within 40 s less. Contrary to male subject, the optimum stimulus duration in female subject was 5 min. In order to establish the relation between stimulus time and gender difference, we need recruit more female subjects. In order to identify a link between the disaggregation in rouleau formed RBCs and the duration of PMF stimulus, it is necessary to investigate the correlation between PMF intensity and the stimulus time, the mobility of RBCs, and the number of stacked RBCs.

Keywords: Pulse Magnetic Field, Red Blood Cells, Aggregation, Magnetic Stimulus, Rouleau formation.

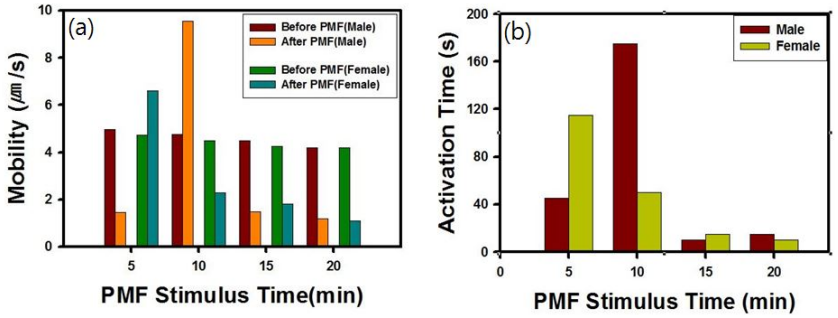

Fig. 1. Effect of PMF stimulus on the dynamic motion of RBCs aggregation. (a) The mobility of RBCs aggregation (b) the activated time taken to stop the motion of RBCs

BM03

Magnetic detection of protein biomarkers by combining a nuclear magnetic resonance biosensor with engineered ferrite nanoparticles

Minhong Jeun[1], Sungwook Park[1,2], Hakho Lee[3], and Kwan Hyi Lee[1,2*]

[1]Center for Biomaterials, Biomedical Research Institute,
Korea Institute of Science and Technology (KIST), Seoul 02792, Korea
[2]Division of Bio-Medical Science &Technology, KIST School,
Korea University of Science and Technology (UST), Seoul 02792, Korea
[3]Center for Systems Biology, Massachusetts General Hospital, Harvard Medical School, Boston, MA, USA
[*]kwanhyi@kist.re.kr

Magnetic-based biosensors are considered as one of the more probable detection methods for on-site detection due to their intrinsic magnetic characteristic not being affected greatly by biological samples. We present a highly sensitive magnetic biosensor which is combines a nuclear magnetic resonance (NMR) device with nanoferrite particles (NFPs). The magnetic properties of the NFPs can be identified by the transverse relaxation rate (R2) of the NMR device; this transverse relaxation rate can be identified as the sensing performance of the device. By controlling the Mn and Mg cation concentration and distribution we have developed magnetically engineered NFPs (MnMG-NFP), NMR agents, which show greater magnetization and subsequent improved (R2) rate. The MnMg-NFPs and miniaturize NMR system showed high sensitivity and stability for the detection of a small amount of nucleoprotein biomarkers.

Use of Dual-type GMR-SV Device below the Center of μ-coil and PR μ-channel to Observe and Measure the Properties of Magnetic Beads Combined with Red Blood Cell

Jong-Gu Choi[1*], Jang-Roh Rhee[2], and Sang-Suk Lee[1†]
[1]Department of Oriental Biomedical Engineering, Sangji University, Wonju 26339, Korea
[2]Department of Nanophysics, Sookmyung Women's University, Seoul 04310, Korea

The GMR-SV sensor is widely used as a displacement and position sensor such as non-contact detection of movement of an in-cylinder piston in an automobile as well as a nano-biosensor. This technology is a successful case of nanotechnology in a relatively short period and can be considered to be very effective in other nanotechnology fields. The frequency response can maintain any steady status from dc to 1 MHz but sharply attenuates at higher frequencies. In this study, a dual-type GMR-SV biosensor for detecting of red blood cell(RBC) was prepared to fabricate a composited device pattern with a line width of several μm. The GMR-SV thin film is optimized with Ta/NiFe/CoFe/Cu/CoFe/IrMn/CoFe/Cu/CoFe/NiFe/Ta multilayer structure. We have studied magnetoresistive properties to detect MBs coupled to RBCs with GMR-SV device, one or multi turn μ-coil, and PR μ-channel fabricated by Ar-ion milling, electrode deposition, and photolithography, respectively.

Fig. 1(a) shows two GMR-SV devices. Fig. 1(b) is a photograph in which the center portion of the coil coincides at the same position of GMR-SV device. Fig. 1(c) shows two actual shapes for a single and multi turn μ-coils and GMR-SV device structure fabricated by patterning two PR μ-channels. The edge electrodes of GMR-SV devices other than the center portion of the electrode material of all PR was coated by SiO_2 insulating layer.

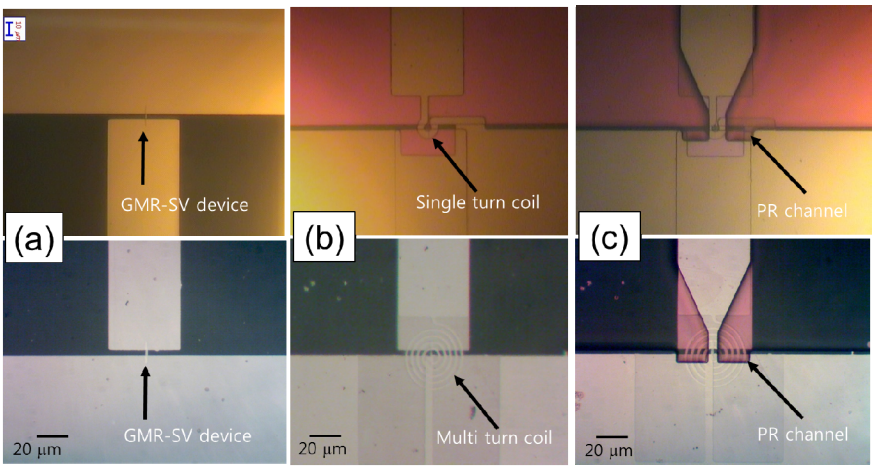

Fig. 1. Photographs of the complex structure composed of dual-type GMR-SV μ-device, μ-coil, and PR μ-channel; (a) dual-type GMR-SV μ-devices, (b) a single turn μ-coil and multi turn μ-coil, and (c) PR one μ-channel.

Two GMR-SV devices were designed to immerse a physiological saline liquid containing RBCs combined with MBs to flow into the microtubule injector and toward the center of the complex structure with the pressure difference. The matching MBs coupled to RBCs in normal saline are to be free to move according to the flowing

path of the liquid, as shown in Fig. 2(a) and 2(b). Fig. 2 shows two side views for different flowing status on the complex structure composed of μ-device of GMR-SV and turn μ-coils. There are exit RBCs with MBs through to a valley in the 8 μm thickness and the 10 μm width of PR as an actual motion, as shown in the right side of Fig. 2(a) and 2(b).

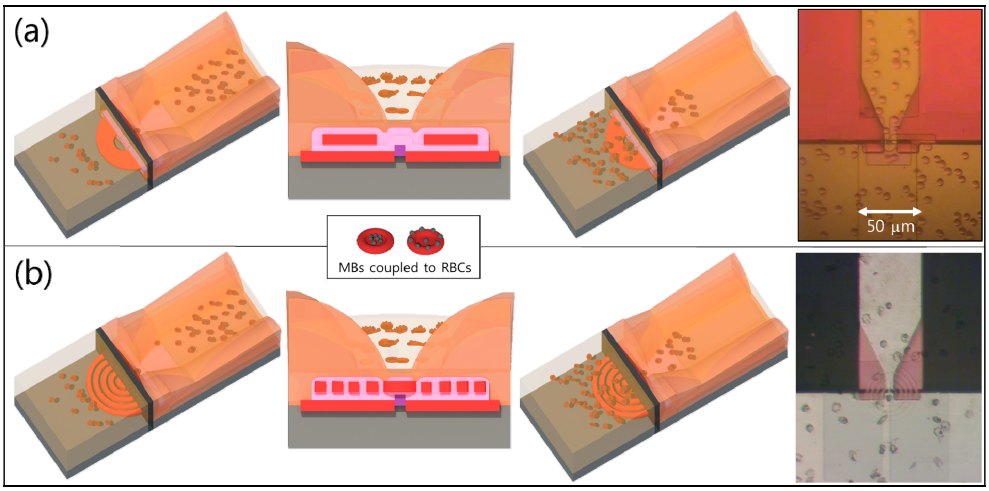

Fig. 2. Visualization of the flow with side views of two states and front cross view for MBs coupled to RBCs passed through (a) a single μ-coil and (b) multi turn μ-coil with PR μ-channel above GMR-SV device. There are two photographs of right side for an actual motion of RBCs combined with MBs pass to PR μ-channel above GMR-SV device and two μ-turn coils.

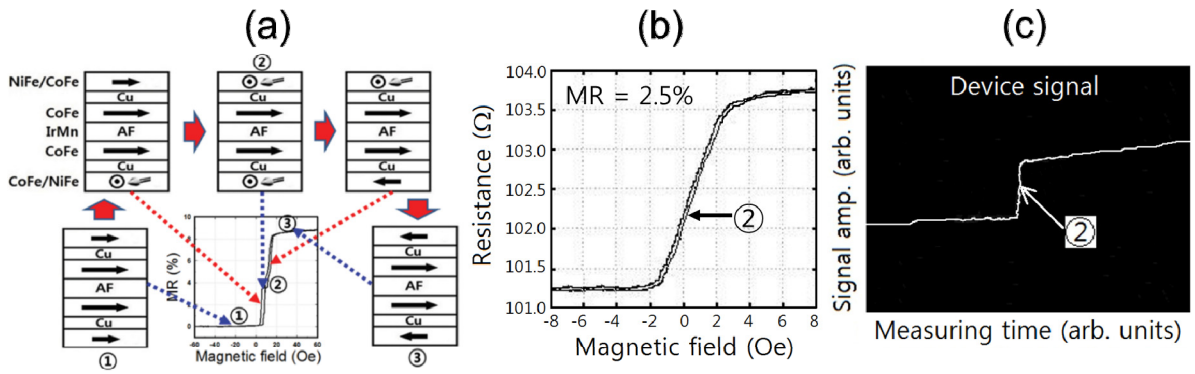

Fig. 3. Minor MR curves of dual-type (a) GMR-SV film and (b) GMR-SV device. The schematic of detailed process for the changing stages of magnetization spin arrays of typical magnetic domains from ① point to ② and from ② to ③ point on the dual-type GMR-SV multilayers. (c) Magnetic signal versus measuring time of the order of ms around the adjacent of composite bio-device with multi turn μ-coil and μ - PR channel with MBs coupled to RBC.

Fig. 3(a) shows the detailed magnetization spin arrays and the minor MR curve when changing from the dual-type GMR-SV film consisting of two pinned layers and two free layers with an antiferromagnetic IrMn thin film. The red and blue arrows shown in Fig. 3(a) which represents the steps corresponding to the magnetization spin arrangement of the multilayer structure. We have already presented several MR curves showing typically high MR properties for GMR-SV thin films. In the step ① and ②, the magnetization spin arrangement of the ferromagnetic material in the dual-type GMR-SV multilayer structure is parallel to the left and antiparallel to the

right, so that the MR due to the spin-dependent scattering effect becomes the minimum and maximum value, respectively.

Fig. 3(b) shows that the gentle MS of 1.0 %/Oe, the Hex of 0.5 Oe, and the MR ratio of 2.4 % are measured from the minor MR curve of GMR-SV device. When MBs coupled to RBC passing to of multi turn μ-coil, as shown in Fig. 2, a MR of the GMR-SV element was kept at a constant value before dropping RBC with MBs. The output signal for the notation ② of Fig. 3(a) and 3(b) corresponding to one of Fig. 3(c) means before and after passing in the center of GMR-SV device with the change of the sensing position of the minor MR curve by the abrupt variation of the sensing field in the presence of MBs coupled to RBC. It suggests that several statuses of versatile membrane of RBCs combined with MBs passed through the center of μ-coil and PR μ -channel can be analyzed by the output MR signals of GMR-SV device.

Acknowledgments

This work was supported by the National Research Foundation of Korea (NRF) funded by the Korea government (Ministry of Education) with the Grant No. of NRF-2016R1D1A1B03936289.

Exchange-coupled Sr-hexaferrite/Magnetite composites

Tae-Won Go*, Kang-Hyuk Lee, Jae-Hyung Yoo, Dami Kim, Sang-Im Yoo†
Department of Material Science and Engineering, Research Institute of Advanced Materials (RIAM),
Seoul National University, Seoul, Korea

Exchange coupled hard/soft magnet has mostly brought interest in powder and layered film applications after the theoretical proposal in 1991 by Kneller and Hawig [ref]. However, its presence in bulk permanent magnets has never been clarified. In this study, we tried to investigate the exchange-coupling effect in bulk hard/soft magnetic composites. Strontium hexaferrite/Magnetite were chosen as the hard/soft magnetic materials, respectively. Sr-ferrite was prepared via molten-salt synthesis, with $SrCO_3$, Fe_2O_3 as raw materials. They were ball-milled and mixed with NaCl in the mass ratio of 1:5. It was calcined at 1050℃ for 2h in air. The calcined powder was washed with DI water to remove NaCl and ball-milled again to break down agglomerates. It was coated with Fe_2O_3 by citrate/nitrate sol-gel combustion route, where $Fe(NO_3)_3 \cdot 9H_2O$ was used for the iron source. The Sr-ferrite/Fe_2O_3 mixture was uniaxially pressed into precursor pellets and sintered at 1200℃ for 2 h in 4% H_2/96% N_2 gas. The samples were characterized by X-ray diffraction (XRD), vibrating sample magnetometer (VSM), and scanning electron microscope (SEM). Details will be presented for a discussion.

Keywords: Exchange-coupled magnet, magnetic composite, strontium ferrite, manganese zinc ferrite

Reference

[1] IEEE TRANSACTIONS ON MAGNETICS, VOL. 27, NO. 4, JULY 1991

Structure and magnetic properties of nanocrystalline MnAl-C prepared by solid state reactions

Hui-Dong Qian[1,2*], Ping-Zhan Si[1†], Jihoon Park[1], Kyung Mox Cho[2], Chul-Jin Choi[1†]
[1]Powder & Ceramic Division, Korea Institute of Materials Science, Changwon, Korea
[2]School of Materials Science and Engineering, Pusan National University, Busan, Korea
[†]Email: cjchoi@kims.re.kr; pzsi@cjlu.edu.cn

The magnetic Mn-Al system has attracted continuous interests for more than half century [1]. The research interests in MnAl-based magnets increase recently with increasing demand for low cost rare-earth free magnets [2]. A number of techniques have been employed for preparation of the metastable τ-phase, which was usually prepared by annealing the high temperature ε-phase that obtained by melting process [3]. In this work, we prepared the MnAl-C alloys by using one-step solid state reaction methods starting from manganese nanoparticles. The τ-phase purity increase when heating longer time at 1100°C because of more ε-phase generated. After 6 hours heat treatment at 1100°C, we obtained samples with 1221.97Oe coercivety and 44.28emu/g saturation magnetization at 4T Field. The structure, magnetic properties, and phase transformation of the samples were studied systematically by using XRD, SEM, TEM, and PPMS.

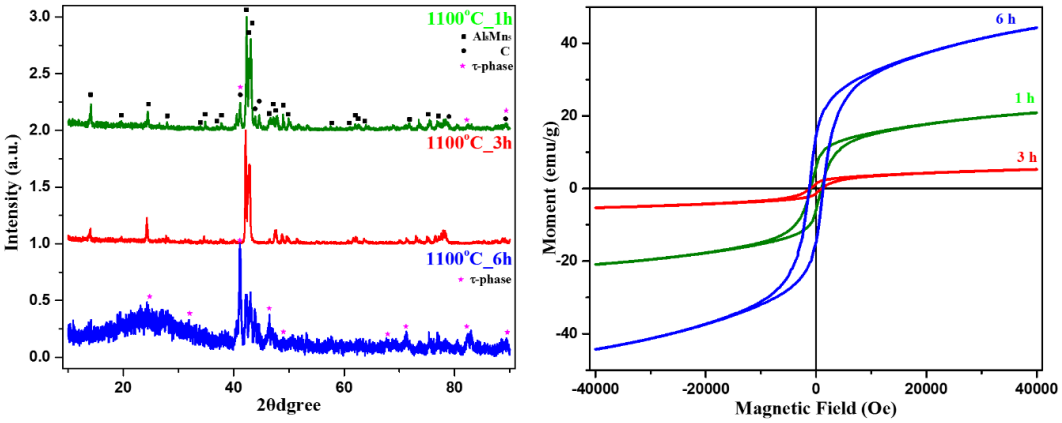

Fig. 1. XRD and M-H loops of Mn-Al-(C).

Acknowledgements

This work was supported by Creative Materials Discovery Program through the National Research Foundation of Korea (NRF) funded by the Ministry of Science, ICT and Future Planning under Grant Number 2016M3D1A1027800, and NSFC (Nos. 11074227, 51671177).

References

[1] H Kono, On the Ferromagnetic Phase in Manganese-Aluminum System, Journal of the Physical Society of Japan, **13**(1958) 1444-1451.
[2] JMD Coey, New permanent magnets, J. Phys. Condens. Matter **26**(2014) 064211
[3] M. A. Bohlmann, J. C. Koo, J. H. Wise, J. Appl. Phys. **52**(1981) 2542

Samarium cobalt nanofibers with ultra-long aspect ratio: a Novel structure based on Electrospinning and Enhanced Magnetic properties

Jimin Lee[1*], Tae-Yeon Hwang[2], Min Kyu Kang[3], Jongryoul Kim[1,3], Yong-Ho Choa[1,2]

[1]Department of Materials Science and Chemical Engineering, Hanyang University, Korea

[2]Department of Fusion Chemical Engineering, Hanyang University, Korea

[3]Department of Materials Engineering, Hanyang University, Korea

Rare-Earth/Transition-Metal (RE-TM) permanent magnets such as Nd-Fe-B, Sm-Co and Sm-Fe-N are essential part in a wide range of applications including direct current (DC) rotating electric motors in automobiles, data storage, magnetoelectronic, electromechanical, and electronic devices. Among these RE-TM permanent magnets, Sm-Co based alloy magnets are the promising materials for high-temperature applications due to excellent magnetocrystalline anisotropy constant (approaching 17.0×10^6 J/m^3) and the higher Curie temperatures (T_c of ~1,190K). Additionally, the researchers predicted that enhanced hard magnetic properties (e.g., coercivity) can be achieved when the dimension of materials reaches the single-domain size (e.g., Sm_2Co_{17} = 0.66 micron). At this condition, the magnetic spin in each single-domain of particle gives highest resistance to demagnetization, leading to greater coercivity. The other way to enhance hard magnetic properties is to create high aspect ratio structures, which will increase shape anisotropy resulting in greater coercivity. That is to say, the enhanced hard magnetic properties are predicted from one-dimensional Sm-Co sub-micron fibers.

In this work, we demonstrated to ability to synthesize Sm-Co fibers with controlled composition and dimension by combining electrospinning and reduction-diffusion process. Synthesized fibers show excellent hard magnetic properties.

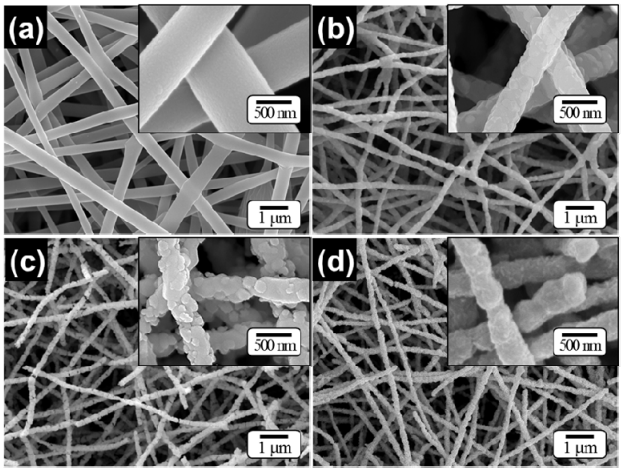

Fig. 1. FE-SEM micrographs of samples obtained after; (A) electrospinning, (B) calcination, (C) 1st reduction and (D) 2nd reduction with subsequent washing (Insets: high magnification images).

Synthesis and Magnetic Properties of Samarium Cobalt Particles using Modified Spray Pyrolysis-Calcination and reduction-diffusion process

Tae-Yeon Hwang[1*], Jimin Lee[2], Gwang-myeong Go[2], Yong-Ho Choa[1,2]
[1]Department of Fusion Chemical Engineering, Hanyang University, Korea
[2]Department of Materials Science and Chemical Engineering, Korea

Samarium-cobalt ($SmCo_5$ or Sm_2Co_{17}) magnets are a kind of rare earth magnet which have high uniaxial magneto-crystalline anisotropy (K_u = 2.0 x 10^8 erg cm^{-3}) and high Curie temperature (T_c = 1020 K). In general, the maximum energy product (BH_{max}) of Sm-Co based magnets (16 – 33 MG*Oe) are lower than sintered neodymium based magnets ($Nd_2Fe_{14}B$, ~64 MG*Oe). But, owing to their high Curie temperature, samarium-cobalt magnets are superior to sintered neodymium magnets at high temperature applications. In addition, working temperature of permanent magnets in electric vehicles or a wind turbine is expected higher than 100°C and thus Sm-Co based magnets seems promising permanent magnet material. However, the limited intrinsic maximum energy product of Sm-Co based magnets and the high cost of Samarium element are still main obstacles.

To overcome these problem, researchers have been dedicated in developing magnetic composite which contain exchange-coupled hard and soft magnetic material. By exchange coupling of hard magnetic materials with soft magnetic materials, the remanences of the soft magnetic material are enhanced due to the anisotropy of magnetic moment of soft material retained by hard material and the overall maximum energy products of the composites are increased. In general, coupling of hard/soft material occurs only in very fine interface and require uniaxial alignment of the magnetization axis of each hard/soft phase. Therefore, developing synthesis method of Sm-Co particles with fine microstructure having a uniaxial magnetization axis is primary object to implement.

So far, Sm-Co particles have been fabricated via ball-milling or melt-spinning and chemical synthesis with Ca or CaH_2 assisted reduction-diffusion process. The Sm-Co particles synthesized by these methods demonstrated $SmCo_5$ or Sm_2Co_{17} phase, which exhibit high magnetic property among Sm-Co related phases, are successfully synthesized. However, the particles showed an isotropic spatial distribution of the easy magnetization directions and thus the use for exchange coupling with soft magnetic materials are limited.

Here, we attempted a synthesis of $SmCo_5/Sm_2Co_{17}$ particles by the combination of salt-assisted ultrasonic spray pyrolysis and reduction-diffusion process by Ca and CaH_2. We observed that the addition of salt during reduction-diffusion process refined the growth of the particles and Sm_2Co_{17} particles successfully synthesized. The morphology and crystal structures were characterized with field effect field effect scanning electron microscope (FE-SEM) and x-ray diffractometer (XRD). The magnetic property was measured by vibrating sample magnetometer (VSM)

Synthesis of Iron Nitride on Fe Foils Using NH_4Cl

K. P. Shinde[1*], M. Ranot[2], P. Z. Si[1], J. H. Park[1], J. W. Kim[3], C. J. Choi[1] and K. C. Chung[1]

[1]Nano functional materials Department, Korea Institute of Materials Science, South Korea

[2]Materials Deformation Department, Korea Institute of Materials Science, South Korea

[3]Functional Ceramic Department, Korea Institute of Materials Science, South Korea

Rare-earth-free magnets are highly considered as a next-generation potential candidate since the supply constraints and environmental issues of rare-earth magnetic materials in recent years. Iron nitride, $Fe_{16}N_2$, has been recognized as one of promising candidates because of its redundancy of Fe and N, large magneto-crystalline anisotropy, and high saturation magnetization.

In this study, we have used the textured Fe foils with the different thickness of 10, 20, and 100 μm to study the nitriding behavior of iron foils using the ammonium chloride (NH_4Cl), which can sublime around 337^{o}C, as a source of nitrogen. Both Fe foils and NH_4Cl were put into a quartz tube and then vacuum sealed. Among the variables of nitriding process, effect of amount of ammonium chloride and nitriding temperature were investigated in order to form α”-$Fe_{16}N_2$ phase. In the nitriding process, the high temperature region of the heating profile was varied from 210-360^{o}C to give a kind of activation energy to the Fe foil and have a better ambient of nitrogen source, and thus for the good nitrogen diffusion into the Fe foils. It was found that α”-$Fe_{16}N_2$ phase can be formed at a temperature of about 330^{o}C and 2 hrs dwelling time with the impurities of iron oxides. Also the synthesis of iron nitride on Fe foils using the normal ammonia flow route are carried out and the comparison is discussed for the formation of α”-$Fe_{16}N_2$ phase.

Magnetic properties of barium-strontium hexaferrite $Ba_xSr_{1-x}Fe_{12}O_{19}$ (x = 0.0 - 1.0) prepared by solid-state reaction

Jun-Ho Park*, Kang-Hyuk Lee and Sang-Im Yoo†
Department of Materials Science and Engineering, Seoul National University,
Research Institute of Advanced Materials (RIAM), Seoul 151-744, Korea

M-type hexaferrties have been used for many applications as a permanent magnet, data storage materials, electrical devices, and micrwowave devices. Nowadays, in order to increase their magnetic properties, researches on the site substitution of M-type hexaferrites are being widely performed. However, the magnetic properties of barium-strontium hexaferrite ($Ba_xSr_{1-x}Fe_{12}O_{19}$, *BSFO*) synthesized by solid-state reaction have not been fully clarified yet. Thus, in this study, we investigated the magnetic properties of BSFO samples prepared by solid state reaction. Calcination condition was 1050˚C for 8 h in air, and sintering condition was 1100˚C for 2 h in air. Samples were characterized by X-Ray Diffraction (XRD), Scanning Electron Microscope (SEM) and Vibration Sample Magnetometer (VSM). The XRD data revealed that BSFO hexaferrite phase coexists with a small amount of α-Fe_2O_3. The sample having x = 0.2 ($Ba_{0.2}Sr_{0.8}Fe_{12}O_{19}$) exhibited the highest magnetic properties of Ms = 72.22 emu/g and Hc = 4996 Oe while the sample having x = 0.4 ($Ba_{0.4}Sr_{0.6}Fe_{12}O_{19}$) possessed the lowest values of Ms = 68.19 emu/g and Hc = 4219 Oe. Details will be presented for a discussion.

Keywords: M-type hexaferrite, $Ba_xSr_{1-x}Fe_{12}O_{19}$, saturation magnetization (Ms), coercivity (Hc)

Effect of initial alloy on hot-deformation behavior of Nd-Fe-B HDDR powder

Jae-Gyeong Yoo[1,2*], Hee-Ryoung Cha[1], Kwang-Won Jeon[1], Youn-Kyoung Baek[1], Dongyun Lee[2], Hae-Woong Kwon[3], and Jung-Goo Lee[1]

[1]Powder & Ceramics Division, Korea Institute of Materials Science, Changwon, Korea
[2]Department of Nano Fusion Technology, Pusan National University, Busan, korea
[3]Department of Materials Science and Engineering, Pukyong National University, Busan, Korea

High performance Nd-Fe-B permanent magnet is widely used in a variety of applications such as traction motor of hybrid and electric vehicles. Since these applications need high operation temperature which results in demagnetization, high coercivity is required. Addition of heavy rare earth (HRE) elements can easily improve coercivity. However, there is a critical problem in supply and demand with HRE. Grain refinement of Nd-Fe-B magnets is one of the effective methods to increase the coercivity without using HRE. Representative methods for refining grains are melt-spinning (MS) process and hydrogenation - disproportionation – desorption– recombination (HDDR) process. Compared to MS powder, HDDR powder can be subjected to heat-treatment at relatively high temperature, because it has larger grain size than MS powder. HDDR and MS powders can be produced to bulk magnets using the hot-deformation (HD) process. HD process consists of two steps. First, hot-pressing (HP) process, Nd-Fe-B powders are hot-pressed into high density compact. Second, die-upsetting (DU) process, the Nd-Fe-B grains are aligned their easy magnetization c-axis parallel to the compression direction. As a result, the aligned grains lead to a high remanence. Numbers of research reveal that rare earth-rich phase is critical factor to the texture formation during the HD process. It is also expected that the microstructure of initial alloy could effect on the deformation behavior during HD process.

In this study, the Nd-Fe-B bulk magnets were produced by HD process using HDDR powders. As-produced and annealing-treated HDDR powders, which have different microstructure, are employed. The magnetic properties and microstructure of hot-deformed magnet were analyzed by VSM and FE-SEM.

The annealed HDDR powders have lower coercivity than untreated HDDR powders. It could be considered that the annealed HDDR powders have non-uniform and discontinuous Nd-rich phase distribution in grain boundary. It could be confirmed through SEM observation that the different of Nd-rich phase distributions in grain boundary in hot-deformed magnet. Based upon these results, effect of initial alloy on hot-deformation behavior of Nd-Fe-B HDDR powder will be discussed.

Effect of quenching speed on the magnetic properties of $Nd_9Fe_{85-x-y}B_6Ti_xM_y$ melt-spun ribbons

Sol Jung[1*], Haein Yim[2]
[1]Department of Physics, Sookmyung Women's University, Seoul 04310, Korea
[2]Department of Applied Physics, Sookmyung Women's University, Seoul 04310, Korea

We investigated the Nd-Fe-B-Ti-M (M=transition metal) melt spun ribbons at quenching speeds from 10 to 40 $m{\cdot}s^{-1}$ in order to optimize the magnetic properties of nanocomposite Nd-based magnets. The nanocomposite magnet is comprised of a mixture of hard and soft magnetic phases with nano-scale grains and has two types such as α-Fe/$Nd_2Fe_{14}B$ and Fe_3B/$Nd_2Fe_{14}B$. This magnet is extensively studied for various striking merits: high saturation magnetization, large maximum energy product and low content of rare earth materials. Moreover, this magnet has the exchange coupling interaction between hard and soft magnetic phases, it endues the magnet with single-phase hard magnetic property and the high theoretical maximum energy product. The efficient exchange coupling interaction requires a homogeneous and fine grained microstructure. In order to satisfy two needs, we try to make Nd-Fe-B-Ti-M amorphous ribbons by melt-spinning process at various quenching speeds and nanocrystalline ribbons through annealing process at various annealing temperatures.

$Nd_9Fe_{85-x-y}B_6Ti_xM_y$ (M = transition metal, x = 0, 1, 2, 3, 4 at.% and y = 0, 1 at.%) ribbons with a thickness of 20 ~ 30 μm and a width of ~ 2 mm were prepared by arc-melting and melt-spinning under an highly purified argon atmosphere. For a homogeneous composition, ingots of Nd-Fe-B-Ti-M were repeatedly melted several times. These ingots were fabricated by melt-spinning onto a cupper wheel at speed of 10 ~ 40 $m{\cdot}s^{-1}$ for rapid solidification. Annealing processes of as-spun ribbons were performed at temperature of 560 ℃ for 5 min under an argon atmosphere. The microstructures of as-spun and annealed ribbons were characterized by X-ray diffraction (XRD) with Cu-Kα radiation. The magnetic properties such as saturation magnetization, coercivity and remanence were measured by vibrating sample magnetometer (VSM) under an in-plane applied magnetic field of -2.8 T ~ +2.8 T. Consequently, the $Nd_9Fe_{85-x-y}B_6Ti_xM_y$ (M = transition metal, x = 0, 1, 2, 3, 4 at.% and y = 0, 1 at.%) ribbons was produced amorphous ribbons at quenching speed of 30 $m{\cdot}s^{-1}$ and above.

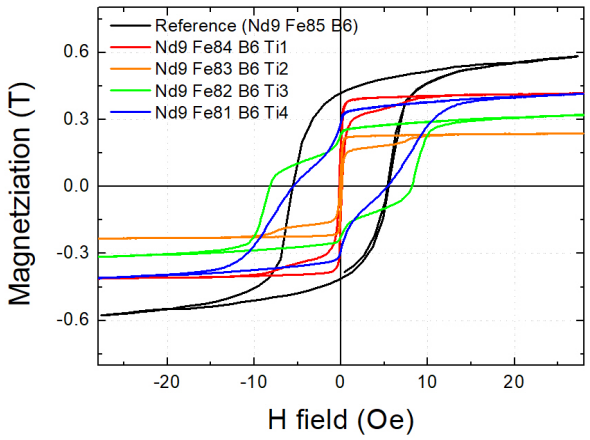

Fig. 1. Hysteresis loops of Nd-Fe-B-Ti-M as-spun ribbons (quenching speed = 18 $m \cdot s^{-1}$)

Magnetic properties of $MnAlC_x$ Magnetic Materials

Sumin Kim*, Hyun-Sook Lee††, and Wooyoung Lee†
Department of Materials Science and Engineering, Yonsei University, 262 Seongsanno,
Seodaemun-gu, Seoul 120-749, Republic of Korea
†Corresponding Author Email: wooyoung@yonsei.ac.kr
††Corresponding Author Email: h-slee@yonsei.ac.kr

Mn-based magnetic materials including MnBi, MnAl and MnGa have received much attention due to their high magnetocrystalline anisotropy and high Curie temperature without rare earth or noble metals. Their maximum energy products (BH)max are between those of ferrite magnets. Especially, MnAl-based permanent magnet have advantage of low cost, which might fill in the gap between the above two mentioned traditional permanent magnets if a well manufacturing process could be developed. The ferromagnetic and metastable τ–phase MnAl, which has the L10 stucture and relatively low density 5.1 g/cm^3, has relatively good intrinsic magnetic properties (K_1 = 1.7 MJ/m^3, Ms = 7.5 kG), suggesting a potential maximum energy product of ~12 MGOe with appropriate microstructural development. The $L1_0$ phase is metastable and forms from the ε phase, which is stable above 870 °C. The equilibrium phases at room temperature that normally result from the decomposition of the ε phase are γ2 and β-Mn. The addition of C tends to increase the stability of the metastable τ phase, likely by suppressing formation of the equilibrium phases. The C addition to the $L1_0$ does not deleteriously affect the intrinsic properties, except for the Curie temperature, which is decreased from 392°C to 331°C with 1.7 atomic percent C.

In this study, we fabricate the $MnAlC_x$ (x=0,1,2,3) ribbons by rapid solidification using melt spinning bypasses the primary solidification of γ2 and β-Mn phases, resulting in single-phase ε in the as-solidified case. Consequently, ribbons were heat treated and milled to particles. The MnAl powder was separated by size through sieves. A relatively high coercivity of about 3.2 kOe and saturation magnetization of ~96 emu/g can be obtained.

Keywords: permanent magnets, MnAl, rapid-solidification, magnetic properties

The effect of Ga-doping on the structure and magnetic properties of MnBi

Yang Yang[1,2*], Qiong Wu[1], Pengyue Zhang[1], Hongliang Ge[1], Jong-Woo Kim[2], Chul-Jin Choi[2]

[1]College of Materials Science and Engineering, China Jiliang University, 310018 Hangzhou, China

[2]Functional Nanopowder Material Department Powder & Ceramic Division, Korea Institute of Materials Science, Changwon, Gyeongnam 51508

Since the high performance permanent magnets based on rare earths are becoming expensive due to the limited rare earth supply, it is essential to develop rare earth free permanent magnets for modern technologies. The MnBi compound has emerged as a potential candidate because of its large magnetocrystalline anisotropy. The effect of Ga-doping on the microstructure and the magnetic properties of MnBi has been investigated in this work. We prepared $Mn_{50}Bi_{50-x}Ga_x$(x=0,1.5,1,1.5,2) by arc-melting and high energy ball milling. The intrinsic coercivity and the M_r/M_s of $Mn_{50}Bi_{50-x}Ga_x$ increase while the saturation magnetization M_s decreases with increasing Ga concentration. This implied that the Ga doping may have caused the magnetic anisotropy of the alloy increases. In addition, the lattice parameter of MnBi decreases with Ga doping. The Curie temperature of $Mn_{50}Bi_{48}Ga_2$ is lower than that of the MnBi.

Keywords: magnetic properties, saturation magnetization, Curie temperature

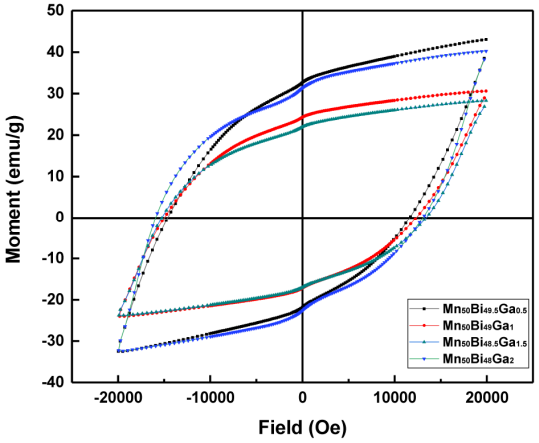

Fig. 1. The magnetic hysteresis loops of the ball milled $Mn_{50}Bi_{50-x}Ga_x$powders.

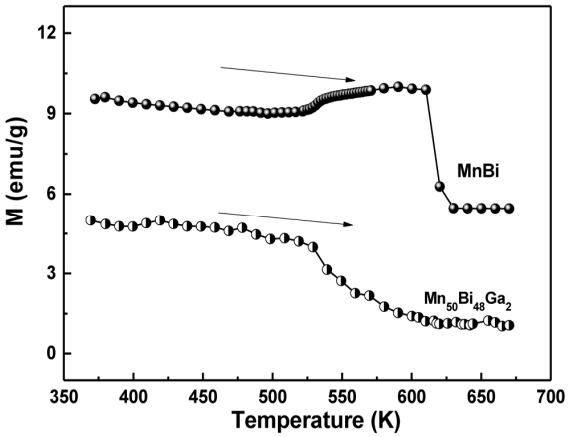

Fig. 2. The M-T curves of $Mn_{50}Bi_{50-x}Ga_x$(x=0,2)alloy.

A Novel DC Motor Employing Anisotropic Bonded Nd-Fe-B Permanent Magnet

Hyo-Jun Kim[1*], Sun-Tae Kim, Sang-Hyup Lee[1], Sang-Myun Kim[1] and Tae-Suk Jang[2]
[1]R&D Center, JAHWA Electronics Co. Ltd., Cheongwon-gu, Chungbuk, 28139, Korea
[2]Department of Hybrid Engineering, Sunmoon University, Asan-si, Chungnam, 31460, Korea

A Direct current (DC) motors employing sintered ferrite magnets (PMs) have been widely used in various automotive applications. In recent years, the PM motors are required to have higher efficiency, better performance with smaller volume, and higher power density. Therefore, the Nd-Fe-B PMs having higher energy density are more attractive to demand the requirements [1].

Conventionally, the isotropic bonded Nd-Fe-B PMs having $(BH)_{max}$ of 80(kJ/m^3) are utilized to a small size DC motors. Very recently, an anisotropic bonded Nd-Fe-B PM, named a MAGFINE having a high-energy product up to 215(kJ/m^3), has been developed by Aichi Steel Corporation [2]. Even though the anisotropic bonded Nd-Fe-B PM gives higher energy product and residual magnetic flux density than the isotropic bonded Nd-Fe-B PM and ferrite PM, its application to the PM motors is still in early stages due to some technical difficulties related with the mass production of the ring-type multi-pole PMs.

In this paper, a ring-type 4-pole polar-anisotropic Nd-Fe-B bonded PM is developed using anisotropic Nd-Fe-B bonded magnetic powder, and applied to a small size DC motor to get higher power-to-volume ratio. Through the comparison with the experimental results, the effectiveness of the proposed PM motor is verified.

This work was supported by the Strategic Core Material Technology Development Program (No. 10043780) funded by the Ministry of Trade, Industry & Energy.

References

[1] V. S. Ramsden, “Application of rare-earth magnets in high performance electric machines,” in Proc. 15th Int. Workshop on REM and Their Applications, 1998, pp. 623-625.

[2] N. Hamada, C. Mishima, H. Mitarai, and Y. Honkura, “Development of Nd-Fe-B anisotropic bonded magnet with 27 MGOe,” IEEE Trans. Magn., vol. 39, no. 5, pp. 2953-2955, Sep. 2003.

Development of High Efficiency Line-Start Permanent Magnet Synchronous Motor from an Industrial Three Phase Induction Motor

Salman Khaliq[1*], Se-hyun Rhyu[1], Hee-chul Yang[2]
[1]Korea Electronics Technology Institute (KETI), Korea
[2]SHIDAE Electric Co. LTD.

Small industrial three phase Induction Motors (IMs) suffer from the lower operational efficiency due to high losses in the rotor and lower power factor. In this paper, Line Start Permanent Magnet (LSPM) is presented which aims to improve power factor and operational efficiency to an IE4 class machine. The proposed LSPM design was developed by inserting the magnets in an off the shelf IM, HHT-05, considering minimum manufacturing cost. Initially, two models of LSPM were designed and analyzed with finite element method (FEM) to assess the performance of both models. The analysis shows a significant increase in the performance improvement compared to the IM. Power factor and efficiency were both improved which will save the operational cost in the proposed models.

Two models of LSPM are analyzed in this paper considering the manufacturing cost and output performance. Fig. 1 shows the rotors of both models. Only rectangular shaped magnet pieces are utilized in both models to keep the manufacturing cost to a minimum. Table I shows the design specifications and output finite element analysis (FEA) performance of both LSPM models along with IM. The outer diameter and stator design were kept precisely same in all the models. However, the stack length was reduced by 10 mm in model 2 to reduce the overall material cost, as only IE4 class motor efficiency is targeted, i.e., 91%. Operational speed in LSPM is 3600 rpm according to the number of poles. Furthermore, model 2 is utilizing 39% lesser magnet volume compared to model 1. FEA analysis shows that the load current in both LSPM models is a little higher than IM which also increases the copper losses in the proposed models. However, there are almost negligible rotor losses in LSPM compared to IM, which increased the overall efficiency in the proposed models. Both LSPM models are showing similar efficiency, however, torque ripple is lower in model two due to a more sinusoidal

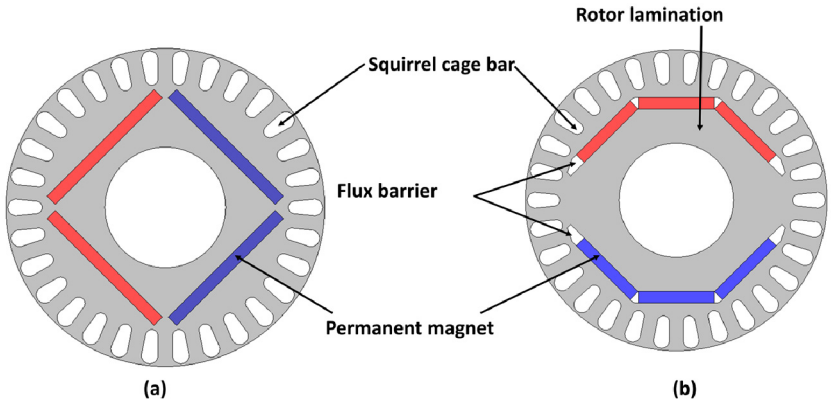

Fig. 1. Proposed LSPM rotor (a) Model 1 (b) Model 2

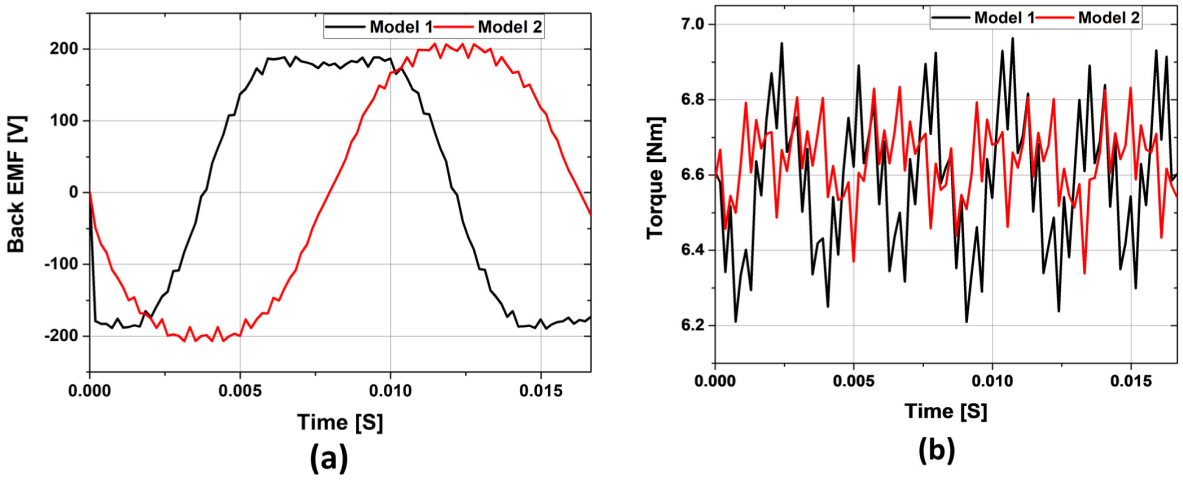

Fig. 2. FEA performance comparison (a) Back EMF (b) Output torque

Table. I Design Specifications and FEA performance comparison

Item	IM	LSPM Model 1	LSPM Model 2
Stack length (mm)	100		90
Supply voltage (V)	220/380		
No. of poles	2		
Magnet volume (mm3)	-	45,000	32,400
Magnet material	-	NdFeB35EH	
Rated speed (rpm)	3530	3600	
3D Finite Element Performance			
Rated current (Arms)	5.32	5.75	5.8
Efficiency (V)	87.5	91.7	91.4
Output power (kW)	2.55	2.60	

spread of permanent magnet (PM) around the rotor core. Furthermore, model 2 is cheaper due to the overall lower material cost, i.e., smaller stack length and lower PM volume. Fig. 2 (a) compares the back EMF and output torque of both models at synchronous speed. Back EMF in model 2 is more sinusoidal compared to model 1. Furthermore, torque ripple is also lower in model 2 as shown in Fig. 2 (b).

As it can be seen from the above analysis that model 2 is showing similar performance with model 1 while exhibiting lower torque ripple. Furthermore, model 2 stack length is smaller by 10 mm, and magnet volume is also lowered by 39%. However, model 1 is more resistant to demagnetization under high temperature condition. The detail demagnetization analysis along with the experimental results will be presented in full manuscript.

Analysis of Electromagnetic Force according to the number of poles and slots for Ultra-high-speed permanent magnet synchronous motors

Jong-Hyun Park*, Young-Hoon Jung, Myung-Hwan Yoon, Jung-Pyo Hong
Department of Automotive Engineering, Hanyang University, Seoul, Korea

This paper deals with the electromagnetic force according to the number of poles and slots for ultra-high-speed permanent magnet synchronous motors. To ensure mechanical stability by vibration, the numbers of poles and slots were determined by considering the maximum speed, and the rotational stability affected by the vibration of the rotor.

1. Introduction

The increasing demand for ultra-high-speed machines in various industry applications, such as direct-drive generators, air blowers, turbo-compressor, and machining spindles, has led to intensive research on the design method for such machines. The use of ultra-high-speed permanent magnet synchronous motors (PMSMs) instead of geared standard motors to improve system reliability, durability, and offers the opportunity to reduce cost. The main advantages of gearless directly coupled ultra-high-speed machines are the elimination of the gear costs and the prevention of oil leakage and maintenance and gear losses. Since no additional transmission system is required, noise and weight can be greatly reduced. While ultra-high-speed machines achieve high power from their high rotational speed and small torque, small and compact motors enable to new integrated system construction [1]. Few academic papers discuss of PMSMs with speeds of up to around 200-krpm, considering the rotor vibration. The authors of [2]–[7] show the design process for a high-speed PMSMs and its diverse applications: as a compressor, pump, machine tool, etc. In such works, however, the magnetic force distributions at the air gap and the vibration of the rotor are not considered when determining the poles–slots number combination. In the case of an ultra-high-speed PMSMs, it is essential to confirm the rotor vibration by the electromagnetic force.

This paper considers vibration to ensure mechanical stability. By determining the pole–slot number, considering vibration characteristics through the appropriate use of finite-element method (FEM) and analytical methods, the mechanical stability of the system can be ensured.

2. Pole-slot number combination

To achieve ultra-high-speed operation, the voltage and current frequency of the inverter must be increased in proportion to the number of poles p. However, the rising signal frequency is burdened on the inverter. The number of poles is limited by the maximum speed of the machine and by the capability of the inverter. Thus, in this paper, p was fixed at 2 to minimize the burden on the inverter [8]. Also, in the case of 2 pole-6 slot distribution winding and 2 pole-12 slot concentrated winding were excluded for reason of the end turn height, 5nd, 7th, etc., harmonic components reduction, and winding factor in advance. This is because it is advantageous for the ultra-high-speed PMSMs to shorten the bearing support portion in consideration of the height of the end coil.

To determine the pole–slot number combination, the magnetic radial force distributions of the 2 pole–3 slot concentrated winding, 2 pole–6 slot concentrated winding, and 2 pole–12 slot distribution winding motors were analyzed using the Maxwell stress tensor, as shown in (1) [9]. This is because the force distribution determines the vibration mode of the machine and affects the rotary stability [10-11]. In (1), P_{mr} is the radial magnetic pressure, B_{mv} and $B_{m\mu}$ are the magnetic flux densities excited by the stator harmonics v and the rotor harmonics μ, respectively, and μ_0 is the magnetic permeability of the free space

$$P_{mr} = \frac{B_{mv} \bullet B_{m\mu}}{2\mu_0} \quad (N/m^2) \qquad (1)$$

Examples of the radial force distribution in the air gap and of the harmonic components of such forces are shown in Fig. 1 and Fig. 2. The rotor contributes the 2nd, 6th, 10th, etc., harmonic components because the components excited by the rotor pole are $(1 \pm 2k)Np$ (N_p: pole number, and k = 0, 1, 2 . . .). Due to the slots and the teeth, the permeance in the air gap is also periodic in space. Thus, the harmonic orders due to the slot are iN_s (N_s: slot number, and i = 1, 2, 3, . . .). In addition, the difference between the harmonic components of the pole and the slot also results in the other harmonic components. In the case of the 2 pole–6 slot and 2 pole–12 slot motors, the 4th, 6th, 8th . . . harmonic components are produced because of the interaction between the flux densities of the rotor and stator in the air gap. Therefore, the 2 pole–6 slot and 2 pole–12 slot motors have no odd harmonic component.

On the other hand, the difference between the harmonic components of the pole and the slot in the 2 pole–3 slot motor can produce odd harmonic components. The 1st harmonic component is produced because the slot and the pole numbers differ by 1, which causes the unbalanced force [9]. In summary, as shown in Fig. 3, which shows the shaft from the axial direction, the geometrical center of the shaft deviates from the rotational center, and consequently, as the shaft rotates, a Mode 1 vibration that vibrates in the radial direction occurs. It has a major negative effect on the vibration characteristics and the rotary stability. However, the 2 pole–6 slot and the 2 pole–12 slot motors have a symmetrically balanced force distribution. Thus, the vibration level of the shaft is relatively low.

3. Conclusion

As a result, the rotary stability and the vibration characteristics of the 2 pole–6 and the 2 pole–12 slot motors are generally much better than those of the 2 pole–3 slot motor. Therefore, the 2 pole–6 slot and the 2 pole–12 slot combination is suitable for a ultra-high-speed motor because it secures the stability of the system.

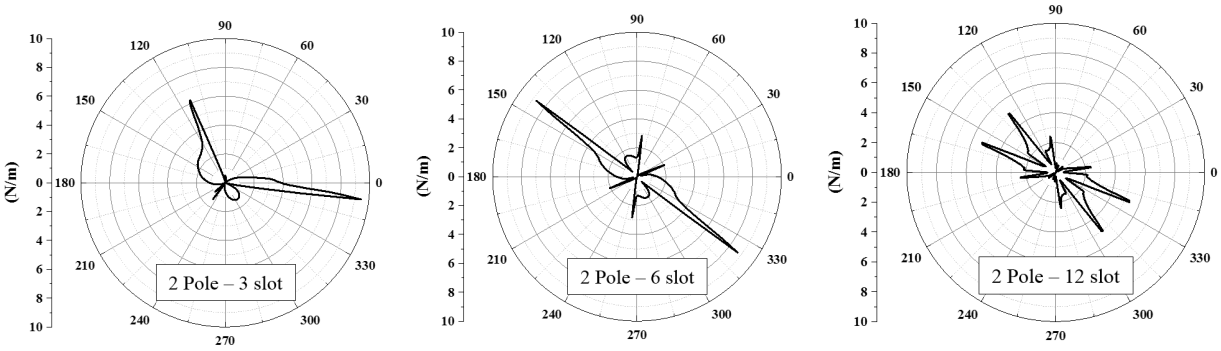

Fig. 1. Radial force distribution

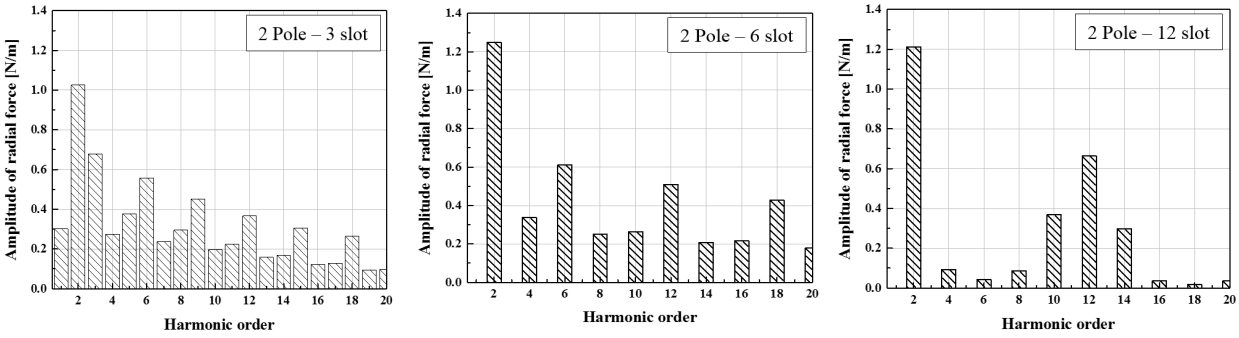

Fig. 2. Space harmonics of the radial forces

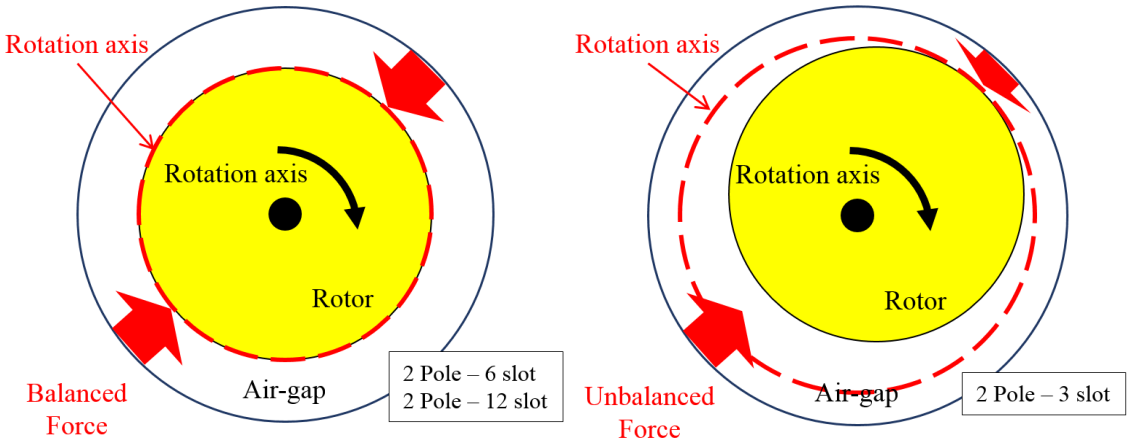

Fig. 3. Vibration of the rotor and shaft

4. Acknowledgement

"This research was supported by the MSIT(Ministry of Science and ICT), Korea, under the ITRC(Information Technology Research Center) support program(IITP-2017-2012-0-00628) supervised by the IITP(Institute for Information & communications Technology Promotion)"

5. Reference

[1] A. Binder, T. Schneider, and M. Klohr, "Fixation of buried and surface mounted magnets in high-speed permanent magnet synchronous motors," in Conf. Rec. IEEE IAS Annu. Meeting, Oct. 2005, vol. 4, pp. 2843-2848.

[2] C. C. Hwang, S. S. Hung, C. T. Liu, and S. P. Cheng, "Optimal design of a high-speed SPM motor for machine tool applications," IEEE Trans. Magn., vol. 50, no. 1, Jan. 2014, Art. ID. 4002304.

[3] S. M. Jang, H. W. Cho, and S. K. Choi, "Design and analysis of a highspeed brushless dc motor for centrifugal compressor," IEEE Trans. Magn., vol. 43, no. 6, pp. 2573-2575, Jun. 2007.

[4] N. Bianchi, S. Bolognani, and F. Luise, "Analysis and design of a PM brushless motor for high speed operations," IEEE Trans. Energy Convers., vol. 20, no. 3, pp. 629-637, Sep. 2005.

[5] M. Sridharbabu, T. Kosaka, and N. Matsui, "Design analysis and improvement high speed hybrid excitation motor for main spindle drive in machine tools based on experimental results of prototype machine," in Proc. IEEE 8th ICPE ECCE Asia, May/Jun. 2011, pp. 1935-1939.

[6] T. Schneider and A. Binder, “Design and evaluation of a 60 000 rpm permanent magnet bearingless high speed motor,” in Proc. IEEE 7th Int. Conf. PEDS, Nov. 2007, pp. 1-8.

[7] P.-D. Pfister and Y. Perriard, “Very-high-speed slotless permanent-magnet motors: Analytical modeling, optimization, design, and torque measurement methods,” IEEE Trans. Ind. Electron., vol. 57, no. 1, pp. 296-303, Jan. 2010.

[8] Myung-Seop Lim, Seung-Hee Chai, Jae-Sik Yang, and Jung-Pyo Hong, “Design and Verification of 150-krpm PMSM Based on Experiment Results of Prototype,” IEEE Trans. Ind. Electron., Vol. 62, no.12, pp. 7827-7836, Dec. 2015.

[9] T. Sun, J. M. Kim, G. H. Lee, J. P. Hong, and M. R. Choi, “Effect of pole and slot combination on noise and vibration in permanent magnet synchronous motor,” IEEE Trans. Magn., vol. 47, no. 5, pp. 1038-1041, May 2011.

[10] J. Boisson, F. Louf, J. Ojeda, X. Mininger, and M. Gabsi, “Analytic approach for mechanical resonance frequencies of high-speed machines,” IEEE Trans. Ind. Electron., vol. 61, no. 6, pp. 3081–3088, Jun. 2014

[11] H. Y. Yang, Y. C. Lim, and H. C. Kim, “Acoustic noise/vibration reduction of a single-phase SRM using skewed stator and rotor,” IEEE Trans. Ind. Electron., vol. 60, no. 10, pp. 4292-4300, Oct. 2013

Magnetic properties of $La_{0.7}Sr_{0.3}MnO_3$ (1-x) and $SrFe_{12}O_{19}$ (x) composites

Young-Min Kang*
Department of Materials Science and Engineering, Korea National University of Transportation, Chungju 27469, Korea

$La_{0.7}Sr_{0.3}MnO_3$ (LSMO), showing the highest curie temperature (T_C) among the perovskite manganites family have been studied extensively because of their magneto-transport properties, half metallic properties and potential applications in low-field magnetoresistive (LFMR) sensors. The electron hopping between mixed valence Mn^{3+} and Mn^{4+} through O^{2-} forms the basis of the double exchange mechanism, which controls the magneto-transport transport properties of the perovskite managanites. Many studies on LSMO-insulator composite systems have been also conducted for an enhancement of the LFMR effect. The second phase at the grain boundary usually obstructs the magnetic spin alignment near the grain boundary region of the manganite and hence increases the tunneling barrier height between the neighboring ferromagnetic grains. However, the studies on the composite of magnetic soft LSMO with magnetic hard oxides have been rarely reported. In this magnetic soft-hard composite, exhibiting double magnetic hysteresis, 4 different magnetization states could be formed according to the relative magnetization direction between the magnetic soft and hard phases. In this study, the magnetic composites of $La_{0.7}Sr_{0.3}MnO_3$ (1-x) and $SrFe_{12}O_{19}$ (x) phases with x = 0, 0.05, 0.1, 0.3, 0.5, 1.0 were prepared by solid-state reaction processes. Fig. 1 shows the M-H curves of LSMO (1-x)-SrM (x) composites. Although the two phases coexist without forming secondary phases the saturation magnetization value of LSMO was largely decreased by the doping of SrM. Clear double hysteresis behavior was exhibited at the samples of x = 0.3 and 0.5 while single soft magnetic hysteresis was obtained at $x \leq 0.1$. In the M-T measurement, the composite with x=0.5 exhibited a diffusive temperature dependence of magnetization compared to that of non-doped LSMO (x=0). Interatomic diffusion between the two phases causes the composite to decrease its saturation magnetization and to exhibit a diffusive temperature dependence of magnetization

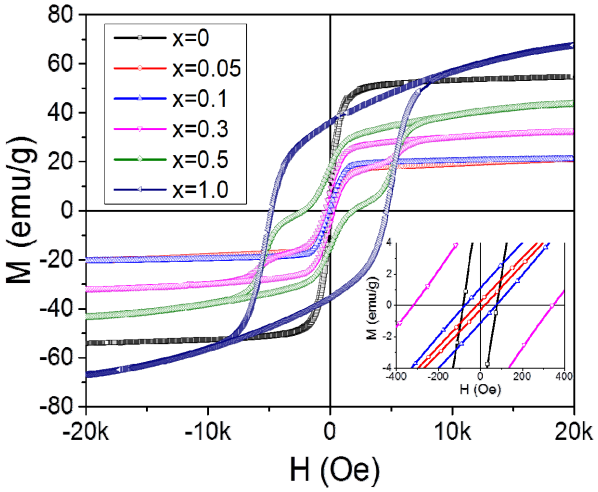

Fig. 1. M-H curves of LSMO (1-x)-SrM (x) composites calcined at 1200 °C.

Synthesis and Characterization of $Ni_xZn_{1-x}Fe_2O_4$

Kwang-Rok Mun, Young-Min Kang*
Department of Materials Science and Engineering, Korea National University of Transportation, Chungju 27469, Korea

Soft magnetic Ni-Zn ferrites are widely used material system in various electromagnetic devices, such as telecommunication, microwave devices, power transformer because of their high magnetic permeability with low magnetic loss and high electrical resistivity. The application into the high-frequency devices can be classified based on the complex relative permeability, $\mu_r = \mu_r' + j\mu_r''$. High μ_r' and $\mu_r'' \approx 0$ are ideal for applications to magnetic field shielding films for radio frequency identification (RFID) and wireless charging, thin film inductors, and thin film transformers. Also, low μ_r' and high μ_r'' are required for the electromagnetic wave absorber in the corresponding frequency range. In this study, $Ni_xZn_{1-x}Fe_2O_4$ samples with $0.2 \leq x \leq 0.8$ were prepared by conventional solid-state reaction method. Double calcination process were employed (calcination at 1000 ℃ for 4 h and 1150 ℃ for 2 h) in order to achieve uniform and fine microstructure. XRD analysis revealed that all the calcined $Ni_xZn_{1-x}Fe_2O_4$ samples ($0.2 \leq x \leq 0.8$) have single Spinel phases and the lattice parameter decreases gradually with increasing Ni content, x. The average grain size of the samples was similar to 1~2 μm regardless of the composition (x). In the M-H measurement, the highest saturation magnetization (M_S) of 78.5 emu/g could be achieved at x = 0.6. The M_S for x=0.4 was 61.8 emu/g and for x=0.8 was 71.0 emu/g. The sample with x=0.2 showed strong paramagnetic behavior without hysteresis. Frequency (1MHz ~1GHz) dependence of the real (μ') and imaginary (μ") part of permeability for $Ni_xZn_{1-x}Fe_2O_4$ ferrites is presented in Fig.1. The applicability of $Ni_xZn_{1-x}Fe_2O_4$ ferrites according to these properties variation with x and correlation between magnetic properties, composition, and microstructure will be discussed.

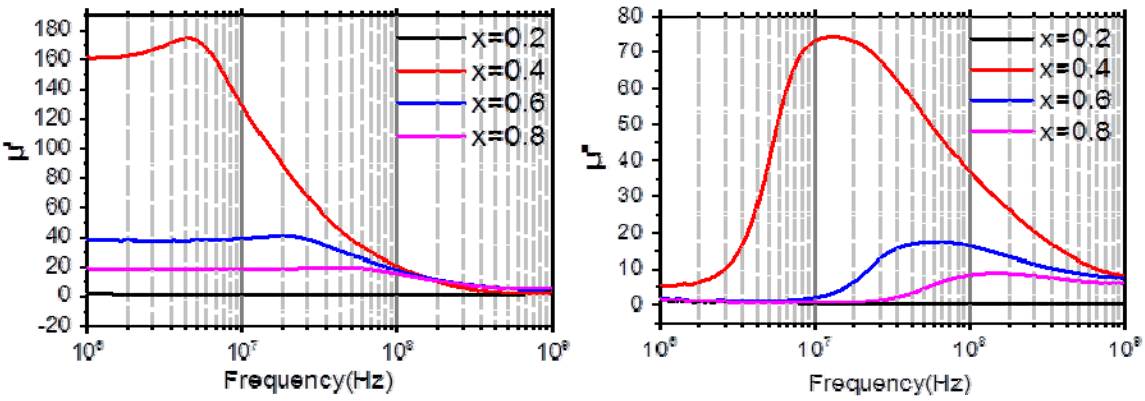

Fig. 1. Frequency (1MHz ~1GHz) dependence of the real (μ') and imaginary part of permeability (μ") for $Ni_xZn_{1-x}Fe_2O_4$ ferrites

Grain alignment dependence of magnetization reversal mechanism in granulated Nd-Fe-B magnet studied by micromagnetic simulation

Shinwon Hwang*, Jae-Hyeok Lee and Sang-Koog Kim
National Creative Research Initiative Center for Spin Dynamics and Spin-Wave Devices, Nanospinics Laboratory, Research Institute of Advanced Materials, Department of Materials Science and Engineering, Seoul National University, Seoul 08826, South Korea

Permanent magnets of high remanence and coercivity have been intensively studied for their promising application in environmentally friendly hybrid vehicles and wind turbines [1]. Nd-Fe-B with uniaxial magneto-crystalline anisotropy is one of the best candidates. In Nd-Fe-B magnets, the performance significantly decreases as the grain alignment parameter(α) decreases [2], which indicates the degree of the grain alignment is one of the key factors to the improvement of the magnet performance. The alignment parameter is a weighted average of deviations of anisotropy axis from the applied field direction. Much researches has been done to obtain perfectly aligned magnets. Growing of the grains in the uniaxial axis [3], applying the magnetic field during sintering [4], Die pressing and press injecting [5] are representative researches. In this regard, we performed a micromagnetic simulations to study the grain alignment dependence of the magnetization reversal mechanisms. The modeled structure consists of a nano-sized cubic ($500x500x500nm^3$) Nd-Fe-B magnets with 27 granular grains [6]. The average sizes of the individual grains (~160 nm) are smaller than the size of a single domain size (200-300nm). For the 27 grains alignment, the grain alignment parameter is set to be α=1(anisotropy), 0.97, 0.89, 0.77, 0.68, 0.62(isotropy) and their distributions are set to follow a half Gaussian distribution [3]. The observed coercivity decreases from 4.3T to 2.9T as the grain alignment parameter decreases from α=1 to α=0.62. This result represents the reversal process of Stoner-Wohlfarth type [7]. We further examined the local magnetization distributions at the nucleation sites of the reversed domains for different misalignment cases. First, when the grains are perfectly aligned, the nucleation of the reversed grain starts at the corner of the grain at the edge of cubic. As the grain alignment parameter decreases, the nucleation begins at the triple junction point of the surface. There are three factors that determine where nucleation begins among the triple junction. The first is the corner shape of the grain, the second is the misalignment of the grain and the last is the grain alignment of neighbor grains. Even though the grains are almost perfectly aligned to the field axis, if two of the three grains of the triple junction are reversed, the unreversed grain can be easily reversed due to the enhanced demagnetization field. As the grain alignment parameter decreases, the misalignment of adjacent grains increases. Increasing the misalignment of the neighboring grains accelerates the magnetization reversal.

Reference

[1] M.J. Kramer, R. W. McCallum, I. A. Anderson, and S. Constantinides JOM 64, 752 (2012)
[2] R. W. Gao et al., Appl. Phys. A 67, 353-356(1998)
[3] P. Tenaud, A. Chamberod and F. Vanoni, Solid State Communications, 63, 303-305 (1987)

[4] S. Z. Zhou et al., J.Appl.Phys, 63, 15(1988)
[5] Zexuan Wang et al., Scientific Reports 6, 38335(2016)
[6] Jae-Hyeok Lee, Jinhyeok Choe Shinwon Hwang and Sang-Koog Kim, Journal of Applied Physics, 122, 073901 (2017)
[7] Stoner E. C., Wohlfarth E. P., Phil. Trans. R. Soc. A 240, 826 (1948).

Nitrogen doped $BiFeO_3$ with enhanced magnetic properties

Yuefa Jia and Chunli Liu*
Department of Physics and Oxide Research Center, Hankuk University of Foreign Studies, Yongin 17035, Republic of Korea

Bismuth ferrite $BiFeO_3$ (BFO) belongs to the perovskite structured (ABO_3) family, which is a widely studied multiferroic material having interesting properties with potential technological applications. In this work, we report for the first time the preparation of N doped BFO(N-BFO) nanoparticles and their magnetic properties. The N-BFO nanoparticles were synthesized using a sol-gel rapid calcination technique, and the influences of N doping on the magnetic properties of BFO was investigated systematically. The XRD patterns of the prepared samples exhibited presence of BFO crystalline phase. The XPS data further confirmed that the nonmetal N element was successfully doped in the BFO nanoparticles. Doping N in BFO drastically boosted saturation magnetization (M_s) values from 0.07emu/g of pure BFO to a maximum value of 0.35emu/g when 12.5 mmol N was used in the precursor (12.5N-BFO). Based on the Mössbauer spectroscopy of BFO and N-BFO, the enhancement in M_s can be attributed to the migration of Fe^{3+} from the B-site to A-site induced by the N doping during the calcination reaction. When too much N precursor was used, M_s decreased sharply. In this case, the impurity phase such as non-magnetic Bi_2O_3 may present in the sample, which led to the reduction of the M_s.

Keywords: N, $BiFeO_3$, saturation magnetization, Mössbauer spectroscopy.

Single-crystalline Gd-doped $BiFeO_3$ Nanowires: *R3c*-to-*Pn2₁a* phase transition and enhancement in high-coercivity ferromagnetism

Jae-Hyeok Lee*, S. K. S. Patel[(a)], Min-Kwan Kim, Biswanath Bhoi, and Sang-Koog Kim

[1]National Creative Research Initiative Center for Spin Dynamics and Spin-Wave Devices, Nanospinics Laboratory, Research Institute of Advanced Materials, Department of Materials Science and Engineering, Seoul National University, Seoul 08826, South Korea

[(a)]Current address: School of Materials Science and Technology, Indian Institute of Technology (Banaras Hindu University), Varanasi 221005, India

$BiFeO_3$ (BFO) material reportedly exhibits antiferromagnetism (AFM) along with very weak ferromagnetism (FM) at room temperature. Owing specifically to its high-ferroelectric Curie (T_C ~ 1103 K) and Neel (T_N ~ 643K) temperatures.[1] Due to its high T_C- and T_N-ordering temperatures, single-phase BFO is the most promising multiferroic material and is expected to find potential applications in spintronics, data storage, and electromagnetic devices.[2] Although BFO below T_N = 643 K is magnetically antiferromagnetic with the G-type spin ordering in the rhombohedral structure, the ferromagnetic phases that can appear by rare-earth-ions (R^{3+}) doping at the sites of Bi^{3+} lead to the suppression of BFO's spin cycloid structure and the enhancement of its magnetization. [3] In accordance with the dependence of BFO's unique inherent properties on its anisotropic dimensions, doped BFO's multiferroic nature is a function of its anisotropic dimensions and different morphologies. One-dimensional (1D) BFO nanostructures are thus gaining significant attention due to their anisotropic-dimensional confinements and modifiable electronic properties. [4]

In this regard, in the present study, we fabricated single-crystalline, Gd-doped $BiFeO_3$ (BFO) nanowires using a hydrothermal technique. The doping of Gd^{3+} ions to the pure-phase BFO nanowire sample effected a remarkable change of both the structural and magnetic properties. X-ray diffraction (XRD) data combined with their Rietveld refinements and high-resolution transmission electron microscopy (HRTEM) revealed pure single-phase crystalline $Bi_{1-x}Gd_xFeO_3$ (x = 0, 0.05, 0.10) nanowires of 40 - 60 nm diameter and their structural transformation from the rhombohedral *R3c* (for x = 0 and 0.05) to the orthorhombic *Pn2₁a* crystal structure (for x = 0.10). The addition of Gd^{3+} ions to the pure-phase BFO leads to remarkable changes in the structural and magnetic properties, which effects are caused by differences in the ionic-radii and magnetic moment between the Bi^{3+} and Gd^{3+} ions. According to the observed magnetization-field (M-H) and magnetization-temperature (M-T) curves, with increasing Gd^{3+} concentration, the saturation magnetization (M_S), squareness (M_r/M_S), coercivity (H_C), exchange-bias field (H_{EB}) and magnetocrystalline anisotropy (K) increased markedly, by M_S = 1.26 emu/g (640 %), M_r/M_S = 0.19 (20.5 %), H_C = 7788 Oe (4560 %), H_{EB} = 501 Oe (880 %) and K = 1.62 × 105 erg/cm^3 (3500 %), for x = 0.10 relative to the data for x = 0. In such Gd-doped BFO nanowire samples, spin-canted Dzyaloshinskii–Moriya interaction, remarkable enhancements in the magnetocrystalline anisotropy as well as uncompensated surface ferromagnetic spin states in the antiferromagnetic core regions also were found.

References

[1] S. V. Kiselev, R. P. Ozerov and G. S. Zhdanov, SoV. Phys. Dokl 1963, 7, 742–744; D. Lebeugle, D. Colson, A. Forget, M. Viret, P. Bonville, J. F. Marucco and S. Fusil, Phys. Rev. B 2007, 76, 024116.

[2] H. Schmid, Ferroelectrics, 1994, 162, 19.; N. A. Hill, J. Phys. Chem. B 2000, 104, 6694.; J. F. Scott, J. Mater. Chem., 2012, 22, 4567.

[3] R. Guo, L. Fang, W. Dong, F. Zheng and M. Shen, J. Phys. Chem. C, 2010, 114, 21390–21396.; G. Catalan and J. F. Scott, Adv. Mater., 2009, 21, 2463–2485.

[4] L. Wu, C. Dong, H. Chen, J. Yao, C. Jiang and D. Xue, J. Am. Ceram. Soc., 2012, 95, 3922–3927.; B. Liu, B. Hu and Z. Du, Chem. Com., 2011, 47, 8166–8168.; S. Li, R. Nechache, C. Harnagea, L. Nikolova and F. Rosei, Appl. Phys. Lett., 2012, 101, 192903.

Characteristic Analysis of Pulse Waveform Reflected by Water Tree in Power Cable

Min-Soo Choi*, Jae-Hoon Shim, Kyu-Jin Jung, Ji-San Park, and Jin-Kyu Byun
Department of Electrical Engineering, Soongsil University, Seoul 06978, Korea

The fault of power cables can cause significant problems in the power system, such as power failures and expensive repair costs. Most cable faults are subjected to various stresses including electrical, mechanical, thermal and chemical stress. In case of distribution cable, it has been investigated that cable deterioration begins to occur after 10 years since cable has been installed and it is known that the main factor of deterioration is caused by water tree and manufacturing defects. Thus, in order to prevent cable faults, it is necessary to diagnose the water tree development of live power cables in advance.

In this paper, for the basic study of the cable degradation characteristics diagnosis, the reflected waveforms of the applied diagnostic pulses are calculated and analyzed according to the shape and size of the water tree models by EM simulations. In the simulation, the cables are modeled as XLPE insulated cables with the length of 10 m and different lengths and depths of the water trees are considered (lengths of 7 mm, 70 mm, 150 mm and penetration depths of 50% and 100%). The power of the reflected pulse waveform is analyzed and also the location of the water tree is identified through the pulse velocity calculation.

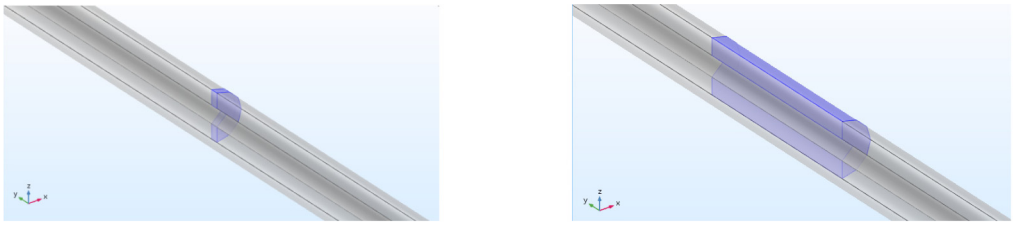

(a) (b)

Fig. 1. Cable water tree models
(a) length: 7 mm. (b) length: 150 mm.

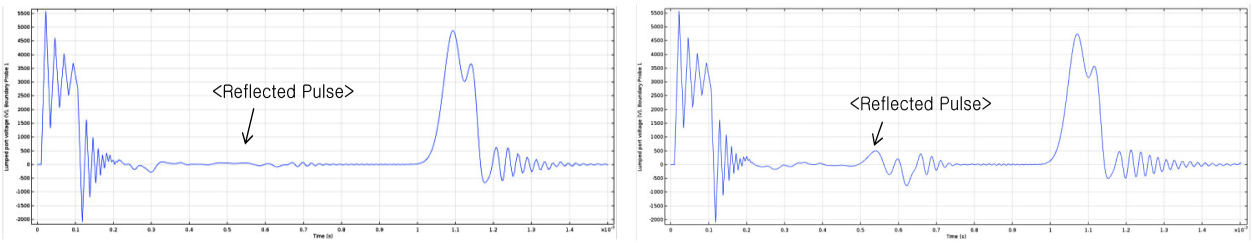

(a) (b)

Fig. 2. Incident and reflected pulse waveforms.
(a) length: 7 mm. (b) length: 150 mm.

Magnetism and magnetocrystalline anisotropy of C- and Pr-substituted τ-MnAl

Jin Sik Park*, S. H. Rhim†, and Soon Cheol Hong†
Department of Physics and Energy Harvest Storage Research Center,
University of Ulsan, Ulsan 44610, Republic of Korea
Corresponding authors: †sonny@ulsan.ac.kr, †schong@ulsan.ac.kr

Ferromagnetic $L1_0$ structured metastable τ-MnAl is one candidate for rare-earth free permanent magnets. Its magnetic moment is measured in experiments to be 1.94 μ_B/f.u. and its lattice constants are a=3.91 Å and c=3.56 Å. The metastable τ-MnAl is stabilized and enhanced in magnetocrystalline anisotropy (MCA) by doping of elements such as C[1], and additional Pr doping further enhances MCA[2].

In this study, we reveal the doping effects of C and Pr on magnetism and magnetocrystalline anisotropy (MCA) of the τ-MnAl, adopting the first-principles calculational method of Vienna Atomic Simulation Package (VASP). For the exchange-correlation potential, the generalized gradient approximation(GGA) is employed as parametrized by Perdew, Burke, and Ernzerhof (PBE). We choose supercell of 2x2x2 for calculating doping effect. The k-meshes of 30x30x30 and 11x11x11 in Monkhorst-Pack scheme are used for the conventional cell and the 2x2x2 supercell, respectively. For wave function expansion, a plane-wave basis set with a cutoff energy of 450 eV is used. Lattice constants of a=3.89 Å and c=3.50 Å are obtained at the total energy minimum, a little bit smaller compared to the experimental values. We have got magnetic moment of 2.30 μ_B/f.u. and MCA energy of +0.27 meV/f.u. without doping. We take 6.25% doping into account by substituting C or Pr for one of the 16 Al or Mn atoms of the supercell. The substitution of C and Pr for the nonmagnetic element Al result in the MCA energies of +0.34 /f.u. and -0.25 meV/f.u., respectively. On the other hand, both magnetic moment and MCA energy are reduced for the substitution of C or Pr for the magnetic element Mn.

References

[1] A. Pasko, M. LoBue, E. Fazakas, L. K. Varga, and F. Mazaleyrat, J. Phys.: Condens. Matter **26** 064203 (2014).

[2] Z. W. Liu, C. Chen, Z. G. Zheng, B. H. Tan, R. V. Ramanujan, J. Mater. Sci.**47** 2333 (2012)

Inductance Comparison of 8-pole 6-slot and 8-pole 12-slot using Equivalent Magnetic Circuit for Actuator of Dual Clutch Transmission

Jin-Cheol Park[1*], Jae-Han Sim[1], Yun-Yong Choi[2], and Jung-Pyo Hong[1]
[1]Department of Automotive Engineering, Hanyang University, Seoul, Korea
[2]Drive Tech Ltd., Bucheon, Korea

Recently, the global EV (electric vehicle) market is expanding by participating actively in the EV market of China and India following major European countries. In addition, A use of dual clutch transmission EV is increasing for stable speed conversion. Thus, the importance and demand of actuators for driving a transmission are growing.

In this paper, Inductance of 8-pole 6-slot and 8-pole and 12-slot are compared using magnetic circuits of actuator for dual clutch transmission. In the initial design, the choice of pole/slot number combination is very important. Especially, the electrical parameters are determined according to the number of pole and slot. Thus, the output power of actuator depends on pole/slot combination in the same actuator size. In the case of inductance among the electrical parameters, the smaller is the inductance, the larger becomes the output power. In other words, as the inductance is reduced in BLDC driving, a larger output can be generated within the same size. As a conclusion, the inductance was compared between 8-pole 6-slot and 8-pole 12-slot using the magnetic circuit in the same size, and it was confirmed that the inductance of 8-pole 12-slot was smaller than that of 8-pole 6-slot. Finally, the inductance is estimated through FEA (Finite element analysis) and the output power of actuator is improved within the same size for 8-pole 12-slot than 8-pole 6-slot.

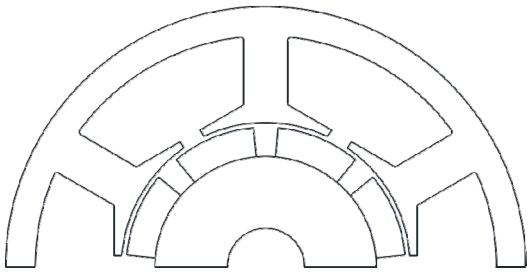

Fig. 1. 8Pole 6slot

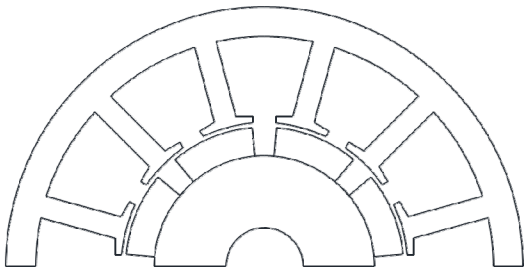

Fig. 2. 8Pole 12slot

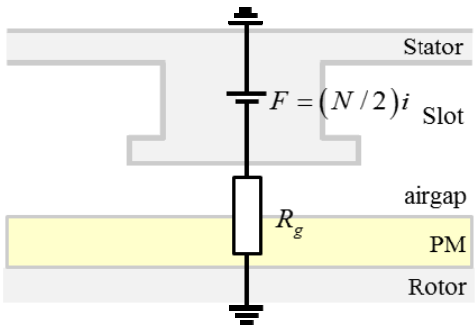

Fig. 3. 8Pole 6slot of equivalent magnetic circuit

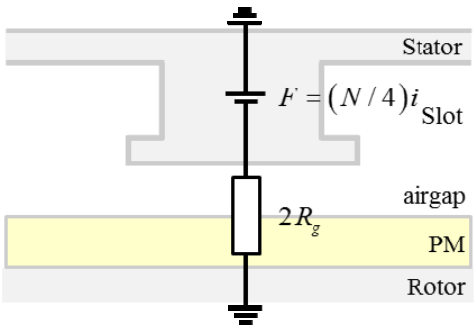

Fig. 4. 8Pole 12slot of equivalent magnetic circuit

Spin accumulation on Cu driven by ultrafast demagnetization of Fe, Co, and Ni

Im-Hyuk Shin[1,2*], Byoung-Chul Min[1], Byeong-Kwon Ju[2], and Gyung-Min Choi[1,3†]
[1]Center for Spintronics, Korea Institute of Science and Technology
[2]Display and Nanosystem Laboratory, Korea University
[3]Department of Energy Science, SungKyunKwan University

Generation of spin current is an essential part of spintronics. Conventionally, spin currents have been generated by applying charge currents or heat currents to ferromagnets. Recently, it has been shown that pulsed laser injected into metallic FMs can generate spin currents by ultrafast demagnetization. However, most experimental evidences were focused on dynamics of magnetization of ferromagnets in a ferromagnet/non-magnet/ferromagnet structure.

In this study, we show measurements of dynamics of spin accumulation on non-magnets surface in a ferromagnet/non-magnet structure driven by ultrafast demagnetization of ferromagnets using time-resolved Magneto Optic Kerr effect. We find that the spin accumulation on a non-magnet, Cu, is well explained by dynamics of demagnetization of ferromagnets, Fe, Co, and Ni, and spin diffusion modeling. We also find that Fe, Co, and Ni generates an order of magnitude larger spin accumulation than previous results with [Co/Pt] and [Co/Ni] multilayers. We interpret that the improvement of the spin accumulation is due to reduced spin relaxation inside ferromagnets.

Overhang Effect Analysis of Spoke-type Interior Permanent Magnet Synchronous Motor Using 3 Dimensional Equivalent Magnetic Circuit Network

Jun-Yeol Ryu*, Dae-Kee Kim, Myung-Hwan Yoon, and Jung-Pyo Hong
Department of Automotive Engineering, Hanyang University, Seoul, Korea

Recently, due to many problems of rare-earth resources such as unstable supply and price fluctuations, there have been many studies on motors that can produce high torque density without using rare-earth permanent magnet (PM). In this reasons, spoke-type interior permanent magnet synchronous motors (Spoke-type IPMSM) using a ferrite magnet are widely used in many industries. In addition, spoke-type IPMSM which has PM overhang is used to improve the torque density. The PM is protruded in the axial direction to produce higher field flux. Due to increased field flux, outputs such as back EMF and torque are improved. Overhang effect of PM can be calculated by using 3 dimensional finite element analysis (3D FEA). However, 3D FEA has difficulties such as hard pre-processing and time consuming. Instead of 3D FEA, overhang effect is calculated by using 3 dimensional equivalent magnetic circuit network (3D EMCN). Fig. 1. shows 3D EMCN. Each element is divided into a rectangular parallelepiped. By using Gauss' law and Kirchhoff's law, flux density in each element is calculated. Not calculating the second-order partial differential equations, the reference model is equated with the 3D circuit network as shown in Fig. 1. And then, Ohm's law is used to calculate. In this reason, computational time can be dramatically reduced in 3D EMCN. Therefore, in this paper, motor outputs such as back EMF and average torque considering overhang effect are calculated by using 3D EMCN and its accuracy and computational time are compared with results of 3D FEA.

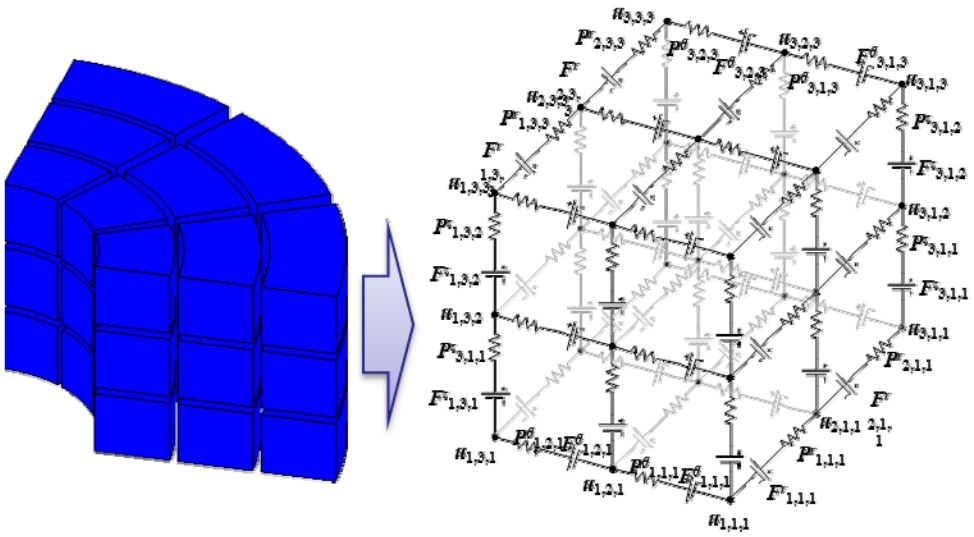

Fig. 1. 3D Equivalent Magnetic Circuit Network

Design of High Power Density Brushless DC Motor for Dual Clutch Transmission of Electric Vehicle based on Space Harmonic Analysis

Jae-Han Sim[1*], Jin-Cheol Park[1], Yun-Yong Choi[2], and Jung-Pyo Hong[1]
[1]Department of Engineering, Hanyang University, Seoul, Korea
[2]Drive Tech Ltd., Bucheon, Korea

The brushless DC (BLDC) motor is an attractive alternative to the brushless AC (BLAC) motor in various applications. As compared with the BLAC motor, the BLDC motor features the inexpensive position sensors and the simple electric control strategies. Furthermore, it has a strength in terms of the power density and is quite suitable for automotive applications other than electric vehicle (EV) traction drives. This paper describes a design process of the BLDC motor for dual clutch transmission of EV to enhance its power density using space harmonic analysis (SHA). The SHA assumes the following 5 aspects; i) the relative permeability of the magnetic core is infinite and isotropic; ii) the permanent magnet shows the linear demagnetization characteristics; iii) the axial end effects are ignored; iv) the stator windings are symmetrical; v) the eddy currents are neglected. The method palliates more computational burden than finite element analysis (FEA) and shows a moderate accuracy within a short computing time. In other words, the SHA can be utilized in order to find out the influence of the geometrical parameters on the performance of the BLDC motor precisely and swiftly. Particularly, the design procedure focused on improving the power density of the BLDC motor in order to decrease its volume. As a result, the 9-slot and 8-pole combination was determined by considering the fundamental winding factor and the end turn length. Here, the geometrical parameters, i.e. rotor diameter, PM thickness, and stack length, were rearranged to improve the power density of the BLDC motor. Consequently, an optimum model was designed and analyzed so as to justify the aforementioned design procedure.

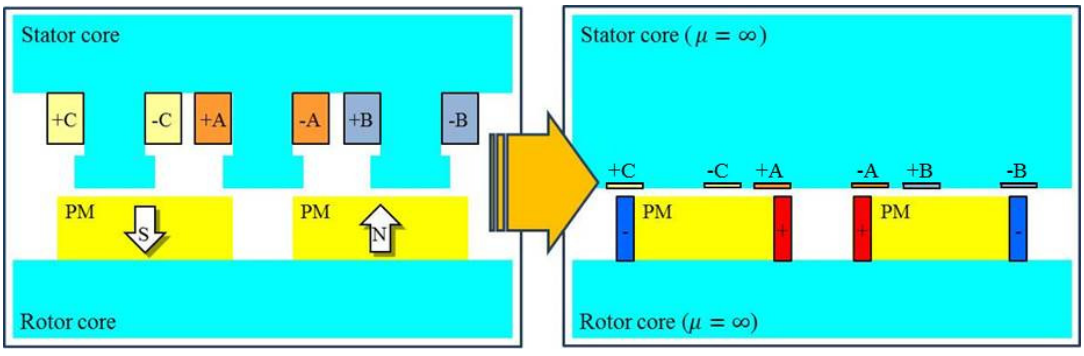

Fig. 1. A practical motor geometry and the corresponding analysis conditions for SHA

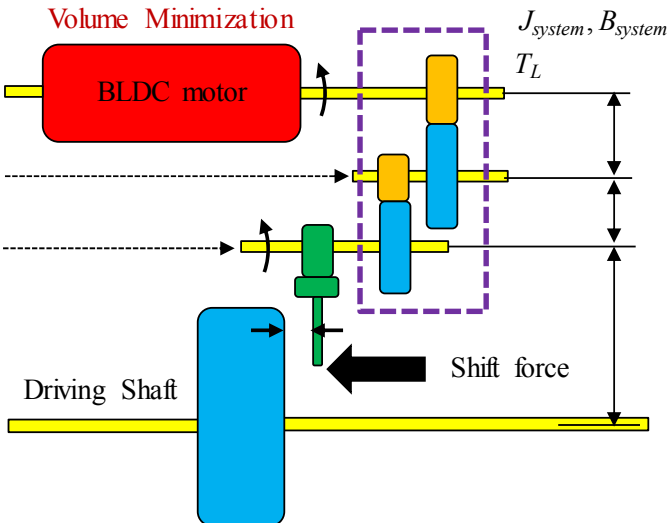

Fig. 2. Schematic view of dual clutch transmission system for electric vehicle

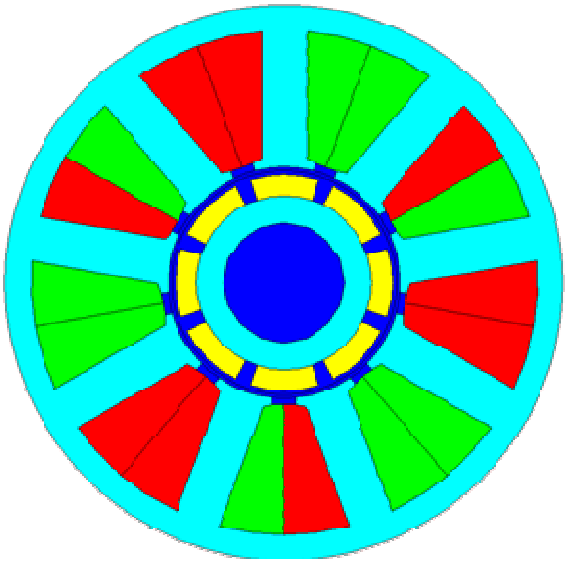

Fig. 3. An optimum 9-slot and 8-pole model(The SHA is used for optimum design process)

First Principles Calculation on Magnetism and Magnetocrystalline Anisotropy of $FeNi_3$

Mun Bong Hong*, S. H. Rhim, and S. C. Hong
Department of Physics and EHSRC, University of Ulsan, Ulsan 44610 Korea

$FeNi_3$ alloy is a typical soft magnetic material which has high saturation (100 emu/g), high Curie temperature (575), and high permeability. Soft magnetic materials are widely used in electronic devices such as magnetic sensors and magnetic recording heads. $FeNi_3$ has the structure consisting of one iron atom and three nickel atoms per unit cell. It is experimentally known that the lattice constant of $FeNi_3$ is a=5.63 Å, the magnetic moments of iron and nickel are 2.81 and 0.62, respectively.

In the present calculation, at total energy minimum unstrained lattice constant is 5.64 Å and the magnetic moments of iron and nickel are 2.81 μ_B and 0.62 μ_B, respectively. To investigate strain effects on magnetism and magnetocrystalline anisotropy (MCA) of $FeNi_3$, we take lattice constants of the ab plane from -3% to +3% and optimize the c-axis. At the -3% strain, the magnetic moments of iron and nickel are 2.81 μ_B and 0.62 μ_B, respectively and the MCA is +0.727 meV. At the +3% strain, the magnetic moments of iron and nickel are 2.79 μ_B and 0.61 μ_B, respectively and the MCA is +0.13 meV. The results, which both of positive and negative strains result in the same sign of MCA energy, is interesting. We will discuss the mechanism of the MCA energies with band structures.

Intrinsic Spin Hall Effect in Ferromagnetic Metal-Heavy Metal Interface

Do Duc Cuong*, Soon Cheol Hong† and S. H. Rhim†
Department of Physics and Energy Harvest Storage Research Center, University of Ulsan, Republic of Korea
†schong@ulsan.ac.kr, †sonny@ulsan.ac.kr

Recent developments in spintronics have focused in utilizing various material classes, where ferromagnetic metal (FM) -heavy metal (HM) superlattice or interface is one example. It is expected to have non-negligible spin-orbit coupling in this heterogeneous material combination, either or both intrinsic or/and interfacial one. Spin Hall effect, a generation of transverse spin current from longitudinal current, is expected in FM/HM interface, whose application is needless to emphasize. Here, we investigate various types of FM/HM interfaces (FM=Fe and Co) and (HM=Pt, Pd, Ta, W) using density functional theory with Wannier function approach to explicitly calculate the transverse spin Hall conductivity in the framework of Kubo formula. Analysis of *k*-resolved Berry curvature as well as traditional band structure elucidates spin-orbit splitting in superlattice, inherently more complicated than simple metal cases.

A study hall effect on CoSiB/Pt/CoSiB structure

Y. K. Kim*, Hana Lee†, T. W. Kim†
Sejong Univ., Gunja-dong, Gwangjin-gu, KS013, Seoul, Korea

magnetic recording media and magnetic sensors using Magnetic recording films. Magnetic recording films were extensively studied using magnetic recording media and magnetic sensors. Natural hall effects of metal and alloys resulting from spin orbital interaction are much larger than conventional Hall effects due to roundworm forces. Some materials show a wide range of hall effects suitable for Hall sensors. The study conducted an experiment on Hall effect.

The manufacture of the thin film manufacturing equipment was used by the souttering system, and the deposition conditions were fixed to CoSiB-0.4Å/s, Pt- 0.8-Ås, Ta-5.0Å/s, and evaporation stacks Ta80 / Pt 30/CoSiB 15/Pt 8/CoSiB15/Pt30Å. To check the difference between bulk and patterng, 5 inch crome mask was produced and compared.

When measured during the Bulk condition and pattered, the coercivity value indicated a small piece of soft graph indicating a soft graph, and the resistance was about 2 %. Even in the case of pattern, the Coercivity value represented a gradient of 1, and the resistance was slightly smaller than the bottom of the buckle.

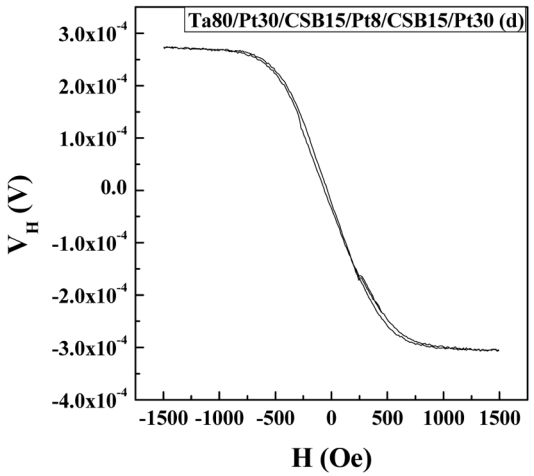

Fig 1. This is the graph measured Ta80 / Pt30 / CoSiB15 / Pt8 / CoSiB15 / Pt30Å stack

『This work was wupprted by the Korea Evaluation Institute of Industrial Technology(10054578)』
『This work was wupprted by the sejong Univ.(20170172)』

Bio-selective logical separation for magnetically driven superparamagnetic beads and cells using multi-frequencies on the Micro-magnetic ellipsoid pathways

Jonghwan Yoon*, Yumin Gang, Yehri Kim, Simsung Bae, Yuna Kim,
Jiwon Chae and Cheol Gi Kim†
Department of Emerging Materials Science, DGIST, Daegu 42988, Korea
cgkim@dgist.ac.kr

We demonstrate a separation method for the mixture of superparamagnetic beads and cells using ellipsoid pathways under an in-plane rotating magnetic field. The non-linear dynamics of the beads moving along the micro-magnetic disk pathways at multi-frequencies can be divided into three regimes, including phase-locked regime, phase-slipping regime and phase-insulated regime at each specific critical frequency. In this work, theoretically we demonstrate that the beads rotating along the periphery of the ellipsoid pathways exploits other dynamic regimes in addition to the three dynamic regimes to achieve bio-selective functionality. Here, we can control the bead jumping location and jumping distance by tuning the geometrical parameters of ellipsoid pattern and by changing the size of the beads/cells when they are rotating along the ellipsoid pathways. In this work, from the complex mixtures of beads + cells, we separate the beads from cells and created the single-cell environmental platform.

Keywords: Superparamagnetic beads, cells, dynamic regimes, ellipsoid pathways, Jumping location, Jumping distance, logical separation

References

[1] Byeonghwa Lim et al. Nat. Commun. 5,3846 (2014).
[2] Xinghao Hu et al. J. Appl. Phys. 118, 203904 (2015).
[3] X. H. Hu et al. IEEE Trans. Magn. 49, 1 (2013).
[4] Byeonghwa Lim et al. NPG Asia Mater. 9 e369 (2017).

Annealing Temperature Influence on Spin Pumping in a CoFeB/Pt Structure

Nyun Jong Lee*, Sang-Il Kim, and Seung-Young Park†
Spin Engineering Physics Team, Division of Scientific Instrumentation, Korea Basic Science Institute, Daejeon 34133, Korea

We investigate the influence of annealing temperature (T_a) on spin pumping in a CoFeB/Pt bilayer structure using a broadband coplanar waveguide ferromagnetic resonance (CPW-FMR). The spin pumping induced spin current has been measured as an enhancement in the Gilbert damping α of the ferromagnetic layer [1-3]. The field derivative FMR absorption spectra were acquired by sweeping the external magnetic field for a set of microwave frequencies. The magnetic damping parameter α extracted from the ferromagnetic resonance field (H_{res}) and the peak-peak line width obtained by fitting the absorption data. The intensity of the generated spin current is sensitive to the FM/NM interface properties. A crystallization of CoFeB film can induce a structural change at the CoFeB/Pt interface. Several temperatures between 300 and 400°C were chosen as T_a because an amorphous CoFeB thin film is crystalized by annealing at 375°C [4]. A CoFeB/Cu bilayer system is comparatively studied in order to rule out T_a dependence of the intrinsic damping. The T_a dependence of α can be understood in a perspective of interfacial structure with presence and absence of the magnetic proximity effect (MPE) [5].

References

[1] Y. Tserkovnyak, A. Brataas, and G. E. W. Bauer, Phys. Rev. Lett. 88, 117601 (2002)
[2] T. Taniguchi and H. Imamura, Phys. Rev. B 76, 092402 (2007)
[3] T. Taniguchi and H. Imamura, Mod. Phys. Lett. B 22, 2909 (2008)
[4] J. Hayakawa, et al., Jap. Journ. Appl. Phys. 44, L587 (2005)
[5] A. Conca, et al., Phys. Rev. B 95, 174426 (2017)

Modulating Magnonic Band Structure in The Presence of Inhomogeneous Dzyaloshinskii-Moriya Interaction

Seung-Jae Lee[1*], Jung-Hwan Moon[2], Hyun-Woo Lee[3], and Kyung-Jin Lee[1,2]
[1]KU-KIST Graduate School of Converging Science and Technology, Korea University, Seoul 02841, Korea
[2]Department of Materials Science and Engineering, Korea University, Seoul 02841, Korea
[3]PCTP and Department of Physics, Pohang University of Science and Technology, Pohang 37673, Korea

1. Introduction

In magnetic systems with an inversion asymmetry and large spin-orbit coupling, the anti-symmetric exchange interaction called the Dzyaloshinskii-Moriya interaction (DMI) becomses non-negligible[1,2]. Recently the DMI effect on the spin wave propagation are expected on opening rich the spin wave physics and wide application in functional devices based on spin waves[3]. The magnonic crystal is a magnetic metamaterial with alternating magnetic media that serve as periodic potential for spin-waves passing through it and construct spin-wave band structure[4]. For practical application of magnonic devices, however, there are some challenges from a small on/off ratio of spin-wave signal. For this purpose, like traditional electronic logic devices based on field-effect transistors, we demonstrate modulating the spin-wave bandgap by and external things with magnonic crystals by using inhomogeneous DMI. In this work, based on theoretical approach and micromagnetic simulation, we demonstrate modulating magnonic band structure either by an external magnetic field or an electric voltage.

2. Simulation Scheme

We investigate spin-wave propagation in magnonic crystal with alternating DMI by using spin-wave version of the Kronig-Penny model and Landau-Lifshitz-Gilbert equation. We use following parameters; nanowire length is 4 μm, the unit cell size along the spin-wave propagation direction is 2 nm, the saturation magnetization is 800 emu/cm^3, damping constant is 0.01, exchange stiffness constant is 1.3 x 10^{-6} erg/cm, DM constant in region 1 is 0 erg/cm^2, the external magnetic field is 5000 Oe, the effective perpendicular magnetocrystalline anisotropy Ku is assumed 0 erg/cm^3.

3. Result and Discussion

Figure 1 (b) and (c) show that magnonic band structure can be modulated by the direction of external magnetic field and ΔD ($=D_2-D_1$). In Fig. (b), we find that the change in the second forbidden band in magnonic band structure can be very large with varying $\theta = 0$ to $\theta = \pi/2$. In Fig. (c), we also find the magnonic band structure can be large modulated with varying D_2 = 1 erg/cm^2 to D_2 = 3 erg/cm^2. These large tunability of magnonic band structure can be reproduce on/off ratio of spin-wave signals.

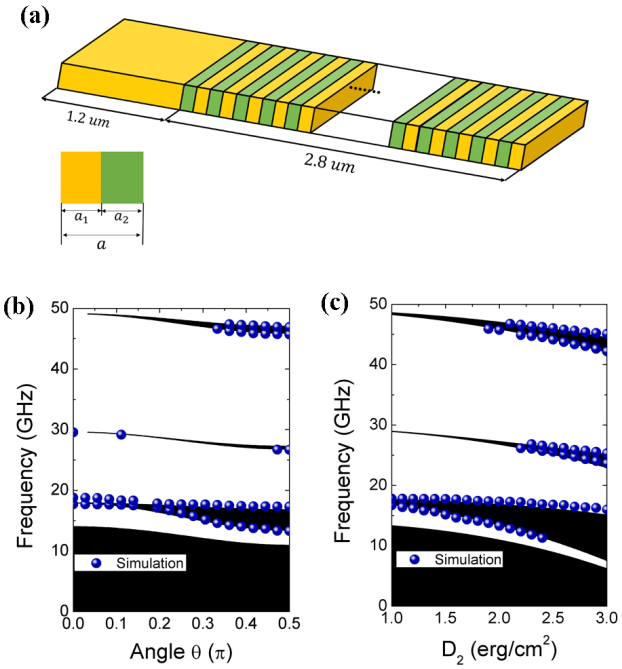

Fig. 1. (a) The schematic diagram of a magnonic crystal with alternating DMI. (b) The spin-wave frequency versus the angle. (c) The spin-wave frequency versus D_2

Correction of thermoelectric artifacts in second harmonics measurements

Eun-Sang Park[1,2*], Byoung-Chul Min[2], Kyung-Jin Lee[1,2,3]
[1]KU-KIST Graduate School of Converging Science and Technology, Korea University
[2]Center for Spintronics, Korea Institute Science and Technology
[3]Department of Materials Science and Engineering, Korea University

Recent study of spin-orbit torque (SOT) shows a new route to control the magnetization of nano magnets, and it becomes a very important part of the spintronics. The SOT have shown interesting physical features, for instance, such as unusual angular dependence, that cannot be simply explained by spin Hall effect. To understand the features, it is important to quantitatively measure the magnitude, symmetry, and angular dependence of SOT. Harmonics measurements, the one of several methods for SOT measurements, are frequently used for determining the magnitude of SOT because of its simplicity [1]. If a temperature gradient exists in the sample, thermoelectric artifacts can be included in the SOT harmonics measurement.

Here we have studied those thermoelectric artifacts in SOT harmonics measurements, and how to eliminate them. A nominally measured Hall signal can be influenced by several artifacts such as Seebeck, Nernst, Ettingshausen, Righi-Leduc effects as well as misalignment and Ohmic offsets. We find that the thermoelectric artifacts contaminate the second harmonic signals. The measured SOT contaminated by thermoelectric artifacts can be either overestimated or underestimated depending on the current bias and magnetic field direction. We have shown that those artifacts can be eliminated by considering the sign symmetry of current and field in the second harmonics. The correction of thermoelectric artifacts in second harmonics measurements shows that the angular dependence of SOT could be significantly distorted by those artifacts and the overestimation of SOT could be as twice large as the pristine magnitude of SOTs.

Reference

[1] Pi, U. H. et al. *Appl. Phys. Lett.* **97**, 162507 (2010)

Experimental Observation of Spin Memory Loss in FMR Spin Pumping Across CoFeB/Pt Interface

Sang-Il Kim[1,2*], Dongjoon Lee[3], Oukjae Lee[4], Seung-Young Park[2], and Kyung-Jin Lee[1,3]

[1]Department of Materials Science and Engineering, Korea University, Seoul 136-713, South Korea

[2]Spin Engineering Physics Team, Division of Scientific Instrumentation, Korea Basic Science Institute, Daejeon 305-806, South Korea

[3]KU-KIST Graduate School of Converging Science and Technology, Seoul 136-713, South Korea

[4]Center for Spintronics, Korea Institute of Science and Technology, Seoul 02792, South Korea

Recently spin-orbit-torques have attracted a lot of attention because the utilization of pure spin current (J_s) provides more efficient methods for the magnetic switching [1]. So far the spin pumping and inverse spin-Hall effect (ISHE) has been used as one of the electrical methods to detect J_s [2]. In addition, Ref. [3] recently proposed an advanced spin-pumping theory, taking account of both Rashba spin orbit coupling (RSOC) at the interface of ferromagnet (FM)/heavy-metal (HM) and the backflow of J_s from the HM to FM. According to the theory, due to the interfacial RSOC, the amount of transmitted J_s is significantly lost at the interface, which is referred to as a spin-memory loss (SML) [3]. Therefore, it is important that during the spin-pumping experiments using the FM/HM structure we should consider the effect of SML in the transmission of J_s through the interface.

Here we experimentally investigated the Gilbert damping constant (α) in CoFeB(10 nm)/Pt(t_{Pt}) bilayers as a function of the Pt thickness (t_{Pt}), using ferromagnetic resonance and coplanar waveguide method. By now, it was very difficult to observe the SML because the value of α is almost constant for the thick Pt layer($t_{Pt} > \lambda_{Pt}$, spin diffusion length of Pt) and the magnitude of α gradually decreases to zero($t_{Pt} < \lambda_{Pt}$)[4]. But we observed that the values of α, which were obtained using the f_0-sweeping FMR, steadily increases as t_{Pt} decreases, especially when it is less than the λ_{Pt} as seen in Figure 1. From the analysis based on the theory, we supposed that the SML magnitude at the CoFeB/Pt interface is about 90% because J_s is considerably dissipated. We additionally

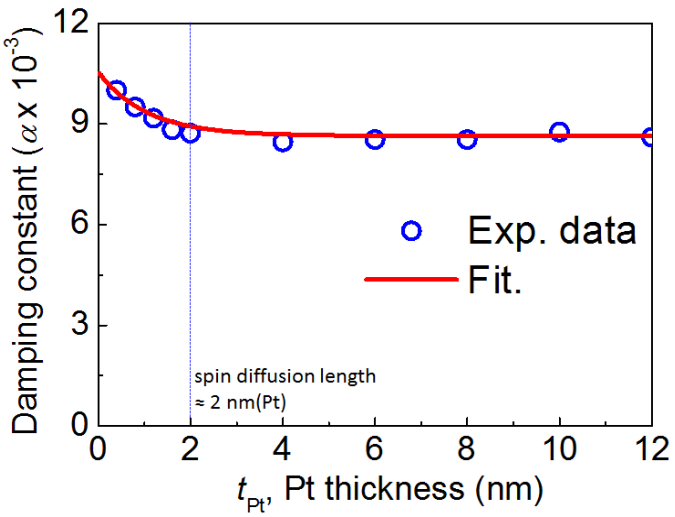

Fig. 1. The measured α as a function of t_{Pt} in the CoFeB(10nm)/Pt(t_{Pt})

performed structural analyses using the X-ray reflectometry (XRR) and the transmission electron microscopy (TEM) in order to support the behavior, the enhancement of α with decreasing t_{Pt} (when < λ_{Pt}). The results provide more insight into the variation of α in the CoFeB/Pt(t_{Pt}) bilayers as we will provide more in this presentation.

References

[1] L. Liu et al., Science **336** 555 (2012).

[2] E. Saitoh et al., Appl. Phys. Lett. **88** 182509 (2006).

[3] K. Chen et al., Phys. Rev. Lett. **114** 126602 (2015).

[4] M Belmeguenai et al., J. Phys. D: Appl. Phys. **50** 135002 (2017).

Huge Domain-Wall Speed Variation with Respect to Ferromagnetic Layer Thickness in Ferromagnetic Pt/Co/TiO_2 Films

Dae-Yun Kim*, Min-Ho Park, Ji-Sung Yu, and Sug-Bong Choe
Department of Physics and Astronomy, Seoul National University, Korea

Here, we investigate the influence of ferromagnetic layer thickness on magnetization process. A series of ultrathin Pt/Co/TiO_2 films exhibits domain-wall (DW) speed variation over 100,000 times depending on the ferromagnetic layer thickness, even under the same magnetic field. From the creep scaling analysis, such significant variation is found to be mainly attributed to the thickness dependence of the creep scaling constant, in accordance to the creep scaling theory with the linear proportionality between the creep scaling constant and ferromagnetic layer thickness. Therefore, thinner film shows faster DW speed. The domain-wall roughness also exhibits sensitive dependence on the ferromagnetic layer thickness: thinner film shows smoother DW roughness. The present observation guides the optimal design rule of the ferromagnetic layer thickness for better performances of the domain-wall-based devices.

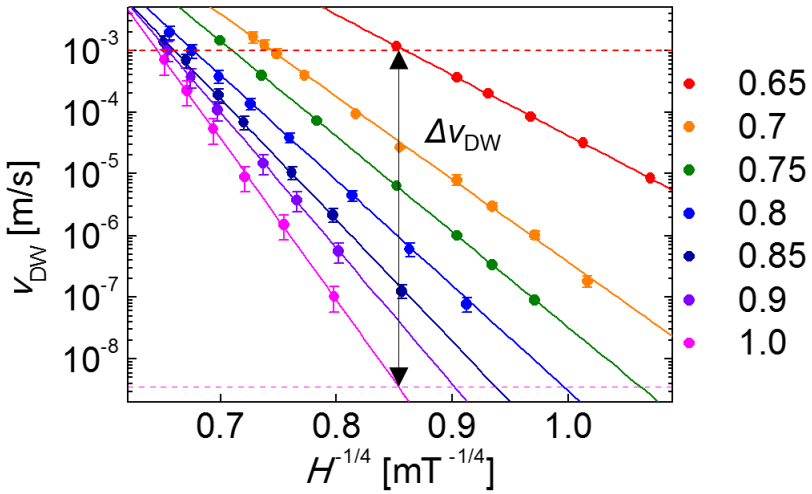

Fig. 1. Plot of DW speed v_{DW} as a function of $H^{1/4}$.

Collective breathing modes of 1D skyrmion lattices in nanostrips

Junhoe Kim*, Jaehak Yang, Young-Jun Cho, Bosung Kim, and Sang-Koog Kim
National Creative Research Initiative Center for Spin Dynamics and Spin-Wave Devices, Nanospinics Laboratory, Research Institute of Advanced Materials, Department of Materials Science and Engineering, Seoul National University, Seoul 08826, South Korea

Magnetic skyrmions are topological solitons that have been intensively studied due to the fundamental and technological perspectives [1]. For example, single skyrmions in geometrically restricted magnetic dots exhibit unique GHz-range dynamic motions such as lower-energy gyration modes and higher-energy breathing modes [2,3]. Therefore, microwave generators and detectors have been proposed based on their inherent dynamic modes [4,5]. Very recently, the collective gyration modes in coupled individual skyrmions have been explored as information carriers [6], as analogous to propagating gyration modes in physically connected or separated vortex-state disks [7,8]. Here, we report on a delicate study, using micromagnetic numerical simulations, of dynamic coupling of breathing modes in one-dimensional (1D) skyrmion lattices periodically arranged in thin-film nanostrips. The coupled breathing modes exhibit characteristic concave-down dispersions that represent the in-phase high-energy mode at zero wavenumber (k=0) and the anti-phase low-energy mode at the Brillouin zone boundary (k=k_{BZ}). The band width of the allowed modes increases with decreasing inter-distance between nearest-neighboring skyrmions. Furthermore, the collective breathing modes propagate well through the thin-film nanostrips, as fast as 200 ~ 700 m/s, which propagation is controllable by the strength of magnetic fields applied perpendicularly to the film plane. The breathing modes in 1D skyrmion lattices formed in such nanostrips possibly can be used as information carriers in information processing devices.

References

[1] A. Fert, V. Cros, and J. Sampaio, Nature Nanotechnol. 8, 152 (2013).
[2] M. Mochizuki, Phys. Rev. Lett. 108, 017601 (2012).
[3] Y. Onose, Y. Okamura, S. Seki, S. Ishiwata, and Y. Tokura, Phys. Rev. Lett. 109, 037603 (2012).
[4] C. P. Chui and Y. Zhou, AIP Advances 5, 097126 (2015).
[5] S. Zhang *et al.* New J. Phys. 17, 023061 (2015).
[6] J. Kim, J. Yang, Y.-J. Cho, B. Kim, and S.-K. Kim, Sci. Rep. 7, 45185 (2017).
[7] D.-S Han *et al.* Sci. Rep. 3, 2262 (2013).
[8] H.-B. Jeong and S.-K. Kim, Appl. Phys. Lett. 105, 222410 (2014).

Chirality-dependent standing spin-wave modes in soft magnetic nanotubes

Jaehak Yang*, Junhoe Kim, Bosung Kim, Young-Jun Cho, Jae-Hyeok Lee, and Sang-Koog Kim
National Creative Research Initiative Center for Spin Dynamics and SW Devices, Nanospinics Laboratory,
Research Institute of Advanced Materials, Department of Materials Science and Engineering,
Seoul National University, Seoul 08826, South Korea

With the increasing demand for magnetically controlled nanostructures of novel functionalities in the fields of spintronics [1, 2] and bio-applications [3, 4], advanced technologies enabling exploration of novel dynamic properties as well as synthesis and characterization of nano-scale magnetic structures have been subjects of growing interest. In fact, over the past few decades, nanometer-scale non-uniform magnetic structures [5, 6] such as magnetic domain walls, magnetic vortices, antivortices, and skyrmions in nanodots and nanowires have been attracting increasing attention for their potential applications as data-storage devices and information carriers. Magnetic nanotubes distinguish themselves from magnetic nanowires by their avoidance of magnetic point singularities along the tube axis. Thereby, they exhibit various and intricate magnetic properties such as controllable and faster reversal processes.

In the present study, spin-wave modes excited in cylindrical nanotubes of finite length were investigated using finite-element micromagnetic simulations [7]. From the simulation results along with the relevant analytical interpretation, we found unique dynamic modes representative of a variety of standing spin-wave modes. Those modes are controllable not only according to the geometric confinements of given nanotubes but also by the relative configuration of the vortex-chirality at both ends of the nanotubes. Using a simple analytical model, we estimated the quantized dispersions of the excited modes that agree with the simulation results. This work facilitates further understanding of discrete standing spin-wave modes in three-dimensional curvilinear nano-elements such as cylindrical nanotubes, and opens up a broader and deeper perspective on chirality-dependent spin-wave modes.

References

[1] C. Chappert, A. Fert, and F. N. Van dau, “The emergence of spin electronics in data storage”, Nature Materials **6**, 813 (2007).

[2] R. Lavrijsen, J.-H. Lee, A. Fernández-Pacheco, D. Petit, R. Mansell, and R. P. Cowburn, “Magnetic ratchet for three-dimensional spintronic memory and logic”, Nature **493**, 647 (2013).

[3] D. -H. Kim, E. A. Rozhkova, I. V. Ulasov, S. D. Bader, T. Rajh, M. S. Lesniak, and V. Novosad, “Biofunctionalized magnetic-vortex microdiscs for targeted cancer-cell destruction”, Nat. Mater. **9**, 165 (2010).

[4] D. F. Gutierrez-Guzman, L. I. Lizardi, J. A. Otálora, and P. Landeros, “Hyperthermia in low aspect-ratio magnetic nanotubes for biomedical applications”, Appl. Phys. Lett. **110**, 133702 (2017).

[5] C. Kittel, “Physical Theory of Ferromagnetic Domains”, Rev. Mod. Phys. **21**, 541 (1949).

[6] Skyrme, T. H. R., “A unified field theory of mesons and baryons”, Nucl. Phys. **31**, 556–569 (1962).

[7] D. Suess, and T. Schrefl, FEMME: Finite Element MicroMagnEtics 5.0.9 (SuessCo, http://suessco.com/).

Temperature dependence of magnetizations in GdFe sublattice

Jaegun Sim*, Jae-Hyeok Lee and Sang-Koog Kim
National Creative Research Initiative Center for Spin Dynamics and Spin-Wave Devices, Nanospinics Laboratory,
Research Institute of Advanced Materials, Department of Materials Science and Engineering,
Seoul National University, Seoul 08826, South Korea

Demand for high-density memory devices has increased dramatically over the last few decades. Magnetic storage technologies such as hard disk drives offer the advantage of digital storage because of their superior price and capacity compared with competing technologies. In recent years, research on HAMR (Heat-assisted Magnetic Recording) technology that changes the direction of magnetization using a laser has been underway [1,2]. HAMR's technology significantly increases the amount of data by allowing writing at a much smaller scale than before. However, in order to improve the magnetic memory devices in the future, it is necessary to understand the intrinsic mechanisms in which magnetization processes takes place. Vahaplar et al. observed using a laser pulse to change the direction of magnetization of GdFeCo material [3]. Ostler et al. presented a computational model of crystallographically amorphous GdFe material and compared the experiment results with those of GdFe calculated by a stochastic Landau-Lifshitz-Gilbert equation for atomistic spins and an atomistic spin Hamiltonian [4].

Here, we calculate the temperature dependence of sublattice magnetizations over a range of Gd concentrations [4]. In this calculation, we used VAMPIRE software package that uses a simple text file format to define and run an atomistic simulation [5]. The magnetization directions of Fe and Gd are opposite to each other and therefore exhibit antiferromagnetic coupling between the sublattices. Compensation point exists for Gd concentration in the range 24%-44%, and the point increases linearly with Gd concentration [6]. After the compensation point, on the other hand, the magnetization of the Fe sublattice becomes lager than that of the Gd sublattice. In addition, we confirm that Curie temperature and Gd concentration are inversely proportional. Those results are the same as those reported in Ref. 4. We confirmed that atomistic simulations of magnetic materials can be used to understand the mechanism of laser induced magnetization dynamics.

References

[1] R.E. Rottmayer, S. Batra, D. Buechel, W.A. Challener, J. Hohlfeld, Y. Kubota, L.Li, B. Lu, C. Mihalcea, K. Mountfield, K. Pelhos, C. Peng, T. Rausch, M.A. Seigler, D. Weller, X. Yang, IEEE Trans. Magn. 42, 2417 (2006)

[2] M.H. Kryder, E.C. Gage, T.W. McDaniel, W.A. Challener, R.E. Rottmayer, G. Ju, Y.-T. Hsia, and M.F. Erden, Proc. IEEE 96, 1810 (2008).

[3] K. Vahaplar, A.M. Kalashnikova, A. Kimel, D. Hinzke, U. Nowak,R. Chantrell, A. Tsukamoto, A. Itoh, A. Kirilyuk, and T. Rasing, Phys. Rev. Lett. 103, 117201 (2009).

[4] T.A. Ostler, R.F.L. Evans, R.W. Chantrell, Phys. rev. B. 84, 024407 (2011)

[5] R.F.L. Evans, W.J. Fan, P. Chureemart, T.A. Ostler, M.O.A. Ellis, R.W. Chantrell, J. Phys.: Condens. Matter 26, 103202 (2014).

[6] P. Hansen, C.Clausen, G.Much, M. Rosenkranz, J. Appl. Phys. 66, 756 (1989)

Improvement of Micro-Bead Detection Performance by Using Anisotropic Magnetoresistance Sensor

Dong Young Kim[1*], Seok Soo Yoon[1], Jae Hoon Lee[2], Cheol Gi Kim[2]
[1]Depearment of Physics, Andong National University, Korea
[2]Department of Emerging Materials Science, DGIST, Korea

The micro sized magnetic bead has been used for early stage diagnosis of various diseases. The micro sized magnetic sensor is required to detect such a micro sized magnetic bead. The one of the best candidate sensor is the anisotropic magnetoresistance (AMR) sensor because of low noise properties. In this work, we fabricated the multi-ring sensor by using exchange biased NiFe/MnIr bilayers material and measured the AMR profiles with magnetic field at various angles θ_H. We confirmed that the measured AMR profiles were well fitted with calculated ones. The calculation method was applied to the analysis of bead signal in order to improve the micro sized bead detection performance. The bead signals increased, as the magnetic field angle increased from hard axis. We obtained high detection performance of micro sized bead signal at optimized magnetic field and field angle by using AMR sensor. The calculated bead detection performance will be compared with measured ones.

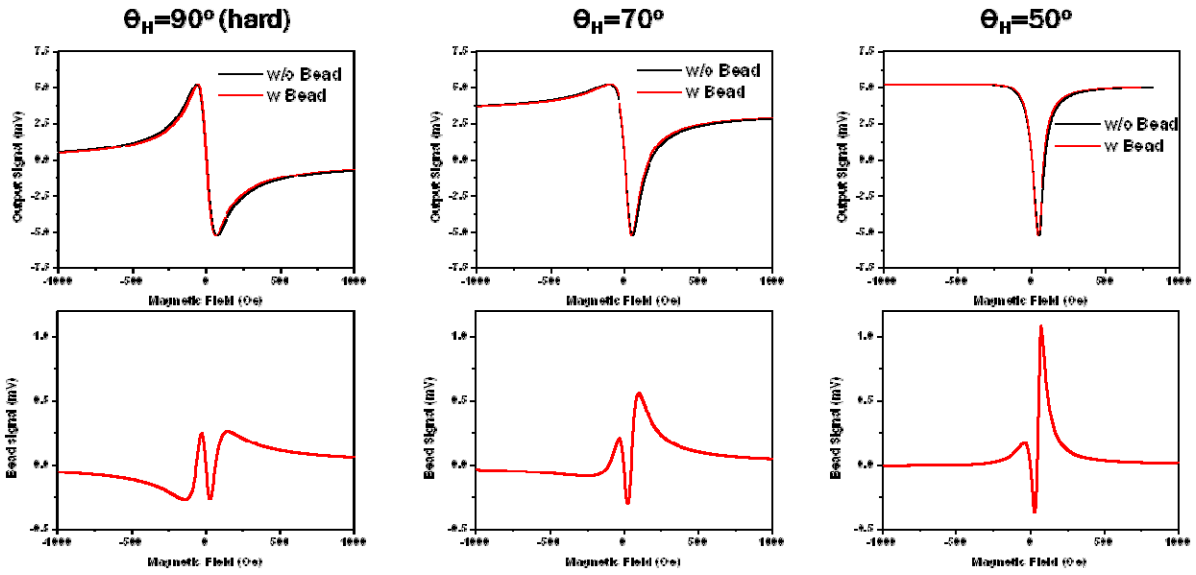

Fig. 1. AMR profiles w/o and w Bead, and bead signal profiles at Θ_H =90, 70, 50°

Acknowledgement

This work was supported by the DGIST R&D Program of the Ministry of Science, ICT and Future Planning (17-BT-02).

Synchronization of parallel-connected spin-torque nano-oscillators

Hee Gyum Park*, Chaun Jang, and Byoung-Chul Min
Center for Spintronics, Korea Institute of Science and Technology, Seoul, Korea

The spin-transfer torque (STT) from spin-polarized current to the local magnetization of magnetic tunnel junction (MTJ) generates a microwave signal under certain conditions of external magnetic field and current bias [1]. This new type of microwave generator – namely spin-torque nano-oscillators (STNOs) – have great advantages in terms of very wide operating frequency ranges, high modulation rates, and fabrication processes compatible with RF CMOS, but it also have critical disadvantages such as lower power and broad linewidth which hinders the real applications of STNO-based wireless communications [2]. The synchronization of multiple STNOs is one of solutions to overcome those disadvantages [3].

We have studied the electrical synchronization of two STNOs connected in parallel. Two STNOs are presumably under the same external magnetic field while each STNO is independently supplied by individual DC current sources and bias tees. The microwave signal measured by a spectrum analyzer showed two distinguished peaks from the electrically-combined two STNOs: one peak at a lower center frequency ($_{C1}$ 2.76 GHz, PSD_1 14 nW/GHz) with a high bias current (I_{DC1} 14 mA), and the other peak at a higher center frequency ($_{C2}$ 3.07 GHz, PSD_2 14 nW/GHz) with a low bias current (I_{DC2} 12 mA). Electrical synchronization of two oscillators was not achieved with various combinations of I_{DC1} and I_{DC2} at zero external magnetic field. As the external field was increased, the two distinguished peaks were gradually merged to a single peak ($_{C}$ 2.7 GHz, PSD 38 nW/GHz). The RF power enhancement and broad linewidth of the merged peak indicate the frequency pulling or partial synchronization of two oscillators.

References

[1] S. I. Kiselev *et al.,* Nature 425, 380 (2003).
[2] H. S. Choi *et al.,* Sci. Rep. 4, 5486 (2014).
[3] B. Georges *et al.,* Phys. Rev. Lett. 101, 017201 (2008).

Magnetic properties and anomalous Hall effect of CoFeB/MgO thin films on the amorphous magnetic FeZr buffer layer

Ji Hoon An[1*], Sang Ho Lim[2]

[1]Department of Semiconductor System Engineering, Korea University, Seoul, 136-716, Korea

[2]Department of Materials Science and Engineering, Korea University, Seoul, 136-716, Korea

It is well known that the large Hall effect is generated from magnetic materials due to anomalous Hall effect (AHE). Using the AHE, magnetic field sensors of which sensitivity is larger than that of conventional semiconductor based Hall sensors can be realized. Because the hall voltage from AHE (V_{AH}) is proportional to a perpendicular component of magnetization (M_z), magnetic materials that exhibit perpendicular magnetic anisotropy (PMA), such as Co/Pt multilayers, $L1_0$-ordered alloys and RE-TM alloys, have been studied for sensor applications. Among these materials, CoFeB/MgO thin films have advantages: high Hall resistivity and tunable PMA. Extremely large sensitivity of 2.376 Ω/Oe is obtained from MgO/CoFeB/Ta/MgO structure [1].

In this study, magnetic amorphous FeZr is used as a boron absorption layer (buffer layer) instead of Ta. Thin films with the stacks of $Fe_{50}Zr_{50}$ (t_{FeZr} = 1–5 nm)/$Co_{20}Fe_{60}B_{20}$ (t_{CoFeB} = 1.0 & 1.2 nm)/MgO (1 nm)/Ta (1 nm) were deposited on the wet oxidized Si substrates using UHV DC/RF magnetron sputtering system and annealed at 175–250°C for 1h. Two important properties, anomalous Hall voltage and saturation magnetic field, were obtained from Hall measurement using Van der Pauw method. These properties depend on t_{FeZr}, t_{CoFeB}, and T_{anneal}, and what plays a key role is B diffusion during annealing (Here, t_{FeZr}, t_{CoFeB}, $T_{annaeal}$ indicate the thickness of FeZr, CoFeB, and annealing temperature, respectively). For this reason, these variables should be set properly for high sensitivity. The maximum sensitivities, S_I = 0.201 mV/Oe (at 1 mA) and S_V = 0.290 mV/Oe (at 3 V) were obtained from FeZr (2 nm)/CoFeB (1.0 nm)/MgO/Ta annealed at 250°C. These values are lower than those from films with Ta due to larger saturation magnetic field. However, FeZr/CoFeB/MgO films are still attractive, in that they generate larger signal owing to AHE from FeZr layer.

Reference

[1] T. Zhu *et al*. Appl. Phys. Lett. 104, 240404 (2014)

Magnetic properties of cobalt based core-shell nanoparticles studied by Mössbauer spectroscopy

Jeongho Park*, Hyunkyung Choi, Sam Jin Kim, Chul Sung Kim
Department of Physics, Kookmin University, Seoul, Korea

We have investigated the magnetic properties of cobalt based core-shell nanoparticles (NP) of CoFe2O4@MgFe2O4 and $CoFe_2O_4$@$AlFe_2O_4$ prepared by the HTTD method. The core-shell NPs has been investigated by X-ray diffraction, vibrating sample magnetometer, hyperthermia and Mössbauer spectroscopy. According to XRD analyzation by Rietveld refinement method, the nanoparticles has single phase and cubic spinel structure with space group *Fd-3m*. The lattice constants were found to be 8.3686 Å for CoFe2O4@$MgFe_2O_4$, 8.4207 Å for $Cofe_2O_4$@$AlFe_2O_4$. The size and morphology of the $CoFe_2O_4$@$MgFe_2O_4$ nanoparticles were confirmed by HR-TEM and using Scherrer's formula. The CoFe2O4@$MgFe_2O_4$ and $Cofe_2O_4$@$AlFe_2O_4$ saturation magnetization were 77.9 emu/g and 52.2 emu/g, respectively. The self-heating temperatures of CoFe2O4@ MgFe2O4 and CoFe2O4@AlFe2O4 were had intermediate values of the materials used as core and shell. The increase in the self-heating temperature of core-shell nanoparticles was observed to be considerable over the first 100 s. The magnetic field was fixed at 250 Oe with a frequency of 112 kHz. The Mössbauer spectra of cobalt based core-shell NPs were performed taken at 4.2 K–295 K. The cobalt based nanoparticles can be considered to have soft-magnetic properties and confirmed by hyperthermia experiments. The core/shell nanoparticles structure investigated in this study has high saturation magnetization and moderate thermal property.

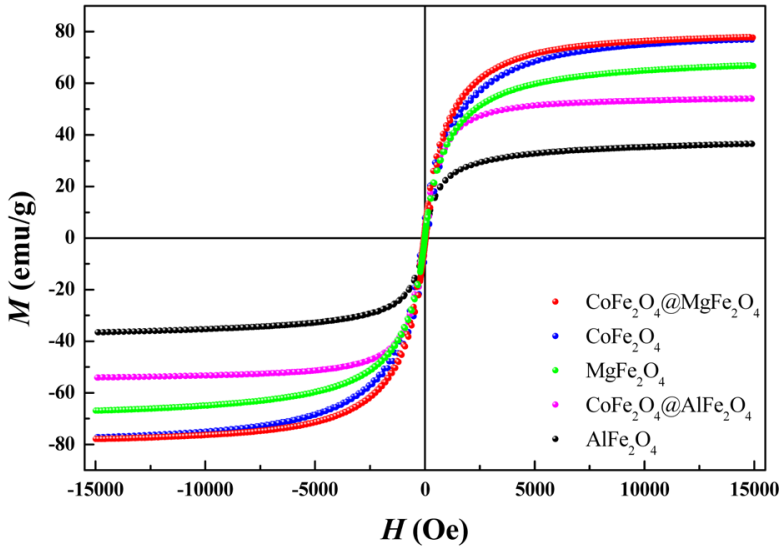

Fig. 1. Hysteresis loops measured at room temperature for the nanoparticles.

Anisotropic Exchange Stiffness Constant in Exchange Biased NiFe/MnIr Bilayers

Dong Young Kim*, Seok Soo Yoon
Department of Physics, Andong National University, Korea

The exchange stiffness constant A_{ex} was linearly propositional to the difference of spin wave resonance field H_{SWR} and ferromagnetic resonance field H_{FMR}. In this work, we measured the H_{SWR} and H_{FMR} with in-plane angles θ in order to compare with the angular dependence of A_{ex} in NiFe and exchange biased NiFe/MnIr bilayers. The A_{exo} of NiFe thin film showed isotropic behavior, which were not depending on the in-plane angles. However, the A_{ex} of exchange biased NiFe/MnIr thin film showed unidirectional anisotropic behavior. The A_{exo} of NiFe thin film was 10.9×10^{-7} erg/cm, while the A_{ex} of exchange biased NiFe/MnIr thin film depend on in plane angle such as $A_{exo} + A_{eb}cos\theta$. The angular dependence of $A_{eb}cos\theta$ in exchange biased NiFe/MnIr thin film was due to the unidirectional exchange bias effect at the interface between NiFe and MnIr.

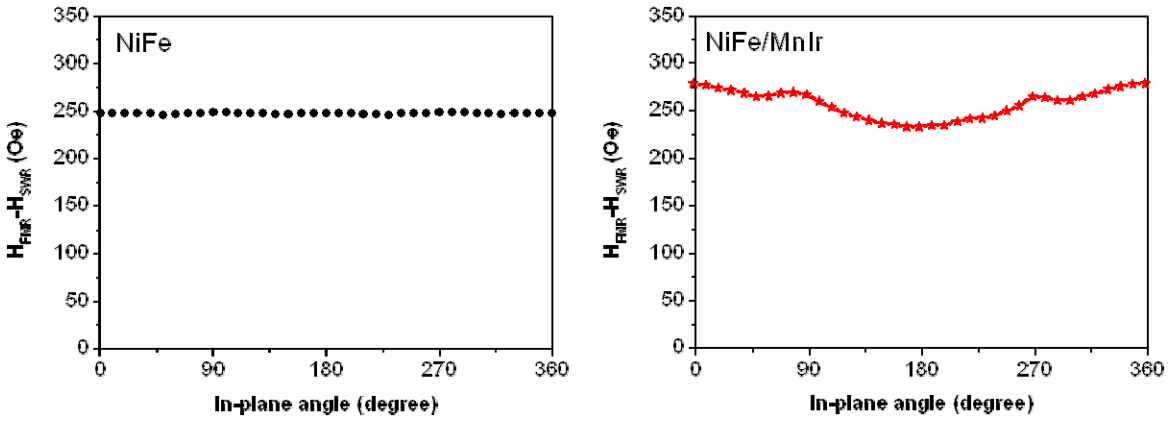

Fig. 1. H_{FMR}-H_{SWR} in NiFe thin film and exchange biased NiFe/MnIr bilayers

Spin Wave Modes in Out-of-Plane Magnetized NiFe Thin Film

Dong Young Kim*, Seok Soo Yoon
Department of Physics, Andong National University, Korea

The spin wave modes were easily excited in in-plane magnetized thin films, which were measured by using the ferromagnetic resonance technique. However, signal amplitude of spin wave resonance measured in out-of-plane magnetized thin film was very small compared with signal amplitude of ferromagnetic resonance. Therefore, the spin wave modes in out-of-plane magnetized thin film had not analyzed yet. In this work, we measured the spin wave resonance field H_{PSSW} and ferromagnetic resonance field H_{FMR} with out-of-plane angles θ_H in NiFe thin film. The perpendicular standing spin wave (PSSW) modes showed two different behaviors with out-of-plane magnetized angle. At low angle, the directions of PSSW and magnetization was perpendicular, the difference of H_{PSSW} and H_{FMR} linearly proportional to $1/cos\theta_H$. Near θ_H = 90°, the directions of PSSW and magnetization was parallel, the difference of H_{PSSW} and H_{FMR} linearly proportional to $1/sin\theta_H$. These two different PSSW modes were analyzed by the transverse and longitudinal propagation of spin wave in NiFe thin film.

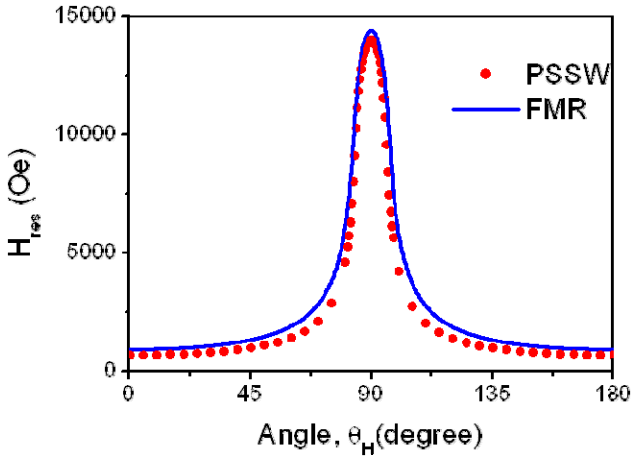

Fig. 1. Spin wave modes in out of plane magnetized NiFe film

Magnetoresistance Properties of Superconductor Hybrid GMR-SV Films with Nb and YBCO Buffer Layers

Woo-Il Yang[1], Jong-Gu Choi[2*], Sang-Suk Lee[2†]
[1]Department. of Applied Physics and Electronics, Sangji University, Wonju 26339, Korea
[2]Department. of Oriental Biomedical Engineering, Sangji University, Wonju 26339, Korea

The enhanced magnetoresistance(MR) properties of Nb, YBCO layers/NiFe(15 nm)/CoFe(5 nm)/Cu(2.5 m)/CoFe(5 nm)/NiFe(7 nm)/IrMn(10 nm)/Ta(5 nm) multilayer structure were investigated. The Nb and YBCO layers are the low and high temperature superconducting layers, respectively. The value of MR (↑↑) is lower than MR (↑↓), and one of remanent magnetization M(↑↑) is larger than M(↑↓). The critical temperature(Tc1) for parallel state is lower than (T_{c2}) for antiparallel state. T_{c1} and T_{c2} is lower than the original critical temperature(Tc) due to the remanent magnetization difference by the proximity effect at the interface of metal and superconductor, as shown in Fig. 1. Hybrid type GMR-SV films with Nb and YBCO buffer layers will be occurred to the variation of critical temperature of superconductor due to the remanent magnetization difference by the proximity effect in the interface of metal and superconductor. The positive MR versus magnetic field curve of hybrid superconductor/GMR-SV films at room temperature is compared with the negative MR versus magnetic field curve of hybrid superconductor/GMR-SV films at the neighborhood of critical temperature. It suggests that the MR curve of hybrid superconductor/GMR-SV films will be measured at the neighborhood of critical temperature can be represented a peculiar giant magnetoresistance ratio.

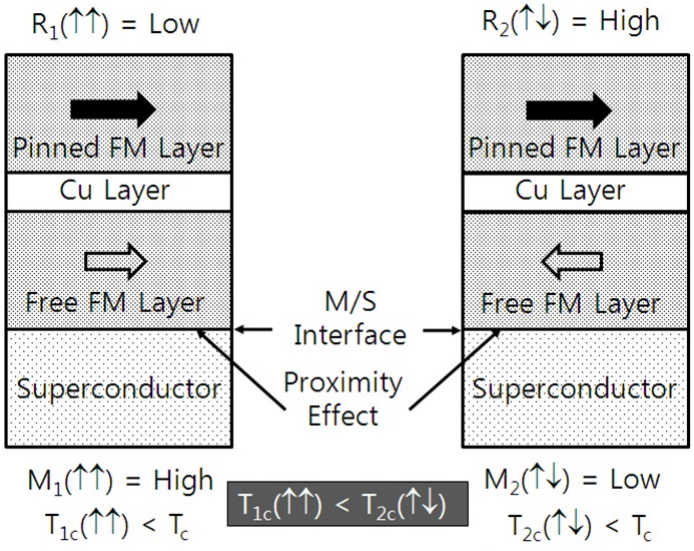

Fig. 1. Schematic for the hybrid superconductor/GMR-SV multilayer structure with parallel (↑ ↑, state 1) and antiparallel (↑ ↓, state 2) magnetization configuration.

Acknowledgments

This work was supported by the National Research Foundation of Korea (NRF) funded by the Korea government (Ministry of Education) with the Grant No. of NRF-2016R1D1A1B03936289.

Phase transition studies of the mixed olivine $LiFe_{0.8}Zn_{0.2}PO_4$ by Mössbauer spectrosocpy

Hyunkyung Choi[1*], Mun Hwan Kim[2], Chul Sung Kim[1]
[1]Department of Physics, Kookmin University, Seoul, Korea
[2]Dongin Semichem Co., Ltd., Hwaseong, Gydonggi-do, Korea

The $LiFe_{0.8}Zn_{0.2}PO_4$ polycrystalline sample has been investigated by X-ray diffraction, vibrating sample magnetometer and Mössbauer spectroscopy. The crystal structure of the $LiFe_{0.8}Zn_{0.2}PO_4$ sample by using Rietveld refinement was determined to be orthorhombic with the space group *P*nma. The lattice constants were a_0 = 10.2918 Å, b_0 = 5.9986 Å, c_0 = 4.6949 Å, respectively. The temperature dependence of zero-field cooled(ZFC) and field-cooled(FC) magnetizaition for $LiFe_{0.8}Zn_{0.2}PO_4$ under an applied field of 1000 Oe. The Néel temperature (T_N) of the sample is determined to be 43 K. The susceptibility curve of $LiFe_{0.8}Zn_{0.2}PO_4$ indicates that the sample antiferromagnetically ordered with decreasing T_N due to Zn substitution. Also, we observed that the change in slope below the spin reorientation temperature (T_S). The value of T_S was analyzed 13 K. The Mössbauer spectra of $LiFe_{0.8}Zn_{0.2}PO_4$ were analyzed at various temperatures in order to verify the hyperfine interaction, state in terms of the Fe nucleus. The spectra of $LiFe_{0.8}Zn_{0.2}PO_4$ sample were a fitted asymmetrical 8-line pattern under T_N. The magnetic hyperfine field (H_{hf}), electric quadrupole splitting (ΔE_Q) and isomer shift (δ) values of the $LiFe_{0.8}Zn_{0.2}PO_4$ at 4.2 K were determined to be H_{hf} = 122.7 kOe, ΔE_Q= 2.74 mm/s, δ=1.24 mm/s. The polar angle (θ) is 10 °, the azimuthal angle φ = 0 °, the asymmetric parameter η = 0.8, the ratio of electric quadrupole interaction to magnetic dipole interaction R = 3.3. From these results, we can be explained that the change of Zn substitution can weaken superexchange interaction that of between the Fe ions.

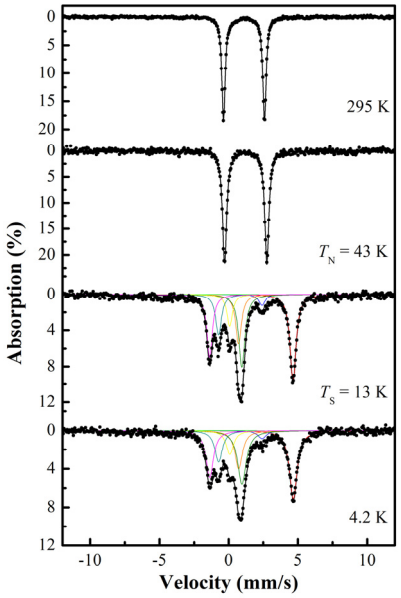

Fig. 1. Mössbauer spectra of $LiFe_{0.8}Zn_{0.2}PO_4$ at various temperature.

Brownian Motion of Magnetic Cube Chain Under External Magnetic Field

Sang-Hyuk Lee[1*], Seung-Young Park[2], You-Jin Lee[3], Gi-Ra Yi[4†], Stefano Sacanna[5], and Dong-Hyun Kim[1†]

[1]Department of Physics, Chungbuk National University, Cheongju 362-763, South Korea
[2]Spin Engineering Physics Team, Korea Basic Science Institute, Daejeon 305-806, South Korea
[3]Center for Research Facilities, Chungnam National University, Daejeon 305-764, South Korea
[4]School of Chemical Engineering, Sungkyunkwan University, Suwon 440-746, South Korea
[5]Department of Chemistry, New York University, New York, New York 10003, United States

We have investigated Brownian motion characteristics of magnetic microcube chains floating in distilled water with control of external magnetic field direction. The dynamics of cube particle has been directly observed by means of optical microscope with ×50 magnitude lens. Images are captured by CCD with 40 *ms* of temporal resolution. The magnetic cube particles are made of Fe2O3 α-hematite with 1×1×1 μm^3 size. The external magnetic field is applied with arbitrary direction by means of 4-pole electromagnet, the field strength is fixed with 150 *Oe*. The direction of cube chain was controlled to be parallel to the external magnetic field, as seen in Fig. 1 (a). The cube chain is formed to be solid since a single magnetic cube particle have a property of magnetic dipole.[1] As in Fig. 1(b), a typical Brownian motion behavior is observed for both *x*- and *y*-directions with field angle of parallel to x-axis. The inset figure shows the x- and y-positions under zero field for comparison, where a similar random Brownian motion is observed. To further understand the Brownian motion characteristics, the mean square displacement (MSD), the growth exponent, and the diffusivity are analyzed based on the Einstein model,[2] where angular dependency of diffusivity is found due to effective cross-section changes along a certain direction under external magnetic field

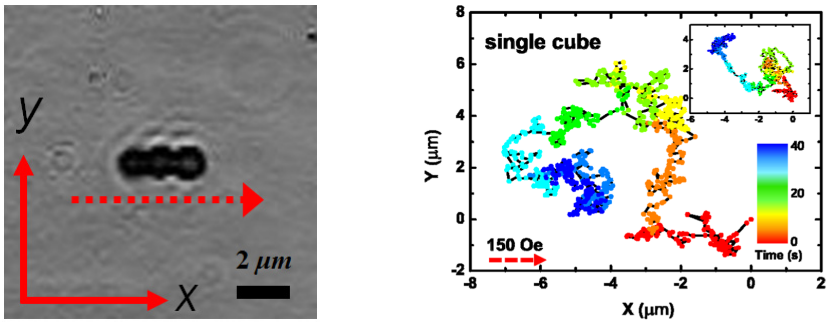

(a) (b)

Fig. 1. (a) Microscopic image of 3-particle chain. Dotted red arrow represents the applied field direction, a scale bar of 1 μm is shown. (b) 3-cube particle trajectory under 150 Oe (red dotted arrow). Inset is a trajectory under zero field. Color code represents an elapsed time during 40 s from red to blue.

References

[1] H.-G. Piao, D. Djuhana, J.-H. Shim, S.-H. Lee S.-H. Jun, S.-K. Oh, S.-C. Yu, D.-H. Kim, J. Nanosci. Nanotechnol. 10, 7212-7216 (2010)

[2] A. Einstein, Ann. Phys. 322, 549-560 (1905)

Thermoelectric voltage of bulk- $Y_3Fe_5O_{12}$ (YIG) prepared by the sol-gel method

Min-Sun Jang*, Ki-Suk Lee
School of Materials Science and Engineering, Ulsan National Institute of Science and Technology (UNIST), Ulsan 44919, Republic of Korea

1. Introduction

Spin-caloritronics, based on the spin Seebeck effect (SSE) has been considered as a prominent candidate for future sustainable green energy technologies [1-3]. Since a single crystal $Y_3Fe_5O_{12}$ (YIG) has been believed to be able to generate sufficiently high SSE signal, most of experiments have been performed with a single crystal YIG fabricated by a pulsed laser deposition (PLD) method [4]. But it is difficult to utilize PLD method for mass-production. Here, we synthesized the bulk-YIG sample by means of sol-gel method which is one of a conventional method for mass-production of metal oxide materials [5-6]. We measured thermoelectric (TE) voltage of bulk-YIG through the inverse spin-Hall effect in Pt electrodes on bulk-YIG sample. It is found that thermoelectric performance of bulk-YIG is almost closed to that of a single crystal YIG by PLD method.

2. Experiments

YIG precursor was prepared by mixing yttrium nitrate ($Y(NO_3)_3.6H_2O$, 99.99%) and iron nitrate ($Fe(NO_3)_3.9H_2O$, 99.99%) powders in a stoichiometric ratio of 3: 5, and adding citric acid ($C_6H_8O_7.H_2O$). The precursor mixture was dissolved in distilled water (100 mL) by stirring (300 rpm) at 27 °C for 18 hours. The solution of the citric acid was maintained at 1pH. The resulting solution (sol) was then stirred for 24 hours at 80 °C to obtain a homogenous gel. Next, a form a dry material (gel) was obtained from the sol by drying the solution, which was decomposed at 100 °C for 5 hours. The YIG powder was obtained by grinding the completely dried gel for 30 min. The calcination process was carried out at 850 °C in the air for 2 hours at a heating rate of the 7.7 °C /min to get rid of residual impurities and the crystallization. After, we did the pressing process to produce the substrate-free as well as the bulk- YIG by pushing 150 MPa for 5 minutes and observed the influence of external mechanics for magnetic properties. Lastly, sintering has been done at 1400 °C for 4 hours. In order to generate spin-currents in bulk-YIG disk with 1.8 mm thickness and 14 mm diameter, we applied 400 Oe magnetic field applied parallel to the disk plane and the temperature gradient was formed along out-of-plane direction (longitudinal SSE configuration). To convert thermoelectric current through the invers-spin hall effect, the 15 nm-Pt electrode was deposited on the bulk-YIG disk.

3. Results & Discussion

After sol-gel synthesis, we identified the complete crystallization of polycrystalline bulk-YIG to be achieved by increasing the degree of oxidation from X-ray diffractometer (XRD; Bruker AXS, D8 ADVANCE) as well as X-ray photoelectron spectroscopy (XPS; ThermoFisher, K-alpha) measurements that the extra surface energy caused by the pressing and sintering process. In addition, the field-emission scanning electron microscopy (FE-SEM; Hitachi, S-4800) images indicate the effect of the pressing and sintering that is grain growth with high

densification and a remarkable reduction of impurities in the microstructure. Because of the microstructure resembled a continuous network of almost hexagonal bubble-shaped particles with no vacancies, consequently, the saturation magnetization was enhanced from 10 emu/g to 26.5 emu/g. From the measurement of the spin-TE module which was composed of the bulk-YIG/Pt structure, we observed that the considerable spin-TE voltage was generated successfully according to various electrode patterns in Fig. 1. Here, we might suggest how to make easily and inexpensively bulk-YIG with enhanced magnetic properties as well as the applicable spin-TE module.

4. References

[1] K. Uchida et al., Nat. Mat. **9**, 894 (2010).

[2] G. E. W Bauer et al., Nat. Mat. **11**, 391 (2012).

[3] K. Uchida et al., J. Phys.: Condens. Matter **26**, 343202 (2014).

[4] N. B. Ibrahim et al., J. Magn. Magn. Mater. **220**, 183 (2000).

[5] R. Kuchi et al., Nanosci. Nanotechnol. Lett. **7**, 738 (2015). [6] M.-S. Jang et al., J. Alloys Compd. **711**, 693 (2017).

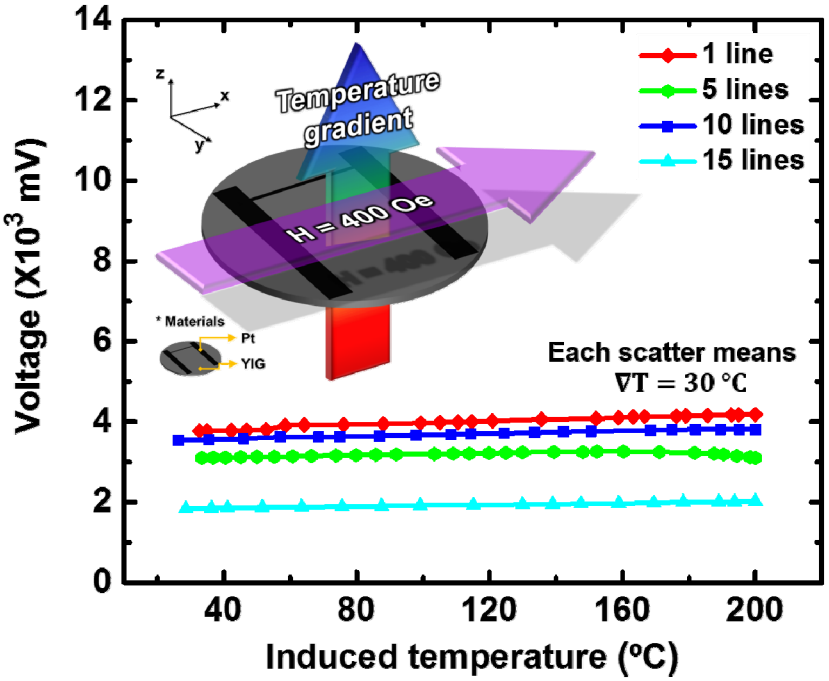

Fig. 1. Schematic illustration of SSE geometry and Spin thermoelectric voltage as a function of the number of Pt electrode lines.

Taguchi Robust Design Considering the Tolerance for Electric Machine

Kyu-seob Kim*, Kyu-Sik Kim†, Byeong-Hwa Lee, Bong-Hyun Lee, Su-Chul Kim
Electric Powertrain R&D Center, Korea Automotive Technology Institute, Daegu, Korea

This paper presents a multi-response Taguchi robust design for back electromotive force (EMF) and cogging torque considering the manufacturing tolerances for electric machines. In mass production, manufacturing tolerances are unavoidably generated in the rotor between the core and the permanent magnet. Because back EMF and cogging torque are influenced by manufacturing tolerance, it is necessary to improvement by changing the specific factors. Because the Taguchi robust design cannot consider a multi-response, a multi-response signal to noise (MRSN) ratio based on Taguchi robust design considering multiple responses is employed. The SN-ratio is not calculated directly by this method; therefore, quality loss is introduced. Total normalized quality loss (TNQL) of each response is calculated and then a weighting factor is applied to each response. As a result, the MRSN ratio is obtained.

Applying the Taguchi method to optimize multi-response processes includes the following considerations. First, the loss functions in the multiple cases are always different for each response. Therefore, the loss for each response cannot be compared and summed directly. The measurement units in the multiple cases are always different for each response. Therefore, the loss caused by each unit for each response could be different. Second, the importance in the multiple cases could be different for each response. Therefore, the weight value for each response is considered.

Thus, an effective method capable of determining the multi-response signal to noise ratio is applied here through the integration of quality loss for all the responses with the application of the Taguchi's SN ratios. Next, the traditional Taguchi method can be applied based on the MRSN ratio.

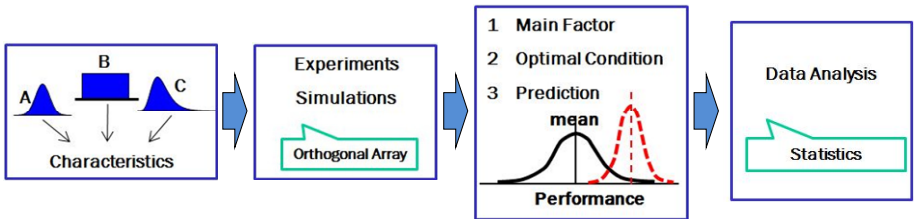

Fig. 1. Process of Taguchi robust design

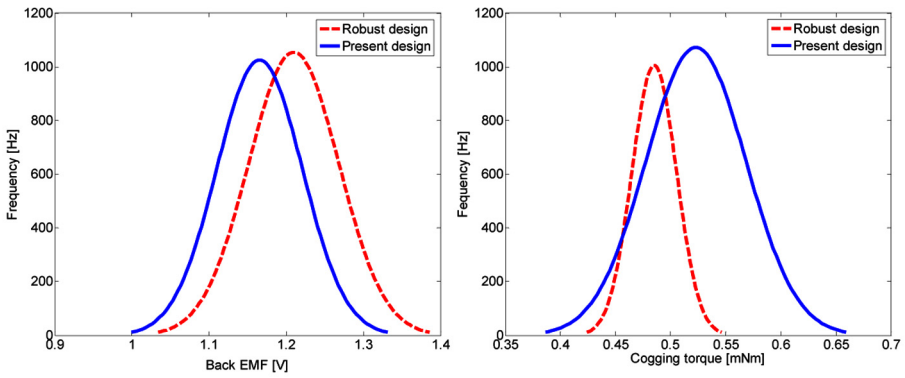

Fig. 2. Comparison using histogram between robust design and present design

Acknowledgement

This research was contributed by the leading Technology Development Project for the next mobility of the Daegu City, Korea.

References

[1] Jang, J., Cho, S.G., Lee, S.J., et al.: 'Reliability-based robust design optimization with kernel density estimation for electric power steering motor considering manufacturing uncertainties', IEEE. Trans. Magn., 2015, 51, (3), pp. 1–4

[2] Wang, C.F., Shen, J.X., Luk, P.C.K., et al.: 'Design issues of an IPM motor for EPS', COMPEL Int. J. Comput. Math. Electr. Electron. Eng., 2011, 31, (1), pp. 71–87

Torque Ripple Reduction of Wound Rotor Synchronous Motor using Rotor Slits

Byeong-Hwa Lee*, Kyu-Sik Kim†, Kyu-seob Kim, Bong-Hyun Lee, Su-Chul Kim, Da-yeon Lee
Electric Powertrain R&D Center, Korea Automotive Technology Institute, Daegu, Korea

Since Interior Permanent Magnet Synchronous Motor (IPMSM) has good performance and high power density, it is used for various applications including electric traction. However, the rise in the price of rare earth magnet caused by its scarcity becomes a troubling issue which the world is facing nowadays.

In this situation, Wound Rotor Synchronous Motor (WRSM) has numerous benefits compared to IPMSM as it does not need magnetic materials and can be operated in a wide range of speeds. So, an alternative solution to IPMSM particularly for the industrial applications is represented by the WRSM [1]. There are lots of advantages of WRSM, but the biggest shortcoming is its relatively high torque ripple. In the case of IPMSM, the optimization of rotor shape is an effective way to solve the problem because the arrangement of permanent magnet influences torque ripple [2]. On the contrary, it is not easy to reduce torque ripple produced in WRSM because the pole angle is closely related with torque value itself. Torque ripple is mainly brought about by the magnetic saturation of pole shoe. Therefore, this paper focuses on a method to decrease it by suppressing magnetic saturation of pole shoe.

In general, rotor slits are utilized a lot in reluctance motor to generate magnetic flux in the d-axis direction. This paper applies this idea to the reduction torque ripple by changing magnetic flux path. To verify it, all the analytical computations are performed by the Finite Element Method (FEM). An analytical model of motor is 60kW WRSM for electric traction. The initial design model of rotor with slits is shown in Fig. 1. Fig. 1 (a) shows rotor with 2 slits per pole and Fig. 1 (b) shows 1 slit per pole. Fig. 2 (a) shows plot of Back-EMF at 1000rpm versus electrical angle and plot of torque versus electrical angle is shown in Fig. 2 (b). Under the same conditions, the torque ripple of rotor with 2 slits per pole reduced from 9.2[%] to 5.7[%] compared with the rotor without slits and the torque ripple of 1 slit per pole reduced from 9.2[%] to 3.6[%]. As for this result, rotor with 1 slit per pole is more effective than the other. Each the average torque value is almost exactly the same.

In later full paper, optimization will be done by Response Surface Methology (RSM). Design variables will be the number of slits, angle, width, length and so on. An objective function will be torque ripple and a constraint is more than 98 percentage of average torque value compared with the rotor without slits. The experimental tests will be done to validate FEM results.

Acknowledgement

This research was contributed by the leading Technology Development Project for the next mobility of the Daegu City, Korea.

References

[1] O. Pyrhonen, M. Niemela, J. Pyrhonen, and J. Kaukonen, “Excitation control of DTC controlled salient pole synchronous motor in field weakening range,” in Proc. 5th Int. Workshop Adv. Motion Control

(AMC), 1998, Coimbra, Portugal, pp. 294–298.

[2] Y. Okada, Y. Kawase, and S. Sano, “Development of optimizing method using quality engineering and multivariate analysis based on finite element method,” in Proc. ISEF2003, vol. 2, Nov. 2003, pp. 737–739.

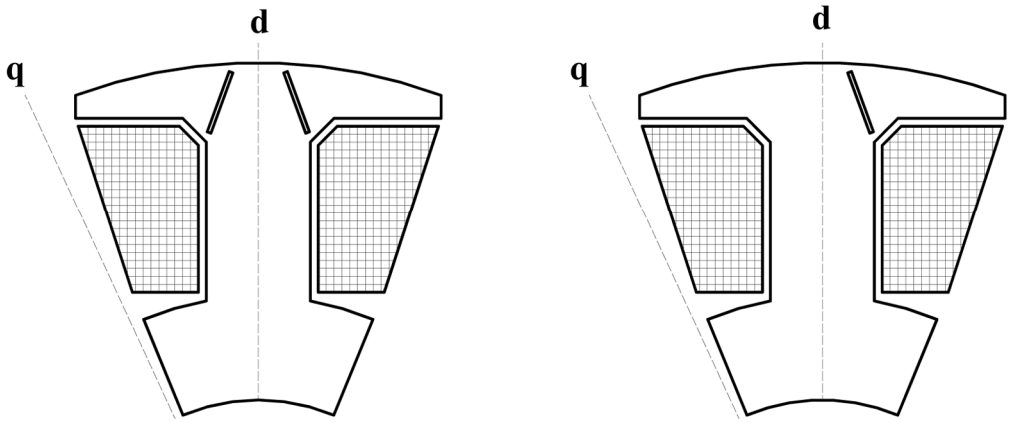

(a) (b)

Fig. 1 The initial design model of rotor with slits. (a) Rotor with 2 slits per pole. (b) Rotor with 1 slit per pole.

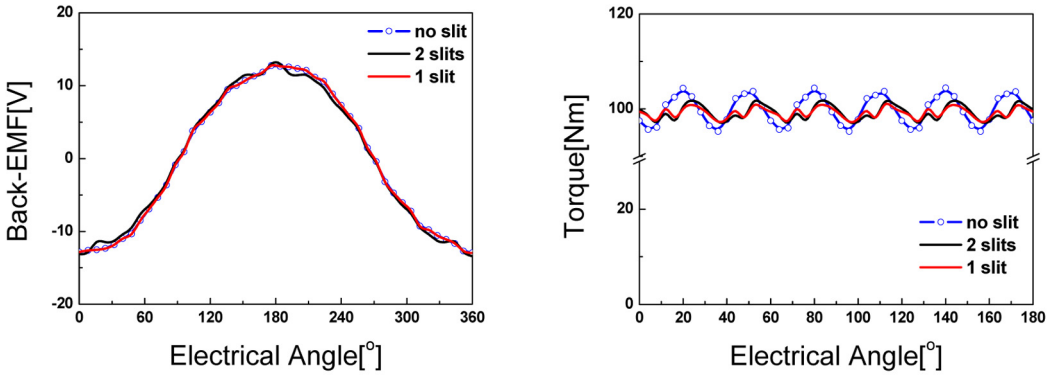

(a) (b)

Fig. 2 (a) Plot of Back-EMF versus electrical angle. (b) Plot of torque versus electrical angle.

The magnetization manipulate in Fe/GaAs/GaMnAs multilayer by spin orbit-induced magnetic field

Sangyeop Lee[1,2*], Taehee Yoo[1], Seul-Ki Bac[1], Seonghoon Choi[1], Hakjoon Lee[1], Sanghoon Lee[1], Xinyu Liu[3], Margaret Dobrowolska[3] and Jacek K. Furdyna[3]

[1]Physics Department, Korea University, Seoul, 136-701, Republic of Korea.

[2]Center for Spintronics Research, Korea Institute of Science and Technology, Seoul 136-791, Korea

[3]Physics Department, University of Notre Dame, Notre Dame, IN, 46556, USA

We investigate the process of selectively manipulating the magnetization alignment in magnetic layers in the Fe/GaAs/GaMnAs structure by current-induced spin-orbit (SO) magnetic field. The presence of such fields manifests itself through the hysteretic behavior of planar Hall resistance observed for two opposite currents as the magnetization in the structure switches directions. In the case of the Fe/GaAs/GaMnAs multilayer, hystereses are clearly observed when the magnetization switches direction in the GaMnAs layer, but are negligible when magnetization transitions occur in Fe. This difference in the effect of the SO-field in the two magnetic layers provides an opportunity to control the magnetization in one layer (in the presence case in GaMnAs) by a current, while the magnetization in the other layer (i.e., Fe) remains fixed. Owing to our ability to selectively control the magnetization in the GaMnAs layer, we are able to manipulate the relative spin configurations in our structure between collinear and non-collinear alignments simply by switching the current direction even in the absence of an external magnetic field.

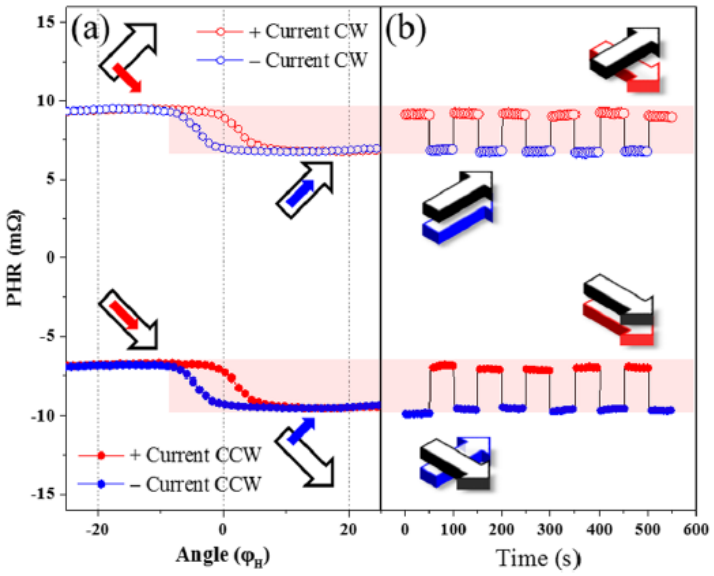

Fig. 1. (a) The angular dependence of PHR for ϕ_H between −25° to +25°. (b) PHR measured as a function of time, showing abrupt switching of PHR as current polarity is reversed every 50 seconds. In both panels the magnetization for the Fe layer is shown by black arrows, and for GaMnAs in color, red for positive and blue for negative current.

Spin-orbit torques and magnetic properties in Pt/GdFeCo/MgO layers

J. H. Kim[1,2*], D. J. Lee[1,3], H. C. Koo[1], B. C. Min[1], K. J. Lee[1,3,4], B. K. Ju[2] and O. J. Lee[1]

[1]Center for Spintronics, Korea Institute of Science and Technology

[2]Graduate School of Electrical Engineering, Korea University

[3]KU-KIST Graduate School of Converging Science and Technology, Korea University

[4]Graduate School of Materials Science and Engineering, Korea University

Recently the quest for appropriate magnetic materials has been extended from ferromagnet (FM) to ferrimagnet (FI)[1,2,3,4,5,6,7] and anti-ferromagnet (AFM)[8,9], because the latter's are expectedly beneficial for no stray field, low-power and fast magnetic manipulation. Amorphous GdFeCo alloy[10], used in this paper, is one of the renowned rare-earth (RE) – transition metal (TM) ferrimagnetic[11] materials. In the alloy, RE Gd 4f magnetic moments and TM FeCo 3d magnetic moments have "indirect" negative exchange interaction. This anti-parallel coupling results from the bridge role of Gd 5d magnetic moments which are parallel to Gd 4f moments through direct exchange but anti-parallel to FeCo 3d magnetic moments via 5d-3d hybridization. The difference between Gd and FeCo magnetic moments results in a small net magnetization, making its magnetic state measurable. It is also well-known that the magnetic properties of GdFeCo can be tuned by temperature and/or its composition, and that the amorphous GdFeCo exhibits to have a bulk perpendicular magnetic anisotropy (PMA).

Here, we report our investigations of magnetic properties and SOT-efficiencies in Pt/GdFeCo/MgO multilayers as functions of MgO and GdFeCo thicknesses. Our studies show that both thicknesses considerably influence ferrimagnetism in the GdFeCo alloy so as to affect the magnitudes of θ_{DL} and θ_{FL}. The measured SOT-efficiencies in the structures, using spin-torque ferromagnetic resonance (ST-FMR) technique, are smaller than conventional Pt/FM/MgO layers, but the magnetic damping of the GdFeCo layer is similar to values in conventional Pt/FM/MgO layers.

References

[1] Xin Jiang et al., Phys. Rev. Lett. 97, 217202 (2006).

[2] Rahul Mishra et al., PRL 118, 167201 (2017).

[3] N. Roschewsky et al., APL 109, 112403 (2016).

[4] N. Roschewsky et al., PRB 96, 064406 (2017).

[5] J. Finley et al., PR Applied, 6, 054001 (2016).

[6] W. S. Ham et al., APL 110, 242405 (2017).

[7] K. Ueda et al., APL 109, 232403 (2016).

[8] P. M. Haney et al., JMMM 320, 1300 (2008).

[9] T. Jungwirth et al., Nature Nano., 11, 231 (2016).

[10] C. D. Stanciu et al., PRL 99,047601 (2007).

[11] K. H. J. Buschow, Rep. Prog. Phys. 40, 1179 (1977).

Capping Layer Dependency of Magnetic Properties in Half MTJ Stack

Min Wook Han*, Byong Guk Park†
Department of Materials Science and Engineering, KAIST, Daejeon

In heavymetal/ferromagnet bilayer structure, in plane current generates torque by spin-orbit interaction of heavy metal layer. This torque is called as 'spin-orbit torque', and it is actively being researched as one possible method for magnetization control in magnetic memory devices. Spin-orbit torque became one of the interesting MRAM model since it does not damage oxide layer because reading current line and writing current line is independent. The most important issue of spin-orbit torque device is modifying strength of spin-orbit torque, and there are many previous researches. For instance, some researchers control the condition of heavy metal film deposition, and some changes thickness of bilayer.

On the other hand, not only modifying spin-orbit interaction of heavy metal layer is unique solution. In magnetic layer, there are many kinds of interactions which can be induced by inversion asymmetry; Rashba effect, Dzyaloshinski-Moryia interaction (DMI), etc.[1] In this work, we select controlled the degree of asymmetry with various capping layer. We used work function difference between capping layer and magnetic layer to generate electric field through the spacing layer, and this potential difference of interlayer between magnetic layer and spacing layer can change asymmetry of the interface. Previous work has shown that capping layer difference may change magnetic anisotropy.[2]

Full stack of the sample is W/CFB/MgO/capping layer/Ta, and we used 5 different capping layer with proper work function gap: Mg(3.66eV), Hf(3.9eV), Ta(4.25eV), Ru(4.7eV), and Pt(5.3eV). Each sample was deposited by magnetron sputtering in W(4nm)/CFB(1.1nm)/MgO(1.8nm)/capping layer(1nm)/Ta(2nm). Magnetic anisotropy, spin Hall magnetoresistance (SMR), spin orbit torque, and current induced switching current was measured for each sample. Magnetic anisotropy was calculated by in plane M-H curve which was performed by vibrating sample magnetometer (VSM) with 1.5T of magnetic field. Spin orbit torque was measured with harmonic hall signal. AC current was applied to Hall bar patterned sample, and Hall voltage was measured with lock-in amplifier which divide Hall signal to first harmonic signal (fig.3.b) and second harmonic signal(fig.3.c). Spin-orbit torque was calculated by equation $H = 2\frac{dv_{2\omega}}{dH} / \frac{d^2 v_{\omega}}{dH^2}$. [3] SMR was measured with γ angle scan in 9T magnetic field with PPMS equipment. As a result, we found that Slonczewski like torque decreases as the work function increases, and SMR has similar tendency except Hafnium. We can expect that this kind of asymmetry control can be one way to modify magnetic property of devices. In addition, magnetic anisotropy and switching current changed by capping layer difference.

References

[1] Toru Moriya, Anisotropic Superexchange Interaction and Weak Ferromagnetism, Phys. Rev. **120**, 91 (1960)
[2] Hiroyuki Yamamoto, *et al*, Dependence of Magnetic Anisotropy in Co20Fe60B20 Free Layers on Capping Layers in MgO-Based Magnetic Tunnel Junctions with In-Plane Easy Axis, Appl. Phys. Express. **5** (2012) 053002
[3] Seonghoon Woo, Maxwell Mann, Aik Jun Tan, Lucas Ceretta and Geoffery S. D. Beach, Enhanced spin-orbit torques in Pt/Co/Ta heterostructures, Appl. Phys. Letters **105**, 212404 (2014)

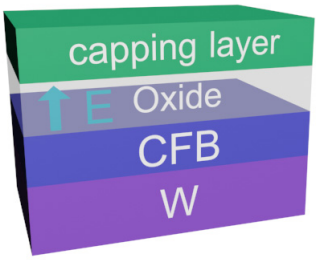

Fig. 1. Schematic of system with electric field with variable capping layer. Sample was deposited with magnetron sputtering, and structure is W(4nm)/CFB(1.1nm)/MgO(1.8nm)/capping layer(1nm)/Ta(2nm). We expected that work function difference between CFB layer and capping layer will generate electric field, and this field may affect as inversion asymmetry.

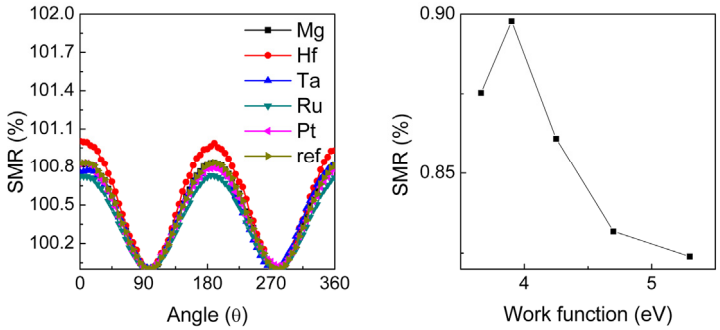

Fig. 2. Work function effect of SMR. SMR was measured with ɣ angle scan in 9T magnetic field with PPMS equipment. Hf has outstandingly large SMR ratio, and other sample has decreasing SMR ratio as work function increases.

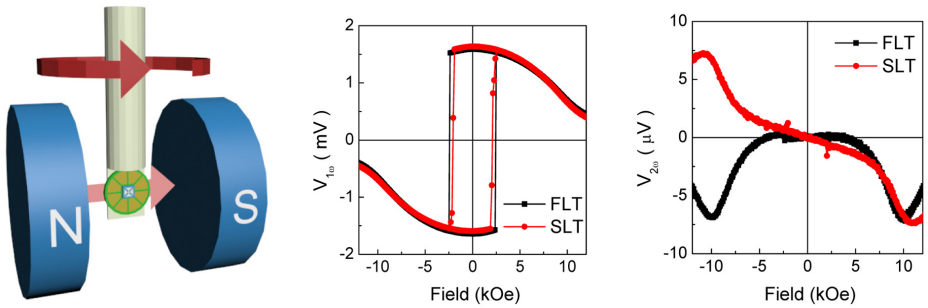

Fig. 3. Measurement of spin-orbit torque. To measure spin-orbit torque, AC current was applied to Hall bar patterned sample, and Hall voltage was measured with lock-in amplifier which divide Hall signal to first harmonic signal(fig.3.b) and second harmonic signal(fig.3.c). Spin-orbit torque was calculated by first order and second order fitting each.

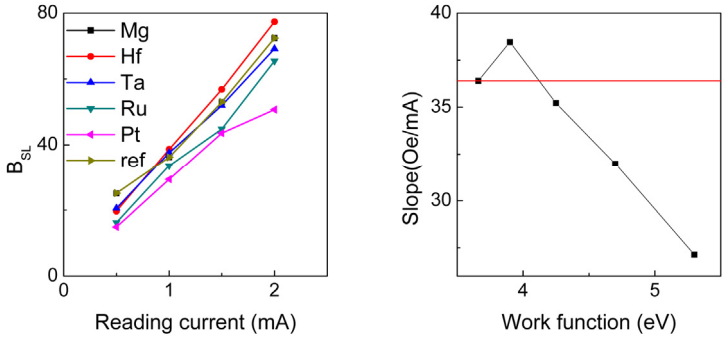

Fig. 4. Work function effect of SLT. SLT has similar tendency with SMR, which is related with spin Hall angle. This agreement show that capping layer difference can affect in magnetic property of MTJ devices.

SO04

Enhancement of spin-thermoelectric voltage by 3-dimentional structure engineering

Jeong-Mok Kim[1*], Dong-Jun Kim[1], Chul-Yeon Jeon[1], Jong-Ryul Jeong[2] and Byong-Guk Park[1]
[1]Department of Materials and Science Engineering, KAIST, Daejeon 34141, Korea
[2]Department of Materials Science and Engineering, Chungnam National University, Daejeon 34134, Korea

Spin thermoelectric devices have recently been studied because of their potential to overcome the Wiedemann Franz law, which is known as the limitation of conventional thermoelectric devices. Since the discovery of spin thermoelectric effect, various methods have been proposed to increase the efficiency of spin-thermoelectric effect. This includes the introduction of ferromagnet (FM)/non-magnet (NM) multilayers that reconciles spin Seebeck effect and anomalous Nernst effect [1], and the formation of the spin thermopile using antiferromagnet [2]. In this work, we report an enhancement of the spin thermoelectric voltage by a 3-dimensional structure engineering which combines the multilayer and thermopile structures. Since the thermopile requires the alternating magnetization of the wire element in order to add their thermoelectric signals constructively, it is necessary for FM/NM multilayer to be exchange-biased by the antiferromagnet layer.

Samples of the CoFeB/NM/CoFeB/IrMn multilayer structure were prepared by magnetron sputtering on oxidized silicon substrate with the base pressure less than 3.0×10^{-8} Torr at room temperature. Here the NM is Pt, Ta, or IrMn. A bar-shaped structure of 10μm1mm and a zigzag-shaped structure were patterned using photolithography and Ar ion milling. The M-H curves of the film were measured by VSM and thermoelectric voltage was measured under the illumination of laser beam of 5μm diameter and 60mW that induces a vertical thermal gradient.

Figure 1 (a) shows the M-H curves of the CoFeB/NM/CoFeB/IrMn multilayer with different NM layers. The samples with Ta or IrMn interlayer show two hysteresis curves corresponding to the top and bottom CoFeB, respectively, indicating they are magnetically decoupled by NM layers. In contrast, the sample with Pt interlayer shows only one hysteresis curve, demonstrating that the CoFeB/Pt/CoFeB layer behaviors as a single FM that are simultaneously exchange-biased by antiferromagnetic IrMn layer. Figure 1b shows the comparison of spin thermoelectric signal between IrMn/CoFeB(6nm) and IrMn/CoFeB(3nm)/Pt(2nm)/CoFeB(3nm). When the Pt layer is introduced in-between the CoFeB layers, spin thermoelectric voltage increases while maintaining the exchange bias. The increase in the thermoelectric voltage is consistent with the previous results [1]. As illustrated in Fig. 1 (c), a thermopile consisting of multilayered structure CoFeB/Pt/CoFeB/IrMn is fabricated [2]. The upper panel of Fig. (c) shows the thermoelectric voltage of the etched (blue) and un-etched (red) wires measured using localized laser heating. The thermoelectric voltage of un-etched (red) wire shows a comparable magnitude, but an opposite sign to that of etched one. Moreover, there is a magnetic field range from 0 Oe to 150 Oe, where both wires have the same sign of the thermoelectric signal, which is due to exchange-bias in un-etched wire. When both wires are heated by laser at the same time, the thermoelectric voltages of two wires are constructively added in the field where two FMs are in antiparallel alignment. In this experiment, we have demonstrated the improvement of the spin thermoelectric voltage by 3-dimensional structural engineering: formation of the spin thermopile using FM/NM multilayers. This results can pave the way toward the realization of practical spin thermoelectric devices.

References

[1] Lee, K-D. et al Thermoelectric Signal Enhancement by Reconciling the Spin Seebeck and Anomalous Nernst Effects in Ferromagnet/Non-magnet Multilayers, Sci. Rep. 5, 10249 (2015)

[2] Kim, D-J. et al Utilization of the Antiferromagnetic IrMn Electrode in Spin Thermoelectric Devices and Their Beneficial Hybrid for Thermopiles, Adv. Funct. Mater.. **26**, 5507 (2016).

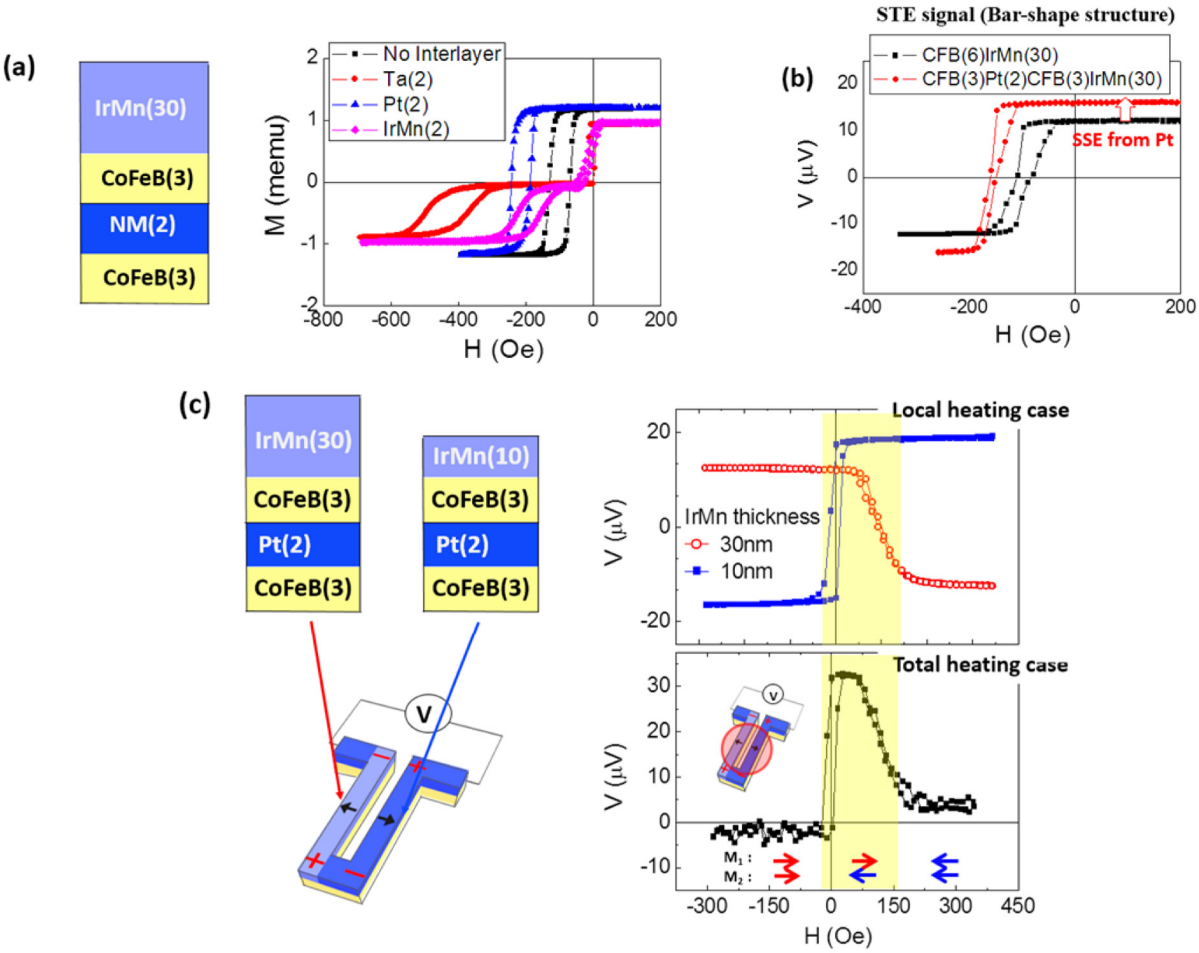

Fig. 1. (a) Schematic of multilayer structure and their M-H curve of CoFeB(3nm)NM(2nm) CoFeB(3 nm)IrMn(30nm) structure (b) M-H curve and spin thermoelectric voltage signal of CoFeB(3nm) Pt(2 nm)CoFeB(3 nm)IrMn(30nm) (c) the spin thermoelectric voltage signal in local heating and total heating in the multilayered thermopile structure. In local heating case, the laser is applied in each part of the wire. In total heating, the laser is applied in both wire.

Effect of interfacial spin-transparency on Pt/Ferromagnet

D. J. Lee[1,2*], J. H. Kim[1,4], B. K. Ju[4], H. C. Koo[1], B. C. Min[1], K. J. Lee[1,2,3] and O. J. Lee[1]

[1]Center for Spintronics, Korea Institute of Science and Technology, Seoul, Korea

[2]KU-KIST Graduate School, Korea University, Seoul, Korea

[3]Materials Science and Engineering, Korea University, Seoul, Korea

[4]Electrical Engineering, Korea University, Seoul, Korea

[*]E-mail: 215353@kist.re.kr

For highly efficient spin memory devices, a reduction of switching current is an issue. While a spin orbit torque driven switching current density is proportional to the spin Hall angle (θ_{SH}), recent researches have shown that the spin-transparency at the interface of heavy metal(HM)/ferromagnet(FM) plays a major role in determining the magnitude of spin Hall angle; e.g. θ_{SH}(Pt|Co)~0.11 vs θ_{SH}(Pt|Py)~0.05 [1,2,3].

The spin Hall effect converts charge current to pure spin current, generating two components of spin-orbit torque; the damping-like torque and the field-like torque . And the HM/FM interface changes these two types of torques.

To identify both efficiencies we compared three ferromagnetic materials (Py, Co and $Co_4Fe_4B_2$) with platinum, where the thickness of the FM layer was varied from 2 to 10 nm. We investigated the magnetic damping () and θ_{SH} in Pt/FM/MgO multilayers by using spin-torque ferromagnetic resonance technique (ST-FMR) and FM/MgO multilayers by using conventional ferromagnetic resonance technique. From the thickness dependence of the damping and the spin Hall angle, we can estimate the values of spin-transparency (T) and spin mixing conductance (). Our results show that the magnitude of SHA is determined by the interface material in contact to the Pt layer which is consistent with the spin-transparency model [1]. However we observed that the interface contribute to the Field-like torque and the Damping-like torque differently.

In this presentation, we will show detailed results and analysis methods from our conventional- and ST-FMR for the different ferromagnetic layer and various thickness ranges.

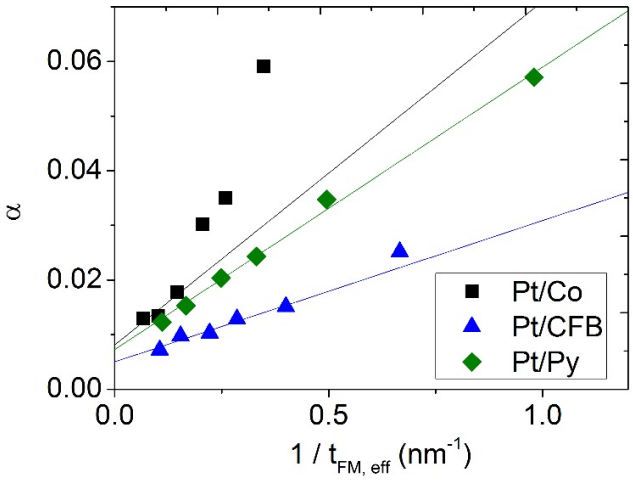

References

[1] Weifeng Zhang, Wei Han, Xin Jiang, See-Hun Yang and Stuart S. P. Parkin, Role of transparency of platinum–ferromagnet interfaces in determining the intrinsic magnitude of the spin Hall effect, Nature Physics, vol 11, (2015) 496-502

[2] Chi-Feng Pai, Yongxi Ou, D. C. Ralph and R. A. Buhrman, Dependence of the efficiency of spin Hall torque on the transparency of Pt/ferromagnetic layer interfaces, Physical Review B 92, 064426 (2015)

[3] Minh-Hai Nguyen, Chi-Feng Pai, Kayla X. Nguyen, David A. Muller, D. C. Ralph, and R. A. Buhrman, Enhancement of the anti-damping spin torque efficacy of platinum by interface modification, Applied Physics Letter, 106, 222402 (2015)

International Symposium on Magnetism and Magnetic Materials 2017

Special Session IV

'Magnetic Materials for Electric Vehicles'

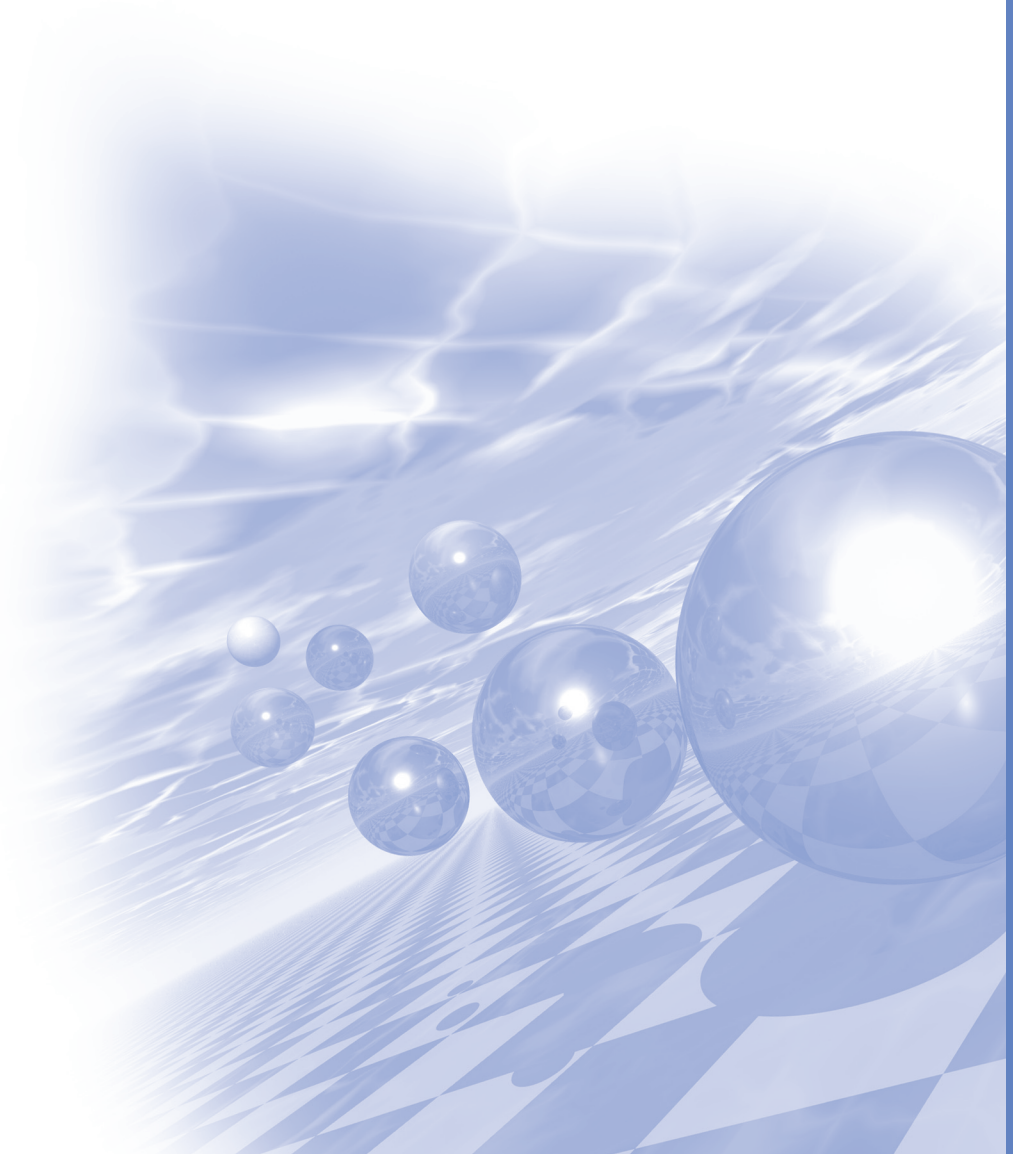

High Performance Nd-Fe-B-type Permanent Magnet with High Electrical Resistivity

H. W. Kwon[1*], K. M. Kim[1], M. S. Kang[1], D. Wu[2], M. Yue[2], J. G. Lee[3], and J. H. Yu[3]

[1]Pukyong National University, Department of Materials Science and Engineering, Busan, Republic of Korea 48513

[2]Beijing University of Technology, College of Materials Science and Engineering, Beijing, China 100124

[3]Korea Institute of Materials Science, Changwon, Republic of Korea 51508

Nd-Fe-B-type magnet is exclusively utilized as permanent magnet part in a traction motor of HEV, EV because of its superior magnetic performance. As Curie temperature of the Nd-Fe-B-type magnet is not satisfactorily high (just above 315 ^{o}C) and operating temperature of the magnet in the traction motor is undesirably high (> 150 ^{o}C), high coercivity is all that matters. Coercivity enhancement in the Nd-Fe-B-type magnet is commonly achieved by substitution of Nd atoms in the magnet by heavy rare earth (HRE : Dy, Tb). However, the HRE-substitution inevitably leads to significant reduction of magnetic performance and cost rise. Recently, finding transition metal (TM)-based new permanent magnetic materials without containing rare-earth has, therefore, become hot issue in the field of hard magnetic materials. In this talk, some TM-based materials are briefly reviewed. Meanwhile, the operating temperature of the magnet in the traction motor is due largely to eddy current caused in the magnet by varying magnetic field from slots of the stator exposing to the magnet during operation. As eddy current is inversely proportional to the electrical resistivity of a material, enhancing electrical resistivity of the magnet is equally important for suppressing the eddy current and hence lowering operating temperature of the magnet. Because the Nd-Fe-B-type magnet is basically metal alloy, enhancing electrical resistivity of the magnet may be by no means easy task. Previously, several attempts have been made to enhance the electrical resistivity of Nd-Fe-B-type magnet using dielectric salts, but to no avail. In this talk, the previous research efforts for enhancing electrical resistivity of Nd-Fe-B-type magnet are reviewed, and an emphasis is placed on the ceramics-bonded Nd-Fe-B-type magnet with high electrical resistivity prepared using an oxide binder with low melting point.

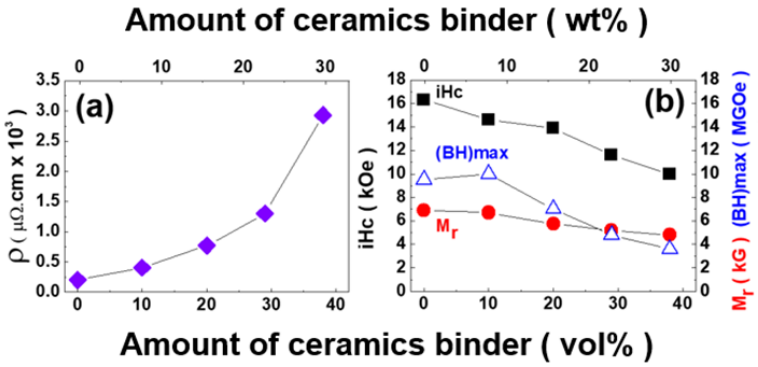

Fig. 1. Dependence of electrical resistivity (a), magnetic performance (b) of the ceramics-bonded magnet on the amount of added ceramics binder.

High-Speed Electrical Machines - Applications, Key Issues and Challenges

Jian-Xin Shen*
Zhejiang University, China
J_X_Shen@zju.edu.cn

In this speech, applications of high-speed electrical machines in the areas of transportation and some others will be introduced, such as exhaust energy recycling and electrically assisted turbo charging for internal combustion engines, air compressor for fuel cells, integrated starter and generator for gas turbines, and electrical spindle for precision machining. As key issues of design and control of the high-speed machines, machine topologies will be reviewed, and design considerations especially those for permanent magnet (PM) AC machines will be presented, including the reduction of electromagnetic losses, thermal analysis and design, rotor stress, and rotor dynamics. Also, sine-wave and square-wave drives for the PM AC machines will be compared. Moreover, challenges such as rotor position sensorless control, field regulation, as well as solution for low PWM carrier-fundamental frequency ratio, under the condition of high-speed operation, will be discussed.

On Electromagnetic Force Density Induced in Dipole Model of Materials

Hong Soon Choi*
Department of Electrical Engineering, Kyungpook National University, Daegu 41566, Korea

When describing the medium in the presence of the electric field, the polarization in the medium and its surroundings have been explained by introducing equivalent bound dipole charges. In a magnetic field, polarization and charge are replaced by magnetization and magnetic charge, respectively. The field change around the medium can be explained by this polarization modeling, but the physical meaning of the distribution of the electromagnetic force induced in the medium due to the bound dipole charges requires attention to interpretation.

In this paper, it is shown that the force on the equivalent unipolar charge on the surface of the medium cannot be the density of the electromagnetic force in the medium. But, the sum of the electromagnetic force on the equivalent unipolar charge distributed on the surface has still valid meaning. It is also shown that the volume force density on the dipole charge induced inside the medium can be an alternative to the surface force density on the unipolar charges which is canceled inside the medium and remained only on surfaces. The field outside the medium has no relation to the viewpoint of the volume dipole charge and the surface unipolar charge. Generally, it is increased by the medium. Numerous dipoles are assembled to form a medium, the force of assembled medium is intended to be regarded as the sum of the forces of simple dipoles. Usually dipoles can be thought of as an atom, the force on a unipolar one in a dipole is not a force on a continuum medium seen in an electromagnetic field, but a force on the half of an atom. The method proposed in this study shows that the force when the medium is in contact can be obtained and the force on a part of the medium can be also obtained. As in Fig.1, for illustrating the properties of bound charge in a medium with polarization P, (a) shows the distribution of the bound charge, which is actually distributed, (b) shows a model in which the distance between the bound charge in the atom is stretched to the boundary between neighboring atoms in order to cancel the bound charge. Fig.1 (b) shows that the value of the unipolar charge with different sign at the boundary can cancel out. The difference between these two models and their meaning will be mentioned in the main paper.

This study is a work of the role of equivalent bound source following the authors' previous work of *On the Physical Meaning of Maxwell Stress Tensor* (Trans.KIEE., APR, 2009). It shows consistent conclusions in both studies.

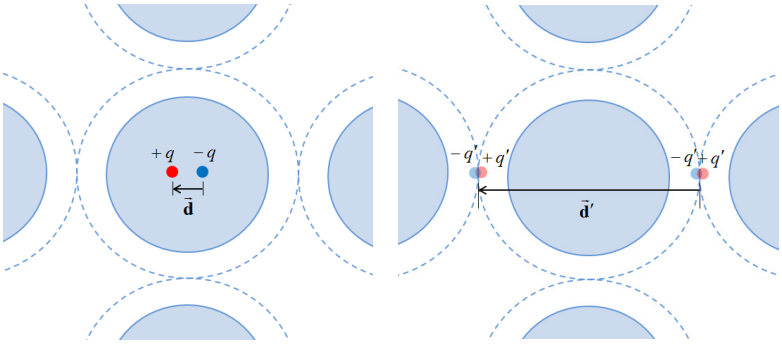

(a) (b)

Fig. 1. Dipole models (a) having real bound charges inside atoms, and (b) having stretched bound charges at inter-atom boundaries.

Fe-rich compounds with promising intrinsic magnetic properties as permanent magnetic materials

Y. Hirayama[1*], Y. K. Takahashi[2], S. Hirosawa[2] and K. Hono[2]
[1]National Institute of Advanced Industrial Science and Technology, Japan (Present address)
[2]Elements Strategy Initiative Center for Magnetic Materials (ESICMM),
National Institute for Materials Science, Japan

The Fe rich compounds, R-Fe_{12}(-N) (R = Sm and Nd), with the $ThMn_{12}$ structure have received revived interest because of their potential as permanent magnetic materials with high saturation magnetization, $\mu_0 M_S$, and high anisotropy field, $\mu_0 H_A$. However, these compounds are not stable in a bulk state. In order to stabilize the $ThMn_{12}$ phase, Fe should be substituted with the structure-stabilizing elements M such as Ti, V, Mo and so on, which substantially reduces the $\mu_0 M_S$ value [1]. Recently, the first principles calculations showed that the $\mu_0 M_S$ values of $SmFe_{12}$ and $NdFe_{12}N$ without M are higher than that of $Nd_2Fe_{14}B$ [1-3] and, Kuno *et al*. reported the enhancement of $\mu_0 M_S$ by preparing $(Sm_{0.8}Zr_{0.2})(Fe_{0.75}Co_{0.25})Ti_{0.5}$ alloy with the $ThMn_{12}$ structure [4].

In order to evaluate the potential of $R$$Fe_{12}$(-N) as a high performance permanent magnetic material experimentally, we have prepared NdFe12Nx and Sm(Fe1-xCox)12 films without M by using the co-sputtering process and evaluated their intrinsic magnetic properties; *i.e.*, $\mu_0 M_S$, $\mu_0 H_A$ and Curie temperature T_C. The detail experimental processes were described in ref. 5-7. The intrinsic magnetic properties are listed in Table 1. By substituting Fe with Co for the $Sm(Fe_{1-x}Co_x)_{12}$ system, T_C increases with increasing Co content up to x = 0.2. The $Sm(Fe_{0.8}Co_{0.2})_{12}$ compound shows higher intrinsic properties than those of $Nd_2Fe_{14}B$ in all temperature ranges. Both $NdFe_{12}N_x$ and $Sm(Fe_{1-x}Co_x)_{12}$ layers can be epitaxially grown at least up to 0.35 μm in thickness, indicating that the $ThMn_{12}$ phase without M can be grown into large crystals once the $ThMn_{12}$ phases are nucleated. In order to put this phase into practical use, we should investigate a new process route to stabilize the R-Fe_{12}(-N) phase in the bulk state as a next step.

Table 1. the intrinsic magnetic properties of $R(FeCo)_{12}$(-N) compounds[5-7]

	$\mu_0 M_S$ (T) @300 K	$\mu_0 H_A$ (T) @300 K	T_C (K)
$NdFe_{12}N_x$	1.66 - 1.7	6 - 8	823
$SmFe_{12}$	1.64	12	555
$Sm(Fe_{0.9}Co_{0.1})_{12}$	1.71	12	710
$Sm(Fe_{0.8}Co_{0.2})_{12}$	1.78	12	859

References

[1] T. Miyake, K. Terakura, Y. Harashima, H. Kino, S. Ishibashi, Journal of the Physical Society of Japan, 83 (2014) 043702.

[2] H. Yosuke, T. Kiyoyuki, K. Hiori, I. Shoji, M. Takashi, First-Principles Study of Structural and Magnetic Properties of $R(Fe,Ti)_{12}$ and $R(Fe,Ti)_{12}N$ (R = Nd, Sm, Y), in: Proceedings of Computational Science Workshop 2014 (CSW2014), Journal of the Physical Society of Japan, 2015, pp. 011021.

[3] W. Körner, G. Krugel, C. Elsässer, Scientific Reports, 6 (2016) 24686.

[4] T. Kuno, S. Suzuki, K. Urushibata, K. Kobayashi, N. Sakuma, M. Yano, A. Kato, A. Manabe, AIP Advances, 6 (2016) 025221.
[5] Y. Hirayama, Y.K. Takahashi, S. Hirosawa, K. Hono, Scripta Materialia, 95 (2015) 70-72.
[6] Y. Hirayama, Y.K. Takahashi, S. Hirosawa, K. Hono, Scripta Materialia, 138 (2017) 62-65.
[7] T. Sato, T. Ohsuna, M. Yano, A. Kato, Y. Kaneko, Journal of Applied Physics, 122 (2017) 053903.

Design of Ferrite Magnet Flux Concentrated Permanent Magnet Synchronous motor with Cross-Laminated Rotor Core

Jaewoo Jung[1*], Jungpyo Hong[2]
[1]R&D Center, Hyundai Mobis, Korea
[2]Department of Automotive Engineering, Hanyang University, Korea

In order to improve the torque density of the flux concentrated permanent magnet synchronous motor (FC-PMSM) utilizing the ferrite permanent magnet (PM), it is important to reduce the leakage magnetic flux flowing through leakage path of the rotor core. Unfortunately, in order to keep the robustness of the rotor assembly, a leakage path is necessarily required in the rotor core. For satisfying the robustness of the rotating body and the improvement of the torque density, we propose a structure in which two types of cores with different shapes are cross-laminated. The proposed rotor structure shown in Fig. 1 consists of a core with a bridge that is necessary for securing the rigidity of the rotor assembly, and a rotor assembly by cross-laminating the segment type rotor cores necessary for minimizing the leakage flux as well as improving the torque density. The complex three-dimensional magnetic circuit of the cross-laminated rotor assembly has been modeled as a two-dimensional (2-D) model based on the mathematical basis using the equivalent magnetic circuit. By using the equivalent 2-D model, the design of the cross-laminated rotor shape and the electromagnetic characteristics were examined comprehensively. At the same time, mechanical stresses due to centrifugal force and slip torque between rotor core and shaft were examined. Finally, after the prototype was made, the validity of the analysis and design method was verified through no-load and load test.

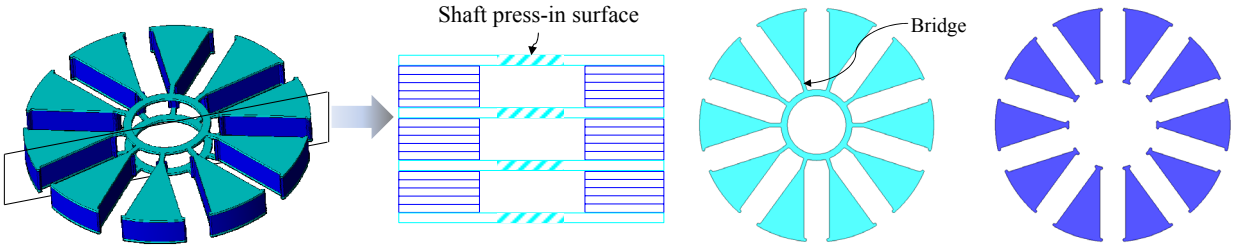

Fig. 1. Shape of cross-laminated rotor core and assembly structure. (a) Rotor core assembly (b) Cross section view of the core assembly(c) Rotor core with bridge (d) Rotor core without bridge

Analysis and reduction of electromagnetic vibration of PM brush DC motors

Shanming Wang*
Tsinghua University, China
wangsm96@mails.tsinghua.edu.cn

Vibration mode of electric machines is an important characteristic of vibration, which is useful for finding the vibration sources with different frequencies, but always neglected before. In this speech, the vibration characteristics, especially vibration mode, of permanent magnetic brush DC motors are studied. Firstly, the air gap flux density distribution and radial force density distribution are derived in detail, and compared with the results of finite element method (FEM). Then two types of vibration modes, called pulsating and bending mode, and their reasons as pulsating force and bending moment are analyzed and elaborated which are not analyzed and verified sufficiently before. In addition, the relationships between these two vibrations and pole width, pole number and slot number are analyzed. The main modal shapes and their frequencies are acquired from the modal test. To confirm the analysis and theory, the multi-probe mode-included test method of vibration acceleration is proposed and emphasized to obtain the vibration mode information of motors, and the experimental results on a PM brush DC motor match well with the simulation results.

In order to reduce the electromagnetic vibration, two effective ways were proposed. One is to skew the PM pole with segments, and the other is to add a copper ring on the pole faces. The analysis and experimental results were included.

Development of Heavy-Rare-Earth-Free Hot-deformed Nd-Fe-B Magnets for Traction Motors

Keiko Hioki[1†], Atsushi Hattori[2*], Yutaka Yoshida[3]
[1]Daido Corporate Research & Development Center, Daido Steel Co., Ltd., Japan
[2]Technical Department, Daido Electronics Co., Ltd., Japan
[3]Daido Steel (America) Inc., USA

Nd-Fe-B magnets are widely used in clean energy applications such as hybrid electric vehicles (HEVs), consumer and other electronic devices, and wind turbines, because these magnets exhibit the highest maximum energy product, $(BH)_{max}$, of all the permanent magnet materials.(1) Especially, the demand of Nd-Fe-B magnets with high remanence and high heat resistance for HEV traction motors have been increasing. On the other hand, the coercivity of these magnets exhibit only around 20 % of anisotropy field which represents the full potential of the material, and its coercivity mechanism has still not been clarified completely. Therefore, heavy rare earth elements (HREEs) with higher anisotropy fields (typically Dy and Tb) are added up to around 10 wt.% in order to improve the coercivity for high temperature applications such as HEVs despite remanence degradation. However, relying on the HREE poses a significant risk as the prices are unstable due to its relative scarcity and uneven distribution as a natural resource. Taking account of the ever increasing demand for clean energy vehicles, it is the most important challenge to reduce HREE consumption in Nd-Fe-B magnets without a significant reduction of coercivity.

Hot-deformed Nd-Fe-B magnets are attractive in reducing or eliminating HREEs. They have a fine crystal grain microstructure (the lateral size of platelet grains is around 300 nm which is almost the same as the single domain grain size of the $Nd_2Fe_{14}B$ phase) due to their unique production process. It was proved that the fine microstructure brings about both the reduction of required HREEs content and better heat resistance.(2) However, their coercivities are still lower than expected from their grain sizes. (3) In order to improve the coercivity, some researches have been conducted and they indicated that magnetically isolating the main phases is effective.(4)(5)(6)

In order to realize a traction motor with HREE-free magnets, we developed high performance hot-deformed magnet as well as modifying the motor design with a collaboration with an automotive manufacturer.(7) Excellent magnetic properties of hot-deformed magnets were achieved without HREE addition by optimizing the chemical compositions and the hot-deformation process. We will present the details of the development method and results in the conference.

References

[1] M. Sagawa, et al., J. Appl. Phys., **55**, 2083 (1984).
[2] K. Hioki, et al., J. Magn. Soc. Jpn., **38**, 79 (2014).
[3] K. Hono, et al., Scr. Mater., **67**, 530 (2012).
[4] H. Sepehri Amin, et al., Acta. Mater., **61,** 6622 (2013).
[5] J. Liu, et al., Acta Mater., **61**, 5387 (2013).
[6] T. T. Sasaki, et al., Scripta Mater., **113**, 218 (2016).
[7] S. Soma, et al., SAE Int. J. Alt. Power. **6**(2), 290 (2017).

International Symposium on Magnetism and
Magnetic Materials 2017

Special Session V

'Medical Science Research'

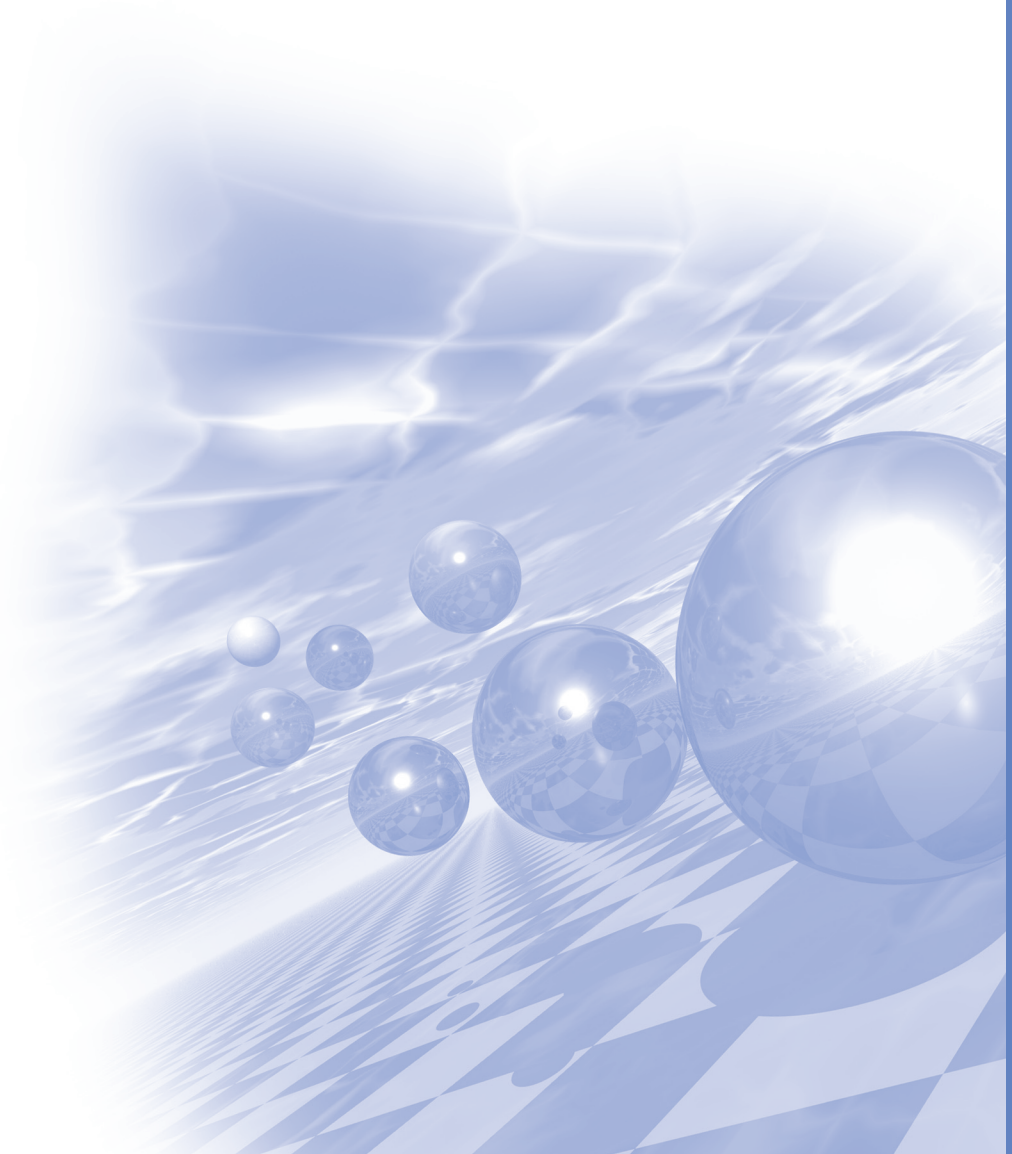

Modified Oblique Sagittal MR imaging of rotator cuff tears: comparison with standard oblique sagittal images

Hyeon Choi Jang[6], Jeong Min Seo[5], Woo Sang Ahn[4], Cheol Soo Park[3], Ham Gyum Kim[2], Myung Sik Ju[1*]

[1]Department of Radiology, Soonchunhyang University Bucheon Hospital, 14584, Korea
[2]Department of Radiological Science, Ansan University, Ansan 15518, Korea
[3]Department of Radiological Science, Hallym Polytechnic University, 24210, Korea
[4]Department. of Radiation Oncology, Asan Medical Center, Gangneung, 25440, Korea
[5]Dept. of Radiological Scienc, Daewon University College, Jecheon, 27135, Korea
[6]Dept. of Radiological Scienc, Suseong College, Daegu, 42078, Korea

Rotator cuff disease occurs in adults is very common cause of shoulder pain causes is known as one of the. Combined oblique coronal and oblique sagittal standard MR imaging is highly accurate for detecting full-thickness rotator cuff tears. However, the accuracy of standard MR imaging is lower for partial-thickness tears. Small rotator cuff tears can be obscured by partial volume effect if the imaging planes are not orthogonal to the surface of the cuff. Angling the oblique sagittal images perpendicular to the lateral 2 or 3 cm of the supraspinatus tendon would reduce the partial volume effect, and might make tears in this region more conspicuous. The purpose of our study was to compare the accuracy for diagnosing rotator cuff tears of oblique coronal images supplemented with standard oblique sagittal images versus thinner-section modified oblique sagittal fat suppressed fast spin-echo T2-weighted images. For full-thickness supraspinatus tendon tears, our study confirms that oblique coronal and standard oblique sagittal images are very accurate for diagnosing tears, and that supplementing oblique coronal images with thinner-section angled oblique sagittal images does not improve diagnostic accuracy for those few full-thickness tears that are missed on standard MR images. In conclusion, there was a slight improvement in accuracy for diagnosing rotator cuff tears, particularly partial-thickness tears, for the staff radiologist using the thinner-section angled oblique sagittal images.

Keywords: MRI, Rotator Cuff, Modified Oblique Sagittal Scan

Development of Multi-purpose Quality Assurance Phantom for Verification of Treatment Plan of Volumetric Modulated Arc Therapy using Linear Accelerator

Hui-Su Won[1,2*], Hyun-Suk Lee[2], Sang-Seok Lee[2], Man-Seok Han[3], Cheol-Soo Park[4], Do-Guwn Hwang[2]

[1]Department of Radiation Oncology, Seoul National University Bungdang Hospital, Seongnam, Korea
[2]Department of Biomedical Engineering, Sangji University, Wonju, Korea
[3]Department of Radiological Science, Kangwon National University, Samcheok, Korea
[4]Department of Radiological Science, Hallym Polytechnic University, Chuncheon, Korea

Purpose: The purpose of this study was to evaluate the feasibility of a multi-purpose quality assurance (QA) phantom for pretreatment verification of volumetric modulated arc therapy (VMAT).

Material and methods: The QA phantom was constructed to perform relative dosimetry using EBT3 film and MapCHECK, as well as the absolute dosimetry using ionization chamber. In order to verify the pretreatment plans, 25 patients treated with VMAT were selected. The pretreatment plans were calculated in the Eclipse treatment planning system using the Acuros XB dose calculation algorithm and CT images for the QA phantom, with the same beam setup and monitor units as those for patient treatment. All plans were delivered to the Varian TrueBeam accelerator equipped with a high-definition multi-leaf collimator.

Results: The multi-purpose QA phantom is developed for convenient VMAT dose verification. By using the QA phantom, all 25 cases passed ±3% acceptability criteria in absolute dosimetry with an ionization chamber for pretreatment verification. The relative dosimetry using EBT3 film and MapCHECK system also showed high agreement of more than 90% for 2%/2-mm and 3%/3-mm criteria.

Conclusion: The results of this study demonstrated the good multi-purpose capabilities of the phantom for the absolute and relative dosimetry. Therefore, the developed multi-purpose QA phantom was applied in our institution for routine VMRT dose verification.

Keywords: volumetric modulated arc therapy, phantom, absolute dosimetry, relative dosimetry

Specific Absorption Rate Evaluation for Multi-Frequency Excitation

Jeung-Hoon Seo[1], Kyoung-Nam Kim[1,2], Yeunchul Ryu[1,3*]
[1]Neuroscience Research Institute, Gachon University, Incheon 21565, Korea
[2]Department of Biomedical Engineering, Gachon University, Incheon 21936, Korea
[3]Department of Radiological Science, Gachon University, Incheon 21936, Korea

In the human magnetic resonance imaging (MRI) research, safety assurance is mainly proved through Specific Absorption Rate (SAR) evaluation. All MR safety researches have focused on a single frequency which is corresponding to the proton excitation. However, the signal from multi-nuclear spin provides meaningful information related to bio-chemical changes in human body. In this research, we introduce the methods to estimate SAR of multi-frequency excitation in the human MR application. All the estimation in this research are based on the electro-magnetic field simulation with digital human model and current safety regulation for MRI system.

Method 1: Summation of individual peak SAR values (pSAR_1)

$pSAR\_1 = Peak\_SAR_{1H} + Peak\_SAR_{31P}$

Method 2: Select of highest individual peak SAR values (pSAR_2)

$pSAR\_2 = max\{Peak\_SAR_{1H}, Peak\_SAR_{31P}\}$

Method 3: Peak of combined SAR (pSAR_3)

$pSAR\_3 = Peak\_(SAR_{1H} + SAR_{31P})$

Separation of photoneutron and photoproton in 10MV and 15MV Medical LINAC

Jeong Ho Kim[1*], Se Jong Yoo[2], Myeong Cheol Park[2]
[1]Department of Radiation Oncology, Konyang University Hospital, Korea
[2]Department of Diagnostic Radiology, Konyang University Hospital, Korea

The photoneutron ray and photoproton ray are occurred according to the use of high-energy electromagnetic radiation of LINACs. Various studies have been conducted to evaluate the effect of such the photoneutron dose on the treatment dose. However, when measuring the photoneutron ray, the measurement of the photoproton ray is added due to the characteristics of the measurement instrument for neutron, so the reliability of the measurement value is low. Therefore, in this study, self-manufactured solenoid was used to measure the photoneutron ray and photoproton ray. And then the calculation formula using reaction cross-section was applied to verify the reliability. For 10 MV LINACs and 15 MV LINACs, the proper conditions of the solenoid were evaluated for application. Then for the distances of 80 ㎝, 100 ㎝ and 120 ㎝ from the source to the measurement instrument, the photoneutron dose value and the sum value of the photoneutron dose and photoproton dose values were read according to the installation of the solenoid in the radiation field of 1X1 ㎠, 2X2 ㎠, and 3X3 ㎠. Finally, the calculation formula according to the reaction cross-section was applied to derive the nuclear reaction process number for the test conditions, and the ratio of photoneutron ray value on the photoproton ray value was compared. The optimum condition of the self-manufactured solenoid was 60[A] or more. The photoproton doses were about 26.3 ± 2.22% of total dose for 10 MV electromagnetic radiation and about 8.59 ± 1.10% for 15 MV electromagnetic radiation as shown in Fig. 1. The index of coincidence between the measured value and the calculated value is about 98.6%. It is possible to separate relatively reliable photoneutrons from photoprotons according to the application of self-manufactured solenoid. In the future, Independent measurement of photoneutrons and photoprotons can be possible by changing the condition of the self-manufactured solenoid.

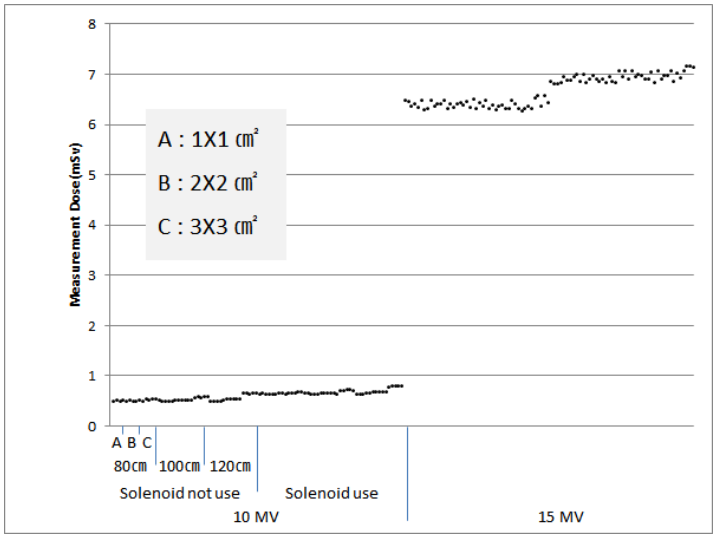

Fig. 1. The graph of measured absorbed dose by each condition

fMRI Brain Network Analysis techniques

Young-Jin Jung[1*], Jang-Woo Park[2], Ujwal Chaudhary[3], Anuradha Godavarty[4], Yongmin Chang[2†]

[1]Dept of Radiological Science, Dongseo University, Busan, South Korea, 47011

[2]Department of Molecular Medicine and medical & Biological Engineering, School of Medicine, Kyungpook National University, Taegu 702-701, South Korea

[3]Dept. of Biomedical Engineering,, Florida International University, Miami, Florida 33174, USA

Brain network analysis of functional MRI data is of great clinical importance for understanding mechanism of diseases and brain activity. However, most of fMRI system can sample the data under 0.5Hz, thereby limiting use of various network estimators. In this study, the analytic signal based causal estimator was demonstrated to estimate the connectivity and causality for low sampled fMRI data. From analytic signal, the instantaneous phase information was extracted and utilized for estimating connectivity and causal networks. To validate the proposed method, the computer based Monte Carlo simulation using fMRI mimicking signals was conducted with various conditions. The simulation results show that the proposed approach can estimate connectivity and causality more accurately than conventional methods. Also, real fMRI data measured from clenching test was applied to identify the brain network and compare with conventional study results. The authors believe that his proposed analytic signal based causal estimator will be found useful, especially when the functional signal was measured with low sampling rate.

Keywords: Analytic Signal, effective connectivity, fMRI, functional connectivity, brain network.

Proposing a low-field bio-imaging method

Sang-Koog Kim*, Jae-Hyeok Lee, and Min-Kwan Kim
National Creative Research Initiative Center for Spin Dynamics and Spin-Wave Devices, Nanospinics Laboratory,
Research Institute of Advanced Materials, Department of Materials Science and Engineering,
Seoul National University, Seoul 151-744, South Korea

Bio-imaging and bio-medicine industries have grown significantly in pursuit of earlier diagnosis of, and more timely therapy for, human diseases. NMRI (Nuclear Magnetic Resonance Imaging) is becoming more widely used to visualize internal organs and structures of the human body. To be able to take full advantage of NMRI's and other bio-imaging techniques' special utility, however, it is essential that their signal sensitivity and spatial resolution be improved to the point that tumor-candidate cells can be isolated and identified. Currently one of the most promising MRI modalities involves the use of contrast agents constituted of super-paramagnetic nanoparticles. Yet this technique requires the application of extremely high magnetic fields (1 - 7 Tesla) to obtain a sufficient number of net signals. The generation of such strong magnetic fields incurs significant cost in superconductor maintenance, and moreover, could have as yet-unknown side-effects on the human body. Thus, it is necessary to find a new, innovative approach - one that entails extremely high-sensitivity, yet low-magnetic- field bio-imaging - and to develop the relevant diverse and proven applications to simultaneous in-vivo diagnosis and therapy.

To this end, we propose a low magnetic-field bio-imaging and therapeutic technique using robust spin dynamics of super-paramagnetic, single-domain, vortex-state nanoparticles, based on resonantly excited precession of individual magnetizations of nanoparticles. The novel spin dynamics may be used to develop new-paradigm bio-imaging techniques as well as hyperthermia therapy with unexpected performance. We conducted micromagnetic numerical calculations of novel spin dynamics for bio-imaging and hyperthermia applications. This concept will provide the original and core technologies that exceed the limitations of conventional bio-imaging tools and therapy to realize the simultaneous implementation of bio-imaging diagnosis and immediate therapy, if tumor targeting technologies using magnetic nanoparticles would be well established.

Author Index

Digests of the International Symposium on Magnetism and Magnetic Materials 2017

The Korean Magnetics Society

International Symposium on Magnetism and Magnetic Materials 2017 Vol. 27, No. 2.

#905 KSTC, (Yeoksam-dong) 22, 7gil, Teheran-ro, Gangnam-gu, Seoul 06130, Korea

TEL. (02)3452-7363, **FAX.** (02)3452-7364

E-mail. komag@unitel.co.kr, **Home-page.** www.komag.org